CO_2 Sequestration in Concrete: Assessing Impacts on Microstructure, Plastic Properties, Mechanical Performance, and Long-Term Durability

by

Clinton Pereira

Bachelor of Engineering-Construction, University of Mumbai, 2000

A Thesis submitted in partial fulfillment of the requirements for the Degree of

Masters of Applied Science

in the Department of Civil Engineering

University of Victoria

We acknowledge and respect the Lək̓ʷəŋən (Songhees and Xʷsepsəm/Esquimalt) Peoples on whose territory the university stands, and the Lək̓ʷəŋən and W̱SÁNEĆ Peoples whose historical relationships with the land continue to this day.

Supervisory Committee

CO_2 Sequestration in Concrete: Assessing Impacts on Microstructure, Plastic Properties, Mechanical Performance, and Long-Term Durability

by

Clinton Pereira

Bachelor of Engineering-Construction, University of Mumbai, 2000

Supervisory Committee

Dr. Rishi Gupta, Supervisor

Department of Civil Engineering

Dr. Thomas Froese, Departmental Member, Supervisory Committee

Department of Civil Engineering

Dr. Rodney Herring, Outside Departmental Member, Supervisory Committee

Department of Mechanical Engineering

Abstract

The 20th century has seen rampant industrialization, a boost in manufacturing, deforestation in urban areas and extensive extraction of natural resources and fossil fuels. With a sudden surge in demand for power, transportation and housing, anthropogenic CO_2 emissions are on the rise and have reached unprecedented levels which the earth never experienced before. With 37.5 billion metric tons of CO_2 emissions released in the atmosphere in 2024, as compared to 4.8 billion metric tons released in 1940, global temperatures are rising aggressively. The power, transport and construction industry have been the fastest growing industries in the recent years. Furthermore, in the construction industry the increase in demand for infrastructure and building materials has indirectly increased CO_2 emissions. Additionally, cement manufacturing alone is responsible for 7% of the global emissions. Hence, all sectors, including the construction industry, are exploring for green and sustainable products and practices to counter global temperature rise. One of the promising approaches is the Carbon Capture, Utilization, and Storage (CCUS) technology, which captures CO_2 from industrial effluent sources for storage or reuse. Recent studies have shown that CO_2 can be effectively utilized to enhance the strength and longevity of concrete. This concept holds a great potential in minimizing anthropogenic CO_2 emissions, but it requires extensive experimental investigation.

Ongoing research has shown that adding CO_2 during the mixing or curing stage of concrete improves its mechanical properties. The purpose of this study was to determine whether adding CO_2 to concrete during the mixing process had any positive effects on microstructural, mechanical, and durability properties. The formation of calcium carbonate ($CaCO_3$) results in densification of the microstructure of concrete. Compressive strength tests showed an improvement of 10-20%, particularly in samples with 0.5% to 0.75% CO_2 dosage, which are mainly attributed to $CaCO_3$ formation. Additionally, compared to control concrete, a 5-10% improvement in the flexural strength was observed in the CO_2-sequestered concrete samples. Thermal Pyrolysis tests confirmed a higher $CaCO_3$ content with CO_2 uptake of 2-3%. Additionally, the microscopy and infrared spectroscopy analysis indicated the presence of $CaCO_3$, thereby confirming the densification and the early carbonation process. Conversely, the concrete slump immediately decreased after CO_2 addition, mainly due to the additional mixing time and formation of carbonic acid and $CaCO_3$ with heat release. Although an additional dose of superplasticizer was used to increase slump in this experiment, balancing the dosage with optimum mixing time and a trade-off between increased strength and workability could be explored. This study has also developed a multi-linear regression model which concrete technologists can utilize to assess the compressive strength of concrete and use the same while designing mixes that employ CO_2.

This study also assessed the long-term effects of adding CO_2 during the mixing stage of concrete on its durability and long-term performance under accelerated conditions. Test results indicated that densification of the matrix enhanced its durability. Lower rapid chloride permeability test (RCPT) and permeability values and higher resistivity readings were observed for dosages between 0.5% and 1% in comparison with control concrete samples. An enhancement in the resistance of concrete to freeze-thaw (F-T) cycles was also observed for CO_2-sequestered concrete samples. CO_2 dosages between 0.5% and 0.75% showed improved performance to F-T cycles, as compared to control concrete, observed by lower mass loss, less surface scaling and

increased stiffness. Concrete slab panels exposed to 50 alternating 24-hour wetting and drying cycles at 50–60 °C with and without NaCl solution showed that CO_2 dosages ranging from 0.5% to 0.75% increased corrosion resistance in a chloride-free environment. CO_2-sequestered concrete indicated a corrosion rate that was approximately 30–35% lower than the control by 50 cycles for CO_2 dosages of 0.5% and 0.75% in the set that had a wetting cycle with potable water at 23 ± 2 °C and a drying cycle at 50 °C. Corrosion rates also decreased by 25–30% for CO_2 dosages of 0.5% and 0.75% in the set with a wetting cycle with potable water at 23 ± 2 °C and a drying cycle at 60 °C in comparison to the control, suggesting improved durability. However, both control and CO_2-dosed concrete suffered extremely high corrosion rates under saline conditions in the set with a wetting cycle with potable water at 23 ± 2 °C and 5% NaCl and a drying cycle at 60 °C. This test shows that in chloride rich environments, only adding CO_2 to concrete without additional changes to the mix design and supplementary protection to steel will not help in resisting corrosion.

A Life Cycle Analysis (LCA) was conducted for CO_2-sequestered concrete with varying CO_2 dosages and the mix with 0.75% CO_2 dosage indicated better environmental performance through a 37% decrease in normalized global warming potential over the control mix. However, challenges pertaining to the high cost of capturing, storing and transporting CO_2 needs to be addressed for large-scale implementation in the construction industry.

In a nutshell, this study experimentally assesses the benefits of CO_2 addition on the microstructure, plastic and mechanical properties and long-term durability, thereby contributing to the development of a sustainable and green construction material. While challenges pertaining to the loss in workability, high cost of CO_2 and acceptance by industry remain, this technology presents a positive approach towards green and sustainable development.

Table of contents

List of Tables

List of Figures

List of Acronyms

Acronym	Definition
AASHTO	American Association of State Highway and Transportation Officials
ACI	American Concrete Institute
AEA	Air-Entraining Admixture
ANOVA	Analysis of Variance
ASTM	American Society of Testing and Materials
ATR	Attenuated Total Reflectance
BSE	Back Scattered Electron
BWC	By Weight of Cement
$Ca(OH)_2$	Calcium Hydroxide
$CaCO_3$	Calcium Carbonate
CCUS	Carbon Capture, Utilization, and Storage
CFH	Cubic Feet per Hour
CO_2	Carbon Dioxide
CSA	Canadian Standards Association
C-S-H	Calcium Silicate Hydrate
DAQ	Data Acquisition
EDX	Energy-Dispersive X-ray spectroscopy
EPS	Expanded Polystyrene
FTIR	Fourier Transform Infrared Spectroscopy
GGBS	Ground Granulated Blast-furnace Slag
GHGs	Greenhouse Gases
GWP	Global Warming Potential
ICOR	Instantaneous Corrosion
IEA	International Energy Agency
ITZ	Interfacial Transition Zone
LC3	Limestone Calcined Clay Cement
LCA	Life Cycle Assessment
LCI	Life Cycle Inventory
LPR	Linear Polarization Resistance
NDT	Non-Destructive Testing
NRMCA	National Ready Mixed Concrete Association
OPC	Ordinary Portland Cement
PPM	Parts Per Million
PLC	Portland Limestone Cement
RH	Relative Humidity
SCMs	Supplementary Cementitious Materials
SE	Secondary Electron
SEM	Scanning Electron Microscopy
SP	Super Plasticizer
$T_{initiation}$	Initiation Time
$T_{propogation}$	Propagation Time

Abbreviations of Units of Measurement

Abbreviation	Unit of Measurement
°C	Degree Celsius
K	Kelvin
%	Percent
m	Meter
km	Kilometer
cm	Centimeter
mm	Millimeter
µm	Micrometer
h	Hour
min	Minute
s	Second
kg	Kilogram
g	Gram
kcal	Kilocalorie
mol^2/L^2	Moles squared per liters squared
cm^3/mol	Cubic centimeters per mole
kg/m^3	Kilograms per cubic meter
m^3	Cubic meter
kN	Kilonewton
MPa	Megapascal
MPa/s	Megapascal per second
kPa	Kilo Pascal
ft^3	Cubic feet
ft^3/h	Cubic feet per hour
kΩ-cm	Kiloohm centimeter
Ω-m	Ohm meter
mV	Millivolt
V	Volt
kV	Kilovolt
J/mol·K	Joules per mole per kelvin
C/mol	Coulombs per mole
µm/year	Micrometer per year
m/s^2	Meters per second squared
kWh/m^3	Kilowatt-hour per cubic meter
CO_2e/kWh	Carbon Dioxide Equivalent per Kilowatt-Hour
CO_2e/m^3	Carbon Dioxide Equivalent per Cubic Meter
kg CO_2e/m^3/year	Kilograms of Carbon Dioxide Equivalent per Cubic Meter per Year

Preface

This research explores utilizing CO_2 gas in concrete production to enhance its properties. The work presented in this thesis is the result of an extensive laboratory investigations and critical analysis conducted during my Master's program at the University of Victoria. This thesis comprises of an introduction, three research papers, a life cycle analysis section and a conclusion. Chapter 2 of this thesis comprises of a literature review presented as a peer-reviewed conference paper, co-authored with Brian Brunell and Dr. Rishi Gupta. This paper was written by me and was critically reviewed by my co-authors. Section 4.4 on Bio sequestration within this paper was authored by Brian Brunell. Chapter 3 presents a journal manuscript that has been published, and Chapter 4 presents a journal manuscript that is currently under review. The original drafts of these papers were written by me and reviewed by Dr. Rishi Gupta. The remaining sections were written by me, and the entire thesis was reviewed by my research supervisor, Dr.Rishi Gupta, and my committee members, Dr. Thomas Froese and Dr. Rodney Herring.

All laboratory experiments were conducted with the assistance of co-op students Hannah Bochmann and Ailish Paterson. The FTIR spectroscopy and data analysis was conducted with the expertise of my colleague Prakriti Raizada. Drs. Cristina Cordoba and Elaine Humphrey from the Advanced Microscopy facility at the University of Victoria helped me with the SEM and EDX analysis. While references to published articles have been made, the text of the thesis is not taken directly from these sources. Grammatical errors in my writing were rectified using Grammarly, an online AI-based tool. My goal for this thesis is to foster innovation and share the findings from my research with both academic and industry professionals.

Acknowledgements

I would like to express my deepest gratitude to my supervisor Dr. Rishi Gupta for his invaluable mentorship and guidance during my Master's journey at the University of Victoria. I am grateful for his technical expertise, financial support and project funding, research materials and equipment, motivation, and ongoing mentorship during both my research and the courses I had taken with him. I am also deeply thankful of my supervisory committee members, Dr. Thomas Froese and Dr. Rodney Herring, for their willingness to serve on my defense committee, their valuable teachings during my graduate studies, and their periodic feedback and support for my research. My sincere thanks goes to the Civil Engineering Department and the entire team at UVic for their continued support throughout my program. I would like to specifically acknowledge Lorrie Barth for her guidance and support during my program.

I grateful to my colleagues , Dr. Loveleen Sharma, Dr. Maryam Monazami, Jay Viradiya, Prakriti Raizada, Perla Rudolfo, Nasrin Nazarisorkhavankalateh, Sanaz Ajabshir, Navid Tutkaboni, Dr. Sreekumari Raghavan and Qiaorong Sun for their support during my Masters journey and during my time in Victoria. I would also like to express my appreciation to FIMIM & CAMTEC for providing their experimental facilities. I warmly acknowledge Dr. Armando Tura, Arielle Garrett , Bastien Lanusse and Solomon Rosenberg from the civil department staff for their experimental assistance. I appreciate the dedicated efforts of co-op students, Madeleine Thorkelsson, Hannah Bochmann, Ailish Paterson, and Brian Read for their support on my experimental projects. I appreciate Dr. Elaine Humphrey and Dr. Cristina Cordoba from the Advanced Microscopy facility at CAMTEC for helping me with the SEM and EDX analysis. I would like to express my gratitude to Butler Concrete & Aggregate and CarbonCure Technologies for their valuable insights and for taking the time to explain the CO_2 sequestration process implemented at their ready-mix concrete plant in Victoria. I would like to sincerely thank my immediate seniors at UltraTech Cement Limited-SB Kulkarni, Devendra Pandey, and Dr. Jayachandran K, for their support in providing references for my Master's program and encouraging my academic pursuits. I also extend my thanks to everyone unnamed, whose guidance and encouragement have been instrumental throughout my Master's journey in Canada.

Lastly, I would like to thank my entire family, whose support and prayers have made this journey possible. My wife, Aarti Pereira, has been my pillar of strength, by supporting me emotionally and financially during this program. She has also helped me in proofreading my papers and thesis. Finally, I thank my daughter Christina Pereira for her silent support which she has rendered always.

Dedication

I would like to dedicate this thesis, first and foremost, to God for granting me wisdom, knowledge, and strength, to my mother for her prayers from above and to my wife for her unconditional support.

Chapter 1 : Introduction

1.1 Introduction & background

Due to a boost in manufacturing after the industrial revolution in the mid-18th century, the world saw a boost in manufacturing which led to a rampant extraction of natural resources, fossil fuels, afforestation and an increase in greenhouse gas emissions [1]. Due to these growing emissions, the earth is currently experiencing climate change and rising global temperatures [2]. Global temperatures are rapidly increasing, with 37.5 billion metric tons of CO_2 emissions pumped into the atmosphere in 2024 compared to 4.8 billion metric tons in 1940 [3]. The world leaders came together and the United Nations in 2015 signed the Paris Agreement which aimed to keep global warming below 2 °C by the end of the twenty-first century in order to lessen the effects of CO_2 emissions on climate change [4]. With growing concerns about climate change and the urgent need to reduce emissions, all sectors including construction need to minimize their carbon footprint. Carbon capture, utilization, and storage (CCUS) technology is one way to lower atmospheric CO_2 levels [5]. It collects CO_2 from the atmosphere and sends it to a carbon sink for storage or usage. However, this system needs to be scaled up, and its implementation costs decreased [6]. Given the significant impact in global CO_2 emissions from the construction industry, exploring mitigation strategies which includes adoption of the CCUS technology within this sector has become imperative. In this context, the cement and concrete industry needs to focus on reducing its environmental impact through process improvements and material innovations.

Concrete is the most popular building material in the world; sales reached $804.58 billion in 2023, expanding at an annual rate of 8.7% [7]. Global cement output reached 4.1 billion metric tons in 2023 [8], accounting for around 7% of global emissions [9]. This large amount of CO_2 emissions can be mitigated by reducing emissions during the cement manufacturing process and by sequestering CO_2 throughout the lifecycle of concrete. During its service life, concrete slowly absorbs atmospheric CO_2, which reacts with hydrated cement products, mainly calcium hydroxide ($Ca(OH)_2$), to form calcium carbonate ($CaCO_3$) by a process termed as natural carbonation [10]. Early-age carbonation can densify the concrete microstructure and improve compressive strength, according to studies [11–14]. However, reluctance to use CO_2 sequestration in concrete has grown due to a lack of information on its impact on concrete properties and due to worries about corrosion caused by carbonation in reinforced concrete structures [15]. This study investigates the impact of CO_2 addition at the mixing stage of concrete on early-age performance, mechanical and microstructural changes and long-term impact on the durability of CO_2-sequestered concrete, providing a comprehensive evaluation of its early age and long-term effects.

1.2 Hypotheses & Objectives

Although several researchers are studying the effect of early-age carbonation on various properties of concrete in plastic and hardened stages, there remains a research gap. The effect of CO_2 addition during the mixing stage on plastic and mechanical properties, microstructural changes, transport properties, freeze-thaw and corrosion resistance and environmental benefits still needs to be better understood. To fill this knowledge gap, this study suggests the following hypotheses and objectives:

Hypothesis 1: Concrete injected with CO_2 during the mixing stage will demonstrate improved workability, compressive and tensile strength and densification of its microstructure compared to conventional concrete.

Objective 1: To investigate the plastic properties of CO_2-sequestered concrete which includes workability, air content, wet density and temperature changes. This includes measuring slump after CO_2 addition to understand its effect on workability. Additionally, measuring air content to determine if CO_2 addition results in changes in the air content of the mix, determining wet density to verify the yield of the mix, and monitoring the temperature of the mix to measure heat release during the hydration reactions. To evaluate the impact of CO_2 addition on the mechanical properties of concrete which includes compressive, flexural and split tensile strength and compare it with those of control concrete to understand the effect of densification on these properties. To analyze the microstructural and elemental changes in CO_2-sequestered over control concrete by using microscopy and spectroscopy.

Hypothesis 2: CO_2 sequestration will increase concrete resistivity, decrease permeability and chloride ion penetration, enhance resistance to freeze-thaw cycles and show a reduced corrosion potential and corrosion rate when subjected to alternative wetting and drying cycles, compared to control concrete specimens.

Objective 2: To assess the long-term durability of CO_2-sequestered concrete in comparison to control concrete, by measuring water permeability, chloride ion penetration and resistivity. Additionally, this study aims to investigate the effect of CO_2 sequestration on the freeze-thaw resistance of concrete by subjecting the specimens to 300 cycles of freezing and thawing and monitoring changes in mass loss, resistivity, ultrasonic pulse velocity (UPV) and dynamic modulus. Furthermore, to determine the effects of CO_2 sequestration on the pH of concrete by measuring pH levels quantitatively using a pH meter and qualitatively using a Phenolphthalein indicator. Lastly, this study aims to assess the corrosion potential, electrical resistivity, and corrosion rate of CO_2-sequestered concrete, by subjecting reinforced concrete specimens to alternative wetting and drying cycles, with and without the presence of corrosive salts and comparing them with control concrete specimens. This study also aims to estimate the service life of CO_2-sequestered concrete using the Tuutti model and compare it with control concrete.

Hypothesis 3: CO_2-sequestered concrete will demonstrate significant environmental benefits and minimize the construction industry’s carbon footprint.

Objective 3: To conduct a Life Cycle Assessment (LCA) to determine the environmental impacts of CO_2-sequestered concrete and compare it to control concrete. This includes quantifying the Global Warming Potential (GWP) reduction achieved by CO_2 sequestration based on the cradle-to-grave emissions and estimate the normalized GWP emissions per year of service life to understand the carbon footprint of CO_2 sequestered concrete over control concrete.

1.3 Methodology

The main philosophy of this research is positivism, with an emphasis on gathering and analyzing empirical data to comprehend the connection between CO_2 sequestration and the characteristics of concrete in both plastic and hardened stages. An experimental model was created to assess

these associations in a novel and effective manner in order to focus our investigation. The study uses controlled experiments and a quantitative research approach to gather numerical data on a range of specific performance criteria.

This study evaluates various concrete mixes with different CO_2 concentrations ranging from 0.1% to 1% by weight of cement (bwc) to assess their fresh and mechanical properties, transport properties, which include permeability and chloride ion ingress, freeze-thaw resistance, and corrosion potential and rate. Furthermore, a comparative analysis is performed for all these tests between CO_2-sequestered concrete and conventional concrete to understand the benefits of CO_2 addition, if any. Microscopic examination using SEM and EDX, FTIR to identify functional groups and thermal pyrolysis is conducted to investigate the morphological and chemical distinctions between CO_2-sequestered and conventional concrete. This study has also developed a predictive model to estimate the compressive strength, which can be used as a starting point for designing CO_2-sequestered concrete mixes. Furthermore, this study adopts Tuutti's corrosion model to estimate the service life of reinforced concrete. It performs an LCA to calculate the GWP and carbon footprint of CO_2-sequestered concrete over control concrete. This study intends to provide the building industry with a green and sustainable building material by experimentally examining the advantages and challenges of adding CO_2 to concrete.

1.4 Contributions and Deliverables

1. This study contributes to enhancing the service life of concrete structures, minimizing their carbon footprint and providing useful information for implementing this technology in the construction industry.

2. The findings from this study demonstrate the effectiveness of adding CO_2 during the mixing stage to enhance early age and later age strength development up to a particular threshold dosage.

3. This study provides information regarding the long-term durability of CO_2-sequestered concrete subjected to harsh environmental conditions.

4. Project findings will be disseminated to industry partners and other stakeholders at events organized by various cement and concrete forums. Additionally, the research outcomes will be published in a concrete materials journal or other relevant publications.

1.5 Thesis Structure

Chapter 1 provides an introduction to this study. Atmospheric CO_2 is one of the critical greenhouse gases responsible for climate change across the globe. This chapter lays out the foundation for the succeeding research phases, which investigates the possibility of adding CO_2 during concrete production and analyzes its impact on early and long-term properties of concrete. It also discusses the hypothesis and motivation for this study, as well as the objectives, methodology, contributions and the thesis outline.

Chapter 2 is presented in the form of a peer-reviewed published conference paper and highlights the work of past studies that have been done in the area of early-age carbonation of concrete. This chapter reviews the approaches to CO_2 utilization technologies within the concrete industry. It delves into techniques like accelerated carbonation, mineralization through CO_2 injection, CO_2 curing, and treatment of wash water enriched with CO_2. Although early-age carbonation of

concrete is one of the promising techniques for CO_2 utilization, this paper also discusses the challenges and barriers to its widespread implementation, which serves as the foundation for future research.

Chapter 3 is presented as a peer-reviewed published journal paper, focussing on the plastic properties, mechanical performance and microstructural changes taking place in CO_2-sequestered concrete. This chapter evaluates the effect of CO_2 addition during the mixing stage on the plastic, hardened and microstructural properties of concrete. Various CO_2 dosages, ranging from 0.1% to 1%, were injected during the mixing stage to analyze the plastic and hardened properties of concrete, and the test results were compared with the control mix. The study also attempts to create a simplified CO_2 sequestration process in concrete, develop a predictive model to estimate the compressive strength and use material characterization techniques to identify the mineralization process.

Chapter 4 is presented in the form of a journal manuscript that is currently under review, focussing on the long-term effect of CO_2 sequestration on the performance and durability of concrete. In this chapter, the impact of varying CO_2 addition during the mixing stage of concrete on the transport properties, resistance to freezing and thawing conditions and the corrosion resistance of embedded rebars subjected to alternative wetting and drying cycles under harsh environmental conditions have been evaluated. Key parameters like water permeability, rapid chloride ion penetration, resistivity, dynamic modulus, corrosion potential and rate were measured to assess the long-term durability. This chapter also uses Tuutti's corrosion model to estimate the service life of CO_2-sequestred concrete over control concrete.

Chapter 5 presents an LCA to understand the reduction in GWP and the carbon footprint of CO_2-sequestered concrete over control concrete.

Chapter 6 provides concluding remarks, contributions, limitations, future scope of work that can be undertaken by researchers and some final thoughts.

Chapter 2 : CO_2 Sequestration in Concrete- A review of Technologies, Innovations and Barriers

Clinton Pereira [1,3][0009-0006-2444-6623], Rishi Gupta[1,4][0000-0002-3402-6095] and Brian C. Burrell [2,5][0000-0001-9722-9677]

[1] Department of Civil Engineering, University of Victoria, Victoria, British Columbia, Canada
[2] Civil Engineer, Hilcon Limited, 420 York Street, Fredericton, New Brunswick, Canada
[3] clintonpereira@uvic.ca
[4] guptar@uvic.ca
[5] bcb.engineer@gmail.com, brian.burrell@hilcon.ca

This chapter is adapted from the paper presented at the Canadian Society for Civil Engineering (CSCE) Conference 2024 held in Niagara, Ontario, which is a part of the conference proceedings. This paper will be published by Springer in conference-style proceedings. This chapter is a literature review of the available technologies and innovations done for sequestering and permanently trapping CO_2 in concrete. It provides a brief overview of the benefits of early-age carbonation on concrete properties, current approaches to active CO_2 utilization techniques in concrete and challenges faced in its widespread adoption.

2.1 Abstract

Rising global carbon dioxide (CO_2) emissions substantially contribute to climate change and global warming. CO_2 emissions from industrial processes continue to increase substantially. The impact of this on climate change cannot be understated, which is why the Paris Agreement of 2015 has strongly emphasized limiting the global temperature rise to 2 °C by the end of this century. This means reducing CO_2 emissions in all sectors, including electricity, transportation, manufacturing, and construction. Currently, the construction industry is the most significant contributor to carbon emissions, and the cement industry is predominantly accountable for most of these emissions. Some recent breakthroughs have revealed that CO_2 can effectively enhance the mechanical properties and durability of concrete. This chapter reviews global CO_2 utilization technologies within the concrete industry. It delves into techniques like accelerated carbonation, mineralization through CO_2 injection, CO_2 curing, and treatment of wash water enriched with CO_2. While the advantages of CO_2 sequestration in concrete, which include enhanced mechanical properties and cost-effectiveness, have been well-documented by researchers, this chapter explores the barriers hindering its widespread adoption in the construction industry. This chapter also includes an exploration of the technical complexities of CO_2 sequestration in concrete and significant policy developments aimed at reducing carbon emissions. With the global production of approximately 15 billion cubic metres of concrete annually, this review emphasizes the significance and potential benefits of CO_2 sequestration in concrete in pursuing a net-zero emissions future.

Keywords: CO_2 sequestration, Concrete, Carbon Capture, Utilization, and Storage (CCUS), Accelerated carbonation, CO_2 injection, CO_2 curing.

2.2 Introduction

Global warming from burgeoning greenhouse gas (GHG) emissions detrimentally impacts the earth's climate, affecting both present and future generations [16]. The increasing atmospheric concentration of GHGs has caused quantifiable climatic warming and a shift in the occurrence, frequency, timing, and severity of weather events. Of all greenhouse gases, carbon dioxide (CO_2) is the most crucial anthropogenic contributor to warming due to atmospheric loadings of CO_2 from various emissions sources [17].

In 2022, CO_2 emissions from fossil fuels and industry were estimated to have reached an unprecedented level of 37.5 billion metric tons [18], with the cement industry alone having an alarming carbon impact, which accounts for approximately 7% of global CO_2 emissions [4, 7]. This large amount of CO_2 emissions can be mitigated by reducing the amount of CO_2 emitted during cement manufacture and by sequestration of CO_2 during the life cycle of concrete. Various strategies can be employed to curtail CO_2 emissions throughout the lifecycle of concrete structures. These encompass designing elements and materials focusing on efficiency during construction, optimizing concrete production methods, and integrating captured CO_2 within concrete [19]. Integration of captured CO_2 into the concrete industry involves processes such as CO_2 mineralization via injection into wet concrete [20], CO_2 curing for precast concrete [21], treatment of concrete wash water [22] and recycled concrete aggregates that are infused with CO_2 [23].The structural design process can be further enhanced through a multi-objective approach of reducing CO_2 emissions through cost-effective designs, construction site productivity, extended service life, and safety measures [24]. Concrete production efficiency can be achieved by fine-tuning mix designs and implementing stringent quality control measures. Introducing supplementary cementitious materials (SCMs) to partially replace Ordinary Portland cement (OPC) not only minimizes CO_2 emissions but also often enhances both the fresh and hardened properties of concrete [10].

A practical method to reduce CO_2 emissions is Carbon Capture, Utilization, and Storage (CCUS), which involves capturing and storing CO_2 generated from industrial facilities and utilization in some manufacturing units [25]. Recent studies suggest that CO_2 can be efficiently employed to improve the mechanical strength and longevity of concrete [26, 27]. This literature review chapter provides insights into the methods and technical complexities of sequestering CO_2 in concrete. It also examines the utilization of these methods to sequester CO_2 within the concrete industry, addressing market constraints and other barriers hindering their widespread adoption. By delving into these aspects, this chapter fosters a holistic view essential for shaping sustainable practices in the construction industry.

2.3 CO_2 emissions in the cement industry

The cement industry, with global production of 4.1 billion tons in 2022 [28], makes a substantial contribution to CO_2 emissions, releasing approximately 0.6 tons of CO_2 per metric ton (MT) of cement produced, based on data provided by the International Energy Agency (IEA) [29]. CO_2 emissions in cement production primarily stem from three sources: approximately 50% arises from the calcination or decomposition of calcium carbonate ($CaCO_3$), around 40% from fuel combustion in kilns, and the remaining 10% from manufacturing operations, including transportation and electricity use [30]. Leading cement industries worldwide are implementing

various strategies to reduce CO_2 emissions [19]. These measures include enhancing clinker substitution with supplementary cementitious materials (SCMs) like fly ash, ground granulated blast-furnace slag (GGBS), and ground limestone [10]. Reducing clinker content offsets emissions linked to limestone calcination, thereby enhancing energy efficiency [31, 32]. Additionally, efforts are focused on reducing fossil fuel usage, increasing the utilization of alternative fuels, and deploying waste-heat recovery systems within cement plants [33]. Furthermore, initiatives involving CCUS technology and infrastructure development are underway. Multiple CO_2 capture technologies like amine scrubbing, calcium looping, direct separation, and oxy-combustion have been developed to extract and capture CO_2 before its release into the atmosphere. These technologies possess distinct advantages and disadvantages, as detailed in Hanifa et al.'s work [30]. Limestone Calcined Clay Cement (LC3) is a promising, sustainable alternative to Ordinary Portland cement (OPC), significantly reducing clinker content by approximately 50% and lowering CO_2 emissions during production. With lower energy consumption than traditional cement processes, LC3 utilizes calcined clay and limestone as low-carbon raw materials, contributing to environmental benefits in the cement industry [34, 35].

2.4 CO_2 Sequestration in Concrete

2.4.1 Natural carbonation process in concrete

Natural carbonation or recarbonation is a slow physiochemical process wherein cement hydration products slowly reabsorb atmospheric CO_2**.** This phenomenon takes place as CO_2 diffuses into the pores of cement-based materials and reacts with calcium hydroxide ($Ca(OH)_2$) to form $CaCO_3$ [10]. The formation of $CaCO_3$ reduces free $Ca(OH)_2$ and densifies the concrete but also results in elevated crystal pressure at a microstructural scale [36]. As time passes, carbonation moves inward from the concrete surface. When it reaches the rebars, corrosion protection decreases, causing cover spalling in moist conditions. Therefore, natural carbonation is generally an undesired process and minimizing it is crucial in concrete design [10]. Due to the unique carbon uptake properties of concrete, industry experts are investigating its inclusion in carbon accounting. Achternboscha et al. [37] noted the absence of reliable models correlating carbonation with concrete age. The Intergovernmental Panel on Climate Change (IPCC) 6th Assessment Report in August 2021 addressed the recarbonation of concrete in carbon accounting [19]. Huang et al. [38] proposed an analytical model to estimate CO_2 uptake from concrete carbonation. While it is not universally accepted, these methods can assess the carbon sink benefit from concrete carbonation throughout its lifespan.

2.4.2 Accelerated carbonation process in concrete

Researchers have shown that CO_2 can be effectively used in concrete production to enhance mechanical properties and improve the durability of concrete [11, 26, 27, 36]. In their paper, Monkman et al. [26] highlighted that intentionally sequestering CO_2 from industrial processes into freshly mixed concrete can improve properties in fresh and hardened states, aiming to reduce the carbon footprint. In another study, Monkman et al. [27] concluded that CO_2 injection accelerates hydration reactions in concrete. They found that the concrete treated with CO_2 exhibited neutral to positive effects on its durability, as indicated by enhanced resistance to chloride penetration, reduced drying shrinkage, and improved performance against freeze-thaw cycles and de-icer salt scaling. The review papers authored by Zhang et al. [36] and Fernández Bertos et al. [11]

conclude that concrete subjected to early-age CO_2 curing exhibited enhanced physical performance and increased resistance to freeze-thaw cycles, sulphate salts, and acids. This improvement is attributed to reduced permeability, porosity, and enhanced strength.

2.5 Reaction kinetics of cement carbonation

As detailed in "Lea's Chemistry of Cement and Concrete," when Portland cement reacts with water, the primary outcome is the formation of the C-S-H phase. Following this, crystalline $Ca(OH)_2$, known as portlandite, becomes the second most prevalent product in hydrated Portland cement pastes [39]. The pH of concrete remains above 12.5 due to the presence of $Ca(OH)_2$, effectively shielding the steel reinforcement from corrosion [40]. The carbonation reaction primarily takes place at the surface of the C-S-H gel. $Ca(OH)_2$ reacts directly with CO_2, leading to the creation of a stable form of $CaCO_3$ and silica gel. Water is not consumed but is needed in the transformation. Equations 1, 2 & 3 usually describe the main carbonation reactions.

$$Ca(OH)_2 + CO_2 \rightarrow CaCO_3 + H_2O \quad (1)$$

$$CO_2 + H_2O \rightarrow H_2CO_3 \quad (2)$$

$$Ca(OH)_2 + H_2CO_3 \rightarrow CaCO_3 + 2H_2O.CO_3 \quad (3)$$

The carbonation process can enhance the mechanical properties and durability of concrete by causing densification of the cementitious matrix. This occurs as a result of carbonation affecting $Ca(OH)_2$ and hydration products, leading to the formation of $CaCO_3$, which has a higher molar volume than $Ca(OH)_2$ [41].

2.6 Approaches to active CO_2 utilization in Concrete

Although natural carbonation can occur slowly in concrete structures, accelerating carbonation of concrete through methods such as mineralization via CO_2 injection, CO_2 curing, and the use of CO_2-enriched wash water are reviewed in this section of this chapter.

2.6.1 Mineralization through CO_2 injection

CO_2 injection and mixing in concrete involve introducing gaseous or liquid CO_2 into cement-based formulations. This is typically achieved by injecting CO_2 into fresh concrete at a ready-mix concrete plant's central mixer or directly into the ready-mixed concrete truck during initial batching and mixing [42]. Certain companies have developed control systems linked to ready-mix plants' batching software. These systems connect to onsite CO_2 tanks and automatically inject precise amounts of CO_2 into the concrete during mixing, like introducing a chemical admixture at the batching plant. When liquefied CO_2 enters the mixing drum, it transforms into a combination of CO_2 gas and solid carbon dioxide snow. This reaction occurs during cement hydration and forms solid nano-sized $CaCO_3$ particles [43].

An innovative method patented by CarbonCure Technologies (Nova Scotia, Canada) [44] designed to curtail the carbon footprint within concrete production, involves adapting concrete production facilities with a system that enables the infusion of captured gaseous or liquid CO_2 into concrete mixers or transit mixers during the mixing process. The CO_2 interacts with the moisture and cementitious elements within the fresh concrete blend, creating $CaCO_3$, an integral part of the mineralization process. Converting CO2 into a mineralized state within the concrete not only

bolsters the strength and endurance of the concrete but also sequesters carbon, significantly reducing its carbon footprint.

2.6.2 Treatment of concrete wash water enriched with CO_2

Wash water from water spraying over powdered suspensions, from the cleaning of equipment (concrete transit mixers, the interior of central mixers, pouring skips, pump lines), and from runoff from production yards is a by-product of ready-mixed concrete production [45]. Because of its highly alkaline nature (with a pH range of 12-14), mainly due to the $Ca(OH)_2$ generated from the dissolution of unhydrated cement particles in an aqueous phase, proper management of concrete washout water is crucial to comply with regulations and prevent environmental harm before discharge into watercourses [22].

Monkman et al. [22] treated industrially sourced wash water with a specific gravity > 1.20 with CO_2. The treatment mineralized CO_2 at 27% by weight of the cement. It reduced or eliminated negative aspects (set acceleration, workability loss, strength reduction with water age) associated with untreated water. The approach allows three waste streams (CO_2, wash-water generated as a by-product of ready-mixed concrete production, and wash-water solids) to be reused to produce concrete sustainably. Wang et al. [23] also discovered through their analysis that the direct use of untreated wash water in concrete can have adverse effects, such as accelerated initial setting time and diminished workability of fresh concrete.

2.6.3 CO_2 curing of concrete

Introducing CO_2 into precast-concrete elements under controlled pressure and temperature is an emerging accelerated curing method gaining traction in the precast industry. Carbonation curing effectively improves early-age properties and provides a stable medium for carbon sequestration and storage [20]. Precast elements, typically mass-produced in a factory, traditionally necessitate steam curing by creating an environment of elevated temperature curing (50–70 °C) and high relative humidity (above 95%), a process known to be highly energy-intensive [36]. The carbonation process described by Shao [21] simulates controlled environmental conditions in a chamber during early concrete curing. It employs static and dynamic systems, where static carbonation places cured concrete in a CO_2 chamber after initial hydration and the dynamic systems expose fresh products to circulating CO_2 for simultaneous preconditioning and carbonation. The pressurized sealed carbonation curing open-inlet system utilizes high-purity CO_2 at up to 500 kPa, ensuring continuous CO_2 supply for concrete reaction and achieving targeted carbon absorption.

The CO_2 curing method exhibits promising potential in non-reinforced applications like concrete blocks, pavers, and aerated concrete blocks. There is a potential for replacing steam or autoclave curing with a comparable or even superior durability performance in such cured products, as indicated by Zhang et al. [36]. The authors have expressed concerns regarding the application of carbonation curing to steel-reinforced members due to challenges associated with pH level alterations and potential corrosion issues on embedded steels. Rostami et al. [46] noticed that initiating early carbonation in precast elements following initial curing facilitated CO_2 absorption and decreased the $Ca(OH)_2$ content at the concrete surface. This chemical alteration could notably enhance sulphate resistance while ensuring that the pH of the pore solution in the core

remains above the corrosion threshold value. Zhu et al.'s [14] microscopic analysis detected that CO_2 curing enhanced the corrosion resistance of inner steel bars by improving the compactness of the concrete matrix at the surface.

The patented Carbicrete method [47] from Quebec, Canada, innovatively cures concrete products, particularly unreinforced hollow concrete blocks, by leveraging CO_2 to enhance the process. The technique involves placing the concrete product with an embedded cavity on a base and sealing it with a cover plate, utilizing its structure as a vessel to maintain pressure. This eliminates the need for an external airtight enclosure. CO_2 is then introduced into the cavity, initiating a carbonation process that improves the curing of concrete, thereby enhancing its strength and durability.

CarbonBuilt (California, USA) utilizes CO_2 to strengthen concrete blocks and pavers by employing it in the curing process of concrete blocks, enabling the implementation of low-carbon concrete solutions [48]. Despite being at an early stage due to technical and economic limitations, carbonation curing is progressively gaining momentum as a viable approach to minimize GHGs and promote sustainability.

2.6.4. Bio-sequestration

Bio-concretes with carbon-sequestering bacteria offer a promising, environmentally friendly means to reduce CO_2 emissions and advance the concrete industry toward a CO_2 net-zero solution [49]. Bio-sequestration accelerates carbonation by utilizing microorganisms with carbonic anhydrase and urease enzymes, converting CO_2 into $CaCO_3$ via bio-mineralization [50]. During concrete hydration, ions interact with carbon-capturing bacteria cell walls, leading to $CaCO_3$ precipitation on the cell surface, enabling concrete to self-heal and improving mechanical and durability properties. Nevertheless, adoption is hindered by higher raw material costs and knowledge gaps compared to other technologies [51].

2.7 Impact of CO_2 Sequestration on Concrete Performance

During the initial stages of concrete carbonation, solid $CaCO_3$ is produced, contributing to increased strength and enhanced material compactness. Studies reveal that early-stage carbonation transforms CO_2 into $CaCO_3$, reinforcing the C-S-H gel and improving concrete durability. This process results in a more compact microstructure, reducing permeability and elevating resistance against freeze-thaw cycles and chloride ion penetration [12, 13, 21, 26, 27]

Upon early-age carbonation in concrete, the primary cementitious by-products consist of $CaCO_3$ and silica gel, derived from the decalcification of the C-S-H gel. This diminishes the specific surface area of the C-S-H gel. While silica gel can absorb and release water during wet-dry cycles, its influence on shrinkage is limited due to its lower presence than $CaCO_3$. In contrast, $CaCO_3$ exhibits notable volumetric stability and chemical inertness within the cement matrix. Consequently, concrete displays improved volumetric stability after undergoing carbonation [12, 26, 27, 46].

2.8 Challenges in commercial use of CO_2 sequestration in concrete

Challenges span the availability and cost of raw materials suitable for carbonation, the availability and price of CO_2 sources, the complexity of carbonation reaction processes, and the lack of relevant codes and guidelines. These are discussed below.

Material Availability and Purity: The availability and cost of raw materials for carbonation hinder the adoption of carbon capture and sequestration technologies. Regional variations in material availability and price can be addressed using recycled materials. CO_2 source compatibility and purity are crucial for effective carbonation reactions. Carbon-capture costs depend on the CO_2 origin, often sourced from concentrated pure CO_2 or industrial flue gas emissions, mainly from cement plants [20]. Presently, CO_2 production demands substantial energy, with around 1.27 GJ needed for one ton of pure CO_2 from flue gas, escalating to about 1.60 GJ after compression and liquefaction [52].

Cost: Currently, there is limited practical use of carbonation treatment in concrete due to complex processes and inconsistent studies. Handling dilute gas streams in cement production and power generation incurs higher expenses, ranging from USD 40 to 120 per ton of CO_2 [53]. Transporting and storing CO_2 has variable costs based on volume, travel distances, and storage conditions, with onshore pipeline transport expenses in the United States ranging from USD 12 to 14 per ton of CO_2 [53]. Global carbon capture and storage initiatives aim to reduce future energy consumption and CO_2-related expenses.

Construction Codes and Standards: Adherence to prevailing construction codes and standards poses a significant challenge, notably in adopting novel methodologies such as early-age carbonation. The lack of relevant codes and guidelines for various concrete capture and sequestration methodologies and products may deter engineers apprehensive of design challenges and liability associated with innovative building materials and infrastructure design. Once various techniques and product specifications related to carbon capture and sequestration techniques are standardized and codified, their adoption should become more widespread.

Uncertainty: The inertia to change, driven by uncertainties in adopting new technologies, poses a challenge in the cement and concrete industries. Initial costs associated with transitioning to new materials and practices may deter widespread adoption. Uncertainties persist until comprehensive, long-term research validates the safety of early-age carbonation. Concerns about carbonation-induced corrosion in reinforced concrete structures increase apprehensions about integrating CO_2 sequestration. Consequently, regulatory adaptation is delayed, requiring potential revisions or new standards within the construction industry.

Early age Carbonation scale-up: Knowledge gaps persist regarding the engineering and costs of upscaling commercial production methodologies for CO_2 sequestration in concrete. Precise control of carbonation parameters, including time, pressure, and temperature, is crucial for desired material characteristics. Transitioning from pilot-scale to commercial production poses challenges in maintaining quality and performance standards, hindering widespread adoption in the cement and concrete industries due to potential initial costs.

2.9 Concluding Remarks

The absorption of infrared radiation by CO_2 is warming the planet and changing regional climates, affecting the ecology, and threatening human health and safety. Yet CO_2 emissions continue to rise substantially, with increasing dire consequences of climate change becoming more likely unless action is taken soon. Anthropogenic CO_2 emissions in all sectors, including construction, must be reduced to limit global temperature rise to 2 °C by the end of this century, as strongly emphasized in the Paris Agreement 2015. As a significant emitter of CO_2, the concrete industry must use industrial CO_2 capture, accelerated carbonation, and other mitigation technologies to reduce its detrimental climate-change impacts. To assess the effects of concrete emission and sequestration of CO_2, a holistic evaluation is suggested as necessary, including consideration of concrete products over their life cycle. A Life-Cycle Analysis (LCA) approach would require consideration of potential sequestration of CO_2 in recycled aggregates and solid wastes diverted from landfills. Nonetheless, it remains crucial that the concrete industry reduce emissions by including CO_2 sequestration.

This chapter contains a review of:

- Natural and accelerated carbonation processes and reaction kinetics,
- Active innovative strategies for CO_2 sequestration in concrete including CO_2 utilization approaches like CO_2 injection, treatment of concrete wash water enriched with CO_2, and CO_2 curing of concrete, and
- CO_2 sequestration on concrete performance, commercial use challenges, and future research recommendations.

In the context of this review, the following conclusions can be drawn:

- The cement industry contributes significantly to CO_2 emissions, prompting the need for innovative strategies to mitigate its environmental impact.
- Accelerated carbonation processes offer potential benefits for improving concrete performance, but scale-up and commercial use challenges remain.
- Methods like CO_2 injection, wash-water treatment, and CO_2 curing show promise in enhancing concrete properties.
- Implementation hurdles exist. Economic factors, regulatory compliance, and limitations in CO_2 retention within concrete pose challenges to widespread adoption.

Furthermore, identified limitations concerning CO_2 sequestration in concrete include:

- CO_2 sequestration in concrete made with OPC exhibits lower efficiency in retaining CO_2 than cement substitutes, limiting its capacity to reduce carbon footprints significantly.
- Adherence to existing construction codes and standards poses a challenge in adopting novel CO_2 sequestration methodologies due to safety concerns and uncertainties.
- Transitioning from pilot-scale methodologies to commercial production while maintaining quality and performance standards presents difficulties.

Future research can enhance our understanding, refine efficacy, and promote efficient implementation of CO_2 Sequestration in Concrete across diverse engineering projects. Specific areas for exploration include:

- Targeting cost and energy reduction in CO_2 capture and utilization in concrete.
- Validating safety and durability to support regulatory adaptation.
- Efficient upscaling of CO_2 sequestration in concrete without compromising quality or performance.

Chapter 3 : Exploring the Impact of CO_2 Sequestration on Plastic Properties, Mechanical Performance, and Microstructure of Concrete

Clinton Pereira [1,2,3,4] and Rishi Gupta [1,2,3,5]
[1] Department of Civil Engineering, University of Victoria (UVic), Canada.
[2] Facility for Innovative Materials and Infrastructure Monitoring (FIMIM) UVic, Canada.
[3] Centre for Advanced Materials and Related Technology (CAMTEC) UVic, Canada.
[4] clintonpereira@uvic.ca
[5] guptar@uvic.ca

Article link: https://doi.org/10.1007/s44290-024-00151-2

This chapter is adapted from a peer-reviewed journal paper published in the Springer Nature-Discover Civil Engineering Journal in December 2024 [54]. This study provides an experimental analysis of the impact of CO_2 addition during the mixing stage of concrete on its plastic and hardened properties. The study focuses on evaluating the effects of CO_2 sequestration on the plastic and mechanical properties of concrete, analyzing microstructural changes, designing a simplified CO_2 sequestration process in concrete, establishing a predictive model to estimate the compressive strength and utilizing material characterization techniques to understand the mineralization process.

3.1 Abstract

In view of global warming, carbon sequestration techniques are being employed across the globe to minimize the damaging effects of greenhouse gases on the environment. Studies have revealed that adding CO_2 during the mixing or curing stage of concrete enhances its mechanical properties and long-term durability. This study aims to examine the effect of CO_2 addition during the mixing stage on the plastic, mechanical and microstructural properties of concrete. Various CO_2 dosages, ranging from 0.1% to 1%, were injected during mixing to analyze the plastic and hardened properties of concrete. CO_2 primarily reacts with calcium hydroxide in concrete to form calcium carbonate ($CaCO_3$), thereby densifying its microstructure and improving its compressive strength by 10-20%. An optimum strength of up to 20% was achieved with 0.75% dosage. Additionally, the results show a 5-10% improvement in flexural and split tensile strength with CO_2 addition over the control mix, with 0.75% dosage yielding optimal strength. Semi-adiabatic calorimetry test on early hydrating concrete shows a 14% peak temperature rise at 0.75% CO_2 dosage compared to control concrete, indicating enhanced early-age strength development. Thermal pyrolysis tests, microscopy and infrared spectroscopy indicated the presence of $CaCO_3$, thereby confirming the carbonation process. However, CO_2 dosages above 0.5% by weight of cement resulted in a drop in the workability of concrete in the plastic stage. This research attempts to create a simplified CO_2 sequestration process in concrete, develop a predictive model to estimate the compressive strength and utilize material characterization techniques to identify the mineralization process.

Keywords: CO_2 sequestration, Recarbonation, Accelerated carbonation, Mineralization, Carbon footprint, Sustainable development.

3.2 Introduction

The temperatures on the Earth have been rising since the late 1850s [2], and this phenomenon is being experienced worldwide [55]. Greenhouse gas (GHG) emissions, mainly CO_2, are rising at an alarming rate due to human activities and industrial development, thus accelerating global warming [56]. In 2023, anthropogenic CO_2 emissions, primarily from the usage of fossil fuels and industrial activities, reached 37.55 billion metric tons [3]. In addition, the average annual atmospheric concentration of CO_2 in 2023 hit a record high of 421.08 parts per million (ppm), resulting in increased GHG emissions [57]. Furthermore, there has been a boom in the construction sector worldwide, resulting in a high demand for cement and concrete, which has a large carbon impact. Concrete is the most widely used construction material worldwide, with global sales reaching $804.58 billion in 2023, and this market is growing at 8.7% annually [7]. Also, cement production reached 4.1 billion metric tons in 2023 [8], accounting for about 7% of world emissions [9]. These large amounts of CO_2 emissions can be reduced by lowering emissions during the manufacturing of cement and decreasing the carbon footprint throughout the lifecycle of concrete. Additionally, studies have explored various end-of-life strategies for different structural elements, from construction to post-use recycling, to mitigate carbon emissions [58, 59]. Building on these insights, this study explores CO_2 sequestration in concrete with an aim to lower its carbon footprint.

Concrete absorbs atmospheric CO_2 during its service life, a process termed as natural carbonation [10]. CO_2 reacts with calcium hydroxide (($Ca(OH)_2$), which is one of the products of cement hydration, to form calcium carbonate ($CaCO_3$) [12]. However, this process slowly results in the consumption of $Ca(OH)_2$ with time, lowering the pH of concrete and making the embedded rebar susceptible to corrosion [27]. In addition, the formation of $CaCO_3$ within the dense microstructure of concrete results in additional pressure on the surrounding concrete, leading to microcracking [60]. Hence, concrete is designed to resist the natural carbonation process [61]. Studies have shown that adding CO_2 during the mixing stage of concrete improves the compressive strength and other mechanical and microstructural properties of concrete without affecting durability, as seen in the natural carbonation process [11–14, 62]. However, gaps still remain related to the accelerated carbonation process, which has slowed its practical implementation in the construction industry. To resolve these gaps, this study focuses on the impact of early-age carbonation on plastic properties, mechanical performance and microstructural changes in CO_2-sequestered concrete.

To test the proposed hypothesis and answer critical research questions regarding the impact of CO_2 sequestration in concrete, this study first measures the plastic and mechanical characteristics of concrete that has been CO_2-sequestered at varying CO_2 concentrations. Slump, air content, density, compressive strength, flexural strength, and split tensile strength are measured and compared to control concrete specimens. Next, the study monitors temperature rise in concrete using semi-adiabatic calorimetry to understand the impact of early hydration on hardened properties for different CO_2 dosages. To predict the compressive strength of CO_2-sequestered concrete, the study has also developed a multi-linear regression model that takes into account variables, including CO_2 dose, cement content, and water-to-cement ratios. Analytical and imaging tools like Fourier transform infrared (FTIR) spectroscopy, scanning

electron microscopy (SEM), and energy dispersive X-ray spectroscopy (EDX) were used to characterize changes at the microstructural level and correlate their impact on mechanical and durability properties. Furthermore, the increasing temperature pyrolysis technique was used to quantify carbonates formed due to the accelerated carbonation process.

By referring to the experimental analysis presented in this chapter, this research will provide valuable insights for industry professionals to explore the practical implementation of CO_2 sequestration in the construction industry to minimize the Global Warming Potential (GWP) and the overall carbon footprint of concrete. In a nutshell, this research aims to provide novel material technologies that enhance the life of concrete and minimize the adverse effects of CO_2 on the environment. This study also contributes to the sustainable development goals by creating resilient infrastructure and promoting well-being and healthy lives for all by minimizing the impact of GHGs on the climate.

3.3 Literature Review

This literature review briefly examines the impact of CO_2 on concrete, evaluates the adverse effects of natural carbonation on long-term durability and explores the potential benefits of accelerated carbonation for enhancing the mechanical properties and microstructure of concrete. Research has also shown that accelerated carbonation may result in a decrease in the workability of concrete. Monkman [27] reported that CO_2 accelerates the hydration process, thereby reducing the initial setting time of concrete by up to 40%. Wang et al. [63] highlighted that CO_2 could act as a coagulant in the fresh stage of concrete and cause a reduction in its workability due to the formation of $CaCO_3$ on the surface of hydrating particles. Bukowski and Berger [64] reported that the dissolution of CO_2 gas in water produces carbonic acid and crystalline $CaCO_3$ involving exothermic reactions, releasing 160 kcal and 288 kcal of heat per mole, respectively. The authors also highlight that the rapid initial reaction rate results in heat release and water loss from the concrete mix. As a result, the concrete workability decreases, which Monkman et al. [27] in their study noted as a parameter which needs further analysis. The authors of this study did not find any published work quantifying the amount of water lost from concrete during early-age carbonation, and this remains an area for future research. Although an increase in early hydration enhances mechanical properties, workability needs to be further analyzed to ensure ease in transportation, placing and finishing of concrete.

3.3.1 Early-age carbonation reactions in concrete

To gain a comprehensive understanding of the early-age carbonation reactions in concrete, the authors of this study have conducted a detailed analysis of the chemical reactions in this section. When water is added to cement, the primary hydration reactions of tricalcium silicate ($3CaO.SiO_2$) and dicalcium silicate ($2CaO.SiO_2$), which form Calcium Silicate Hydrate ($3CaO.2SiO_2.3H_2O$) and calcium hydroxide, [39] are represented by equations 4 and 5 :

$$2\,(3CaO\cdot SiO_2) + 6\,H_2O \rightarrow (3CaO\cdot 2SiO_2\cdot 3H_2O) + 3\,Ca(OH)_2 \quad (4)$$

$$2\,(2CaO\cdot SiO_2) + 4\,H_2O \rightarrow (3CaO\cdot 2SiO_2\cdot 3H_2O) + Ca(OH)_2 \quad (5)$$

When CO_2 is introduced into hydrating cement concrete, it dissolves into the mixing water to form carbonic acid/bicarbonate ion (HCO_3^-). However, due to the high pH environment of concrete, the

carbonic acid is further ionized into H^+ and carbonate ion (CO_3^{2-}) ions. This has been explained by Lagerblad [65] according to reaction equations 6 to 8.

$$CO_{2(gas)} + H_2O_{(liquid)} \rightarrow H_2CO_{3(aq)} \quad (6)$$

$$H_2CO_{3(aq)} \rightarrow H^+ + HCO^-_3 \quad (7)$$

$$HCO^-_3 \rightarrow H^+ + CO_3^{2-} \quad (8)$$

These CO_3^{2-} ions subsequently react with Ca^{2+} ions found in hydrated cement components, such as $Ca(OH)_2$ and C-S-H gel, resulting in the formation of $CaCO_3$ [60].

As explained by Lagerblad [65], $Ca(OH)_2$ reacts directly with CO_2, leading to a stable form of $CaCO_3$ and silica gel. The author also highlights that water is not consumed but is needed in its transformation. As the solubility of $CaCO_3$ (solubility 0.99×10^{-8} mol^2/L^2) is much lower than that of $Ca(OH)_2$ (solubility 9.95×10^{-4} mol^2/L^2), $Ca(OH)_2$ will dissolve and $CaCO_3$ will precipitate during this process [65]. This process can be summarized through equations 9 [66], 10 and 11 [67], (12) and (13) [26].

The primary carbonation reaction is usually described by equation 6, combined with other reactions described by equation 7 & 8 [67]

$$Ca(OH)_2 + CO_2 \rightarrow CaCO_3 + H_2O \quad (9)$$

$$Ca^{2+}_{(aq)} + CO_3^{2-}{}_{(aq)} \rightarrow CaCO_{3\,(solid)} \quad (10)$$

$$Ca(OH)_2 + H_2CO_3 \rightarrow CaCO_3 + 2\,H_2O{\cdot}CO_3 \quad (11)$$

Unhydrated C2S and C3S are also prone to carbonation, as summarised in equations 12 and 13. However, their carbonation does not directly affect the alkalinity of the concrete [66]. Lagerblad [65] further explains that when $Ca(OH)_2$ is completely consumed, the pH of the pore solution drops below 9.2, Ca^{2+} ion concentration also drops, and C-S-H starts dissolving due to the release of Ca^{2+} ions. This can impact the mechanical properties significantly.

$$3\,CaO{\cdot}SiO_2 + (3–x)\,CO_2 + y\,H_2O \rightarrow x\,CaO{\cdot}SiO_2{\cdot}\,y\,H_2O + (3–x)\,CaCO_3 \quad (12)$$

$$2\,CaO{\cdot}SiO_2 + (2–x)\,CO_2 + y\,H_2O \rightarrow x\,CaO{\cdot}SiO_2{\cdot}\,y\,H_2O + (2–x)\,CaCO_3 \quad (13)$$

The x and y variables represent the number of moles of compounds involved in the reaction. x represents the number of moles of $CaO{\cdot}SiO2{\cdot}y\,H_2O$, which is a C-S-H phase formed. y represents the number of moles of H_2O, indicating the water content in the C-S-H phase formed. Additionally, (3-x) and (2-x) represent the number of moles of $CaCO_3$ which are formed during the reaction. The interaction between CO_2 and freshly mixed hydrating concrete, predominantly with the anhydrous cement grains instead of the hydration products of mature concrete, creates a dense microstructure and the obstruction of capillary pores [64]. This occurs as a result of carbonation reactions with $Ca(OH)_2$ and other hydration products, leading to the formation of $CaCO_3$, which has a higher molar volume than $Ca(OH)_2$ [67]. Molar volume of $Ca(OH)_2$: 31.66 cm^3/mol and molar volume of $CaCO_3$: 36.92 cm^3/mol [68].
Although early-age carbonation involves complex reactions, Figure 3.1 provides a simplified illustration of the CO_2 injection process into concrete, along with the basic carbonation reaction.

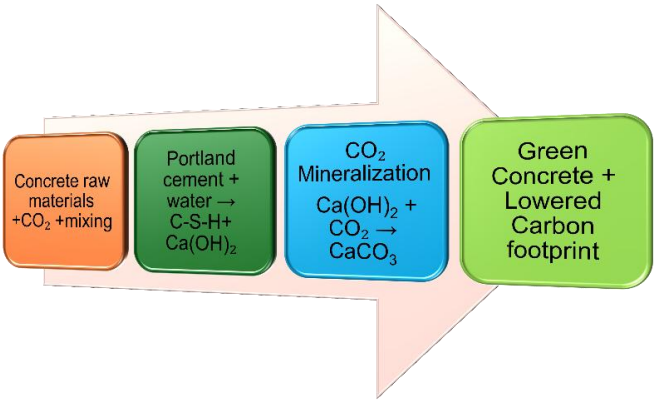

Figure 3.1 Flowchart illustrating a simplified CO_2 sequestration process concrete

3.3.2 Methods for Identifying CO_2 Uptake in Concrete

3.3.2.1 Thermal Pyrolysis method for identification of Carbonates

The thermal pyrolysis method, as explained by Zhang and Shao [69], measures the mass change of a sample as it is heated to reveal information about its composition. Collier [68] describes that quantification of free water, Portlandite, and carbonates is made possible by their thermal decomposition at particular temperature ranges. Bentz and Stutzman [70] claim that at 105 °C, free water is released. According to Scrivener et al. [71], mass loss occurs above 400 °C when bound water, C-S-H, and ettringite phases break down. Portlandite decomposes between 410 °C and 550 °C, according to Alarcon-Ruiz et al. [72]. Zhang and Shao [69] explain that weight loss between 550 °C and 950 °C is usually caused by the breakdown of calcium carbonate. Since CO_2 is released and $CaCO_3$ breaks down into calcium oxide (CaO) during this reaction, it is crucial for measuring the amount of CO_2 absorbed by carbonated concrete. According to Zhang et al. [73], the mass change between these two temperatures was used to compute the quantity of CO_2 using equation 14. In their study, Villain et al.[74] and Kaddah et al. [75] explained that breakdown temperatures of phases such as C-S-H, ettringite, portlandite, and carbonates can be used for mass measurements. Because aggregates are present, Zhang and Shao [69] stressed that the Thermal Pyrolysis method is more feasible for detecting CO_2 content instead of a Thermogravimetric Analyzer (TGA). In light of the difficulties in utilizing a TGA, this work explores the Thermal Pyrolysis technique as a less complicated means of determining CO_2 uptake in concrete.

$$\text{Actual } CO_2 \text{ uptake (\%)} = \frac{(\text{Sample mass at 550 °C} - \text{Sample mass at 1000 °C})}{(\text{Sample mass at 550 °C})} \times 100 \qquad (14)$$

3.3.2.2 Scanning Electron Microscopy (SEM) and Energy Dispersive X-ray Spectroscopy (EDX)

As highlighted by Stutzman [76], SEM allows for high-resolution characterization beyond the capacity of optical microscopy, typically operating in secondary electron (SE) or backscattered electron (BSE) mode. Stutzman further mentions that an SEM equipped with an EDX can also reveal the elemental composition of various concrete compounds through spot analysis, line scans, or mapping. Some researchers have successfully adopted SEM and EDX analysis for the identification of the development of $CaCO_3$ crystals in CO_2-sequestered concrete, paving the way

for future research. Parvan et al. [77] reported SEM images of elongated $CaCO_3$ crystals and flower-like aggregates. Liu et al. [78] observed numerous grainy calcite crystals in CO_2-cured cement paste. The authors highlight that EDX analysis of the same sample indicated high peaks of calcium, oxygen, and carbon, with a lower peak for silicon. Zhu et al. [14] observed needle-like carbonates in the SEM images. Berger et al. [79] suggested that the carbonation reaction products become so intermixed with C-S-H that it is impossible to identify distinct carbonation product morphologies using SEM. Although numerous researchers have identified $CaCO_3$ crystals in CO_2-sequestered concrete using SEM and EDX with success, distinguishing carbonation products remains challenging, as highlighted by different researchers. This experimental work examines whether EDX analysis alone could be adequate to identify $CaCO_3$, given the difficulties with SEM imaging, by identifying carbon in concrete that has been CO_2-sequestered and making suitable inferences.

3.3.2.3 Fourier Transform Infrared Spectroscopy (FTIR)

The results of a study by Kalkreuth et al. [80] indicate that FTIR spectroscopy can detect different chemicals or functional groups in cementitious materials by measuring the absorption or reflectance of infrared light at different wavelengths. Santos et al. [81] state that the presence of different compounds in concrete can be identified as each of these compounds indicates a distinct spectrum according to their functional group, which has been summarized in Table 3.1. As concrete is a homogeneous material made up of hydrated cement paste and aggregates, the interpretation of FTIR spectra can be complex due to the presence of multiple overlapping bands. To counter this issue, and as adopted by Nasrazadani et al. [82] , this study focuses on identifying the functional groups related to $CaCO_3$, C-S-H, and $Ca(OH)_2$, as these groups are mainly found in hydrated cement paste only.

Table 3.1 Compounds, functional groups and the corresponding absorption bands

Compound	Functional group	Absorption band	Vibrational modes	Reference
$CaCO_3$	CO_3^{2-}	1400-1600 cm^{-1}	Asymmetric Stretching	[83]
		Around 870 cm^{-1}	Out-of-Plane Bending	[81]
		Around 765 cm^{-1}	In-Plane Bending	[84]
C-S-H	Si-O	900-1100 cm^{-1}	Si-O Stretching	[85]
		600-670 cm^{-1}	Si-O Bending	[86]
$Ca(OH)_2$	OH^-	Around 3644 cm^{-1}	OH Stretching	[87]

This brief literature review is in tandem with the research problem statement of analyzing the impact of early-age carbonation on plastic properties, mechanical performance and microstructural changes. Although natural carbonation is a very slow process, it can devastate the life of reinforced concrete structures, especially when exposed to high concentrations of atmospheric CO_2. Previous studies on natural carbonation have shown its adverse impact on concrete durability. This occurs due to the reduction of pH of the pore water and the creation of an environment where the protective oxide layer on the steel reinforcement dissolves, making the steel susceptible to corrosion. On the other hand, the addition of CO_2 during the mixing stage of concrete can positively benefit mechanical properties and long-term durability. However, there

remains a research gap in ease of implementation, estimation of compressive strength after CO_2 addition and methods to validate the process. To address these gaps, this study has first developed a simplified sequestration process, which can be adopted in concrete manufacturing units. Research has shown that adding CO_2 during the mixing stage can reduce the workability of concrete and accelerate its hydration, which is often seen as a challenge for field applications. This study investigates these aspects further by studying the impact of CO_2 on plastic properties, analyzing the temperature rise during early hydration and exploring a balance between increased strength and workability. Additionally, a predictive model has been developed to estimate the compressive strength of concrete depending on CO_2 dosage, cement content and water-cement ratio of the mix. This study has also adopted characterization methods to identify microstructural changes due to early age carbonation of concrete. Although earlier studies have utilized individual analytical tools, this study has adopted characterization methods, such as FTIR, SEM, EDX and thermal pyrolysis techniques, to identify microstructural and chemical changes due to early age carbonation of concrete. These findings provide a better understanding of early-age carbonation reactions in concrete. Addressing these gaps will help the concrete industry implement the CO_2 sequestering process and promote the construction of durable, sustainable, eco-friendly structures.

3.4 Methodology

3.4.1 Raw materials

The primary binding agent used was Portland Limestone Cement (PLC), meeting the specifications of CSA A3001-03 GUL (General Use Limestone) or ASTM C595 for type IL (PLC with up to 15% limestone). Locally sourced natural sand and crushed granite were used as fine and coarse aggregates, meeting ASTM C33/C33M-18 [88] specifications. The grading curves for these aggregates, tested as per ASTM C136/C136M-19 [89], are illustrated in Figure 3.2 (a) and (b). Fine aggregates complied with ASTM Standard C33-18 Table 1 requirements, while coarse aggregates met ASTM Standard C33-18 Table 3 specifications. Fine aggregates had a fineness modulus of 2.53, specific gravity of 2.66, and water absorption of 0.38%. Coarse aggregates had a maximum size of 19 mm, specific gravity of 2.68, and water absorption of 0.26%. Coarse aggregates of 19 mm and 9.5 mm sizes were blended in a 55% to 45% ratio in the mix to meet the combined gradation limits for coarse aggregates. To maintain optimal workability, a high range water reducing admixture or superplasticizer (SP), based on polycarboxylate technology, meeting Type F requirements of ASTM C494/C494M-19 [90] and an air-entraining admixture (AEA) meeting the requirements of ASTM C260-10 [91] were used. The SP content varied for different mixes, while AEA was added in fixed amounts per cubic meter of concrete to maintain the air content of the mix between 6-8%. The specific gravity of SP and AEA, provided by the manufacturer, was 1.06 and 1.008, respectively [92].

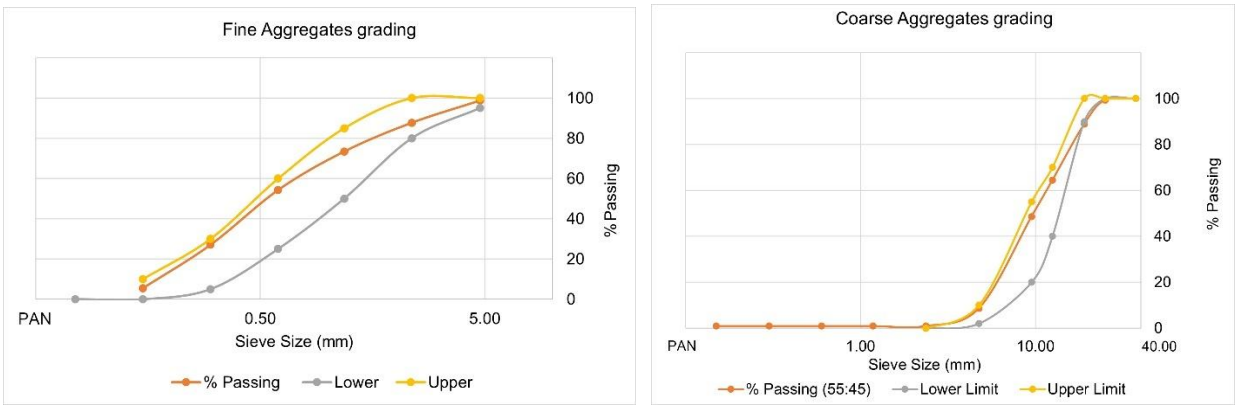

(a) (b)

Figure 3.2 Sieve analysis of (a) fine aggregates and (b) coarse aggregates

3.4.2 Concrete Mix Design

This study involved developing two concrete mix designs with compressive strength (f'_c) of 25 MPa and 40 MPa, as summarized in Table 3.2, adhering to ACI PRC-211.1-91 [93] standards for selecting proportions for normal, heavyweight, and mass concrete.

Table 3.2 Mix design for 25 MPa and 40 MPa concrete

Concrete Ingredients	Grade 25 MPa	Grade 40 MPa
Cement GUL (kg/m^3)	300	400
Water (kg/m^3)	140	160
water/cement ratio	0.46	0.4
Fine aggregate- Natural sand (kg/m^3)	851	712
Coarse aggregate (9.5 mm) (kg/m^3)	464	464
Coarse aggregate (19 mm) (kg/m^3)	567	567
Superplasticizer (% bwc)	0.3	0.3
Air Entraining Admixture (% bwc)	0.3	0.3
Theoretical bulk density (kg/m^3)	2323	2305

The 25 MPa mix was selected to compare the strength gain patterns with control concrete, providing insights into the effects of CO_2 addition during mixing on both early and later age strength development. In contrast, the 40 MPa mix was designed for C2, S2, and A2 class exposure as per the Canadian Standards Association (CSA 23.1:19) [94], with a goal to study both the mechanical properties and long-term effects of CO_2 sequestration on concrete properties. Specific mix proportions for both concrete grades are detailed in Table 3.2. Sample preparation followed ASTM C192/C192M-19 [95] guidelines, using a tilting drum mechanical mixer. Dry ingredients were mixed for 2 min, followed by 3 min of wet mixing. Superplasticizer and AEA were added to the mixing water. For the CO_2-sequestered concrete, CO_2 was injected after initial wet mixing, controlling flow in cubic feet per hour (ft^3/h) and duration in minutes. Additional mixing time for CO_2-injected concrete ranged from 2 to 6 min. Adding CO_2 to concrete resulted in a reduction in workability, which previous researchers have validated. In addition, the extra mixing time adds to moisture loss. For practical applications, concrete needs to be sufficiently workable to ease the process of mixing, transporting, placing, compaction, and finishing at its final

placement location. An extra dose of superplasticizer was added to compensate for the slump drop of the concrete during CO_2 exposure and additional mixing time. An extra quantity of the superplasticizer, ranging from 0.1-0.3% by weight of cement (bwc) depending on CO_2 addition, was added to maintain a slump of 125-150 mm during casting, with an additional minute of mixing time.

3.4.3 CO_2 sequestration process

After the first wet mixing of the concrete, CO_2 was added in a gaseous state as part of the CO_2 mixing process for fresh concrete. The CO_2 cylinder was purchased from an industrial gas supplier for this experiment, which had a vapour pressure of 5730 kPa and a concentration of 99.8%, the cylinder had an industrial-grade CO_2 [96]. Rather than using flue gases, which would have different concentrations of other gases, pure CO_2 was selected. To maintain a sufficient flow of CO_2 gas and regulate the dose, which is expressed in CFH, a gas regulator and flow meter were utilized, as illustrated in Figure 3.3(a). To prevent CO_2 gas from escaping during mixing, a set-up was planned and constructed that included a circular wooden lid and clamps (figure 3.3(b)) to the open end of the tilting drum concrete mixer. Furthermore, a flexible hose was connected to a 10 mm diameter copper pipe, depicted in Figure 3.3(c), that extended into the mixer. To ensure efficient CO_2 mixing, the end of the copper pipe had a 90-degree bend and a swivel connecter to ensure 360^0 rotation and complete immersion of the pipe in the concrete mix during rotation.

(a) (b) (c)

Figure 3.3 CO_2 injection set-up (a) Regulator and flowmeter, (b) CO_2 cylinder and concrete mixer with lid, and (c) CO_2 dosing pipes in the mixer

Table 3.3 CO_2 dosing summary

Mix	% Mass of CO_2/m^3 by weight of cement	Flow rate (ft^3/h)	CO_2 injection Time (min)	CO_2 injected (ft^3)	Mass (kg) of CO_2 for 1 m^3 of concrete
Mix-1	0				0
Mix-2	0.25	14	1.9	0.5	1.0
Mix-3	0.50	14	3.8	0.9	2.0
Mix-4	0.75	18	4.5	1.4	3.0
Mix-5	1.00	18	6.0	1.8	4.0

Note: Cement-400 kg/m^3

Table 3.3 shows the calculations for the mass of CO_2 per cubic meter of concrete derived from the flow and time for mixes 02, 03, 04, and 05 containing CO_2 dosages of 0.25%, 0.5%, 0.75%, and 1%, respectively, for the 40 MPa grade concrete mix. The table highlights the percentage of CO_2 by weight of cement, flow rate in cubic feet per hour (ft^3/h), injection duration (in minutes), total CO_2 volume injected in cubic feet (ft^3), and corresponding CO_2 mass in kg/m^3 of concrete, with a cement content of 400 kg/m^3. The same method was used to calculate the flow rate in cubic feet per hour and the duration of flow in minutes or seconds for the 25 MPa grade concrete mix. Mix 1 served as the control concrete with no CO_2 injection. The CO_2 dosing was regulated by the flow meter by adjusting the flow rate in cubic feet per hour and the duration of flow in minutes or seconds. The following method was used to convert the CO_2 gas being injected into concrete: As per Ideal gas law [97], 1 ft^3 of CO_2 gas contains approximately 1.264 moles of CO_2 at standard temperature and pressure (STP). Table 3.4 provides a calculation of the conversion of 1 ft^3 of CO_2 to mass in grams [98].

Table 3.4 CO_2 weight calculations

Weight of 1 mole of CO_2	44 g
Molar mass of carbon in CO_2	12 amu
Molar mass of oxygen in CO_2	32 amu
Total Molar Mass of CO_2	44 amu
1 cubic feet of CO_2	1.264*44=55.66 g

The CO_2 dosage threshold limit of 1% by weight of cement was selected based on preliminary concrete trials and findings from related studies [26, 27], both of which indicated that higher CO_2 dosages adversely impacted the slump and workability. This upper limit in dosage was chosen to balance the positive effects of CO_2 sequestration with workability and mechanical performance.

3.4.4 Plastic and Hardened Properties of Concrete

Plastic properties are important as they determine the ease of mixing, transporting, placing, compacting and finishing concrete, with the aim of achieving better performance in the hardened stage. This study measures workability and air content in the plastic stage. To monitor and record changes in the workability of concrete due to CO_2 injection, a single-point workability test using the Abrams slump cone was conducted. The procedure for the slump test followed the ASTM C143-12 [99] standard. The pressure method for measuring air content in the concrete was performed according to ASTM C231-09 [100], as shown in Figure A.1(c) in Appendix A . Cylindrical specimens, sized 100 x 200 mm, were cast and cured in line with ASTM C192-14 [95] guidelines. During mixing and casting, the laboratory had a temperature of 15 ± 5 °C and 60 ± 5 % relative humidity (RH). After 24 h of casting, the samples were demoulded and transferred to a curing tank maintained at 23 ± 2 °C until testing. To ensure smooth, plane surfaces for even loading on the moulded face of the cylindrical concrete specimens the surface was ground using a concrete grinding machine as shown in Figure A.2(a) in Appendix A. These specimens underwent compressive strength testing at 7, 28, and 90 days in accordance with ASTM C39-21 [101]. The tests were conducted using a compression testing machine with a load capacity of 2000 kN, as shown in Figure A.2(b) in Appendix A. The load was applied at a stress rate of 0.25 MPa/s ± 0.05 MPa/s. The same compression machine was used to test the split tensile strength of cylindrical

concrete specimens, sized 100 x 200 mm, in accordance with ASTM C496-96 [102]. The load was applied continuously without shock, at a constant rate of 1 ± 0.2 MPa/min, using a jig for aligning the concrete cylinder and wooden bearing strips. To examine the flexural behaviour of materials, third-point loading method tests were performed on prismatic specimens of 100 x 100 x 400 mm, following ASTM C78-09 [103]. A high-stiffness testing machine, equipped with an electronic servo-hydraulic actuator system and a maximum rated load capacity of 250 kN, was used to test the beam specimens, as shown in Figure A.2(c) in Appendix A . A 300 mm span length of the test specimen was maintained between the supporting rollers, with a 50 mm overhang provided on both sides of the beam. A linear variable displacement transformer (LVDT) was used to measure the vertical displacement at mid-span. The results presented for the compression, flexure, and split tensile tests are the average of three samples moulded from the same batch of concrete, cured under the same environmental conditions, and tested at the same age.

3.4.5 Temperature development with time

Using a semi-adiabatic calorimeter created in the lab, the temperature development test was carried out to track the time-based temperature variations in a CO_2-sequestered concrete sample compared to a control concrete specimen, as shown in Figures 3.4(a), 3.4(b), and 3.4(c). The process entails monitoring the temperature increase of a 150 x 150 x 150 mm concrete cube over time (figure 3.4(a)). The cube is housed in an Expanded Polystyrene (EPS) box with a thickness of 25 mm to provide thermal insulation (figure 3.4(b)). To ensure steady curing conditions and avoid external temperature variations, this arrangement was kept inside a temperature-controlled curing box (figure 3.4(c)) with a stable air temperature of 23 ± 2 °C. K-type thermocouple wires were inserted into the centre of the concrete cubes during casting to track real-time temperature changes. These thermocouples linked to a data logger recorded concrete temperatures every 2 min. It is important to note that the temperature recorded at time zero was taken after the concrete was cast in the mould and the assembly placed in the curing box, with both the ambient temperature and the temperature of the raw materials being below 12 °C. This arrangement helped to understand how CO_2-sequestered concrete behaves thermally in comparison to control concrete.

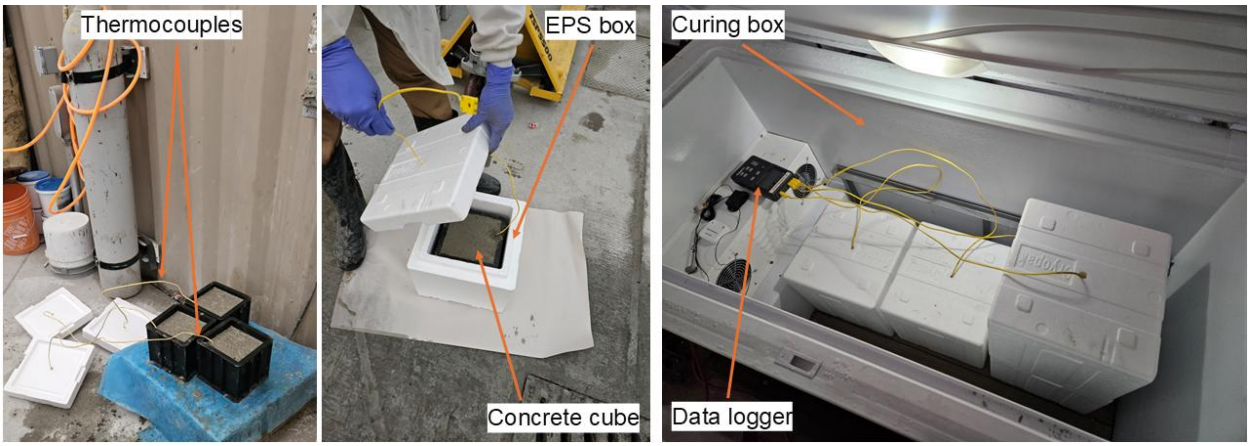

(a) (b) (c)

Figure 3.4 (a) Thermocouples embedded in the concrete cubes (b) Cube placed in an EPS box (c) EPS box placed in a temperature-controlled curing box

3.4.6 Thermal Pyrolysis

The amount of carbonates was measured using the Thermal Pyrolysis method to confirm the carbonation process. This test was conducted in accordance with the procedure described by Zhang and Shao [69]. After testing the cylindrical specimens for 90-day strength, one representative cylinder from the five mixes of 40 MPa concrete was selected for thermal pyrolysis analysis to determine the CO_2 uptake in concrete. The cylinder was broken into smaller pieces using a hammer and placed in an oven at 110 ± 5 °C for 24 h to dry free water. The concrete samples were then crushed into a fine powder using an automatic Marshall impact compactor, as shown in Figure A.3(a) in Appendix A, and the powder was sieved by a 90-micron sieve. The powder samples were subjected to uniform increasing temperature pyrolysis in a muffle furnace, as shown in Figure A.3(b) in Appendix A. Ceramic crucibles were used, and 50 grams of each sample were accurately weighed using a digital balance with a precision of 0.0001 grams, as shown in Figure A.3(c) in Appendix A . The samples were heated from 0 to 550 °C and then from 550 to 1000 °C at an increasing rate of 10 °C/min. The samples were removed from the furnace at these two target temperatures and placed in a vacuum desiccator for 5-10 min, and then their mass was measured. The mass loss occurs in two main stages: dehydration due to the dissipation of bound water (105 to 450 °C) [104], dehydroxylation due to the decomposition of $Ca(OH)_2$ (450 to 550 °C) [72], and dehydration due to calcite decomposition and decarburization (550 to 900 °C) [69]. At 90 days of age after CO_2 injection, the most considerable variation between the mixes was the substantial mass loss that occurred in carbonated samples above 900 °C, corresponding to the decomposition of $CaCO_3$ present in the system.

3.4.7 SEM and EDX analysis

An SEM and EDX analysis was conducted on a CO_2-sequestered sample and compared with a control sample to understand the formation and identification of carbonation products. The Hitachi S-4800 SEM, as shown in Figure 3.5(a), was utilized for X-ray analysis and high-resolution imaging using a cold field emission electron gun. It operates within an accelerating voltage range of 0.5 to 30 kV in 100V increments and offers magnification ranges from 100x to 800,000x in high mode and 30x to 2,000x in low mode. The Bruker Quantax EDX System for X-ray spectroscopy and a ring-type YAG backscatter detector in the SEM facilitate the identification of calcium carbonate in concrete that has been CO_2 sequestered. To ensure that the concrete had undergone adequate hydration and carbonation, in the case of CO_2-sequestered samples, the concrete cylinders were cured for 90 days before the microstructural investigation, producing more dependable test findings. Concrete from the cylinders was cut into thin slices of about 2-3 mm thickness using a diamond-bladed sawing machine. A prismatic sample of about 2x2x2 mm from each slice was cut and polished using a polishing machine, as illustrated in Figure 3.5(b), with abrasive papers of 500, 1500, and 2500 grit for about 2-3 min each with water. The polished samples were washed and dried in an oven at 110 ± 5 °C for 24 h to remove free moisture. Samples were then mounted on SEM stubs using conductive copper tape to ensure good electrical contact between the sample and the stub. Before SEM imaging, the samples mounted onto the stub were placed in a Hitachi zone cleaner for 24 h to remove hydrocarbons and other contaminants using a UV source and vacuum.

Beam deceleration and low vacuum mode were used because the accelerating voltage could not be lowered for EDX analysis. Samples were examined under both secondary electron (SE) and backscattered electron (BSE) modes. For X-ray spectroscopy, an accelerating voltage of 13 keV was selected, as the excitation energy of the Kα X-ray for iron is 6.39 keV. A working distance of 15 mm was chosen for EDX to optimize the collection efficiency and count rate of emitted X-rays. Comparative imaging and X-ray analysis of control and CO_2-sequestered concrete samples were conducted to identify significant differences in morphology and elemental composition to infer if carbonation has taken place.

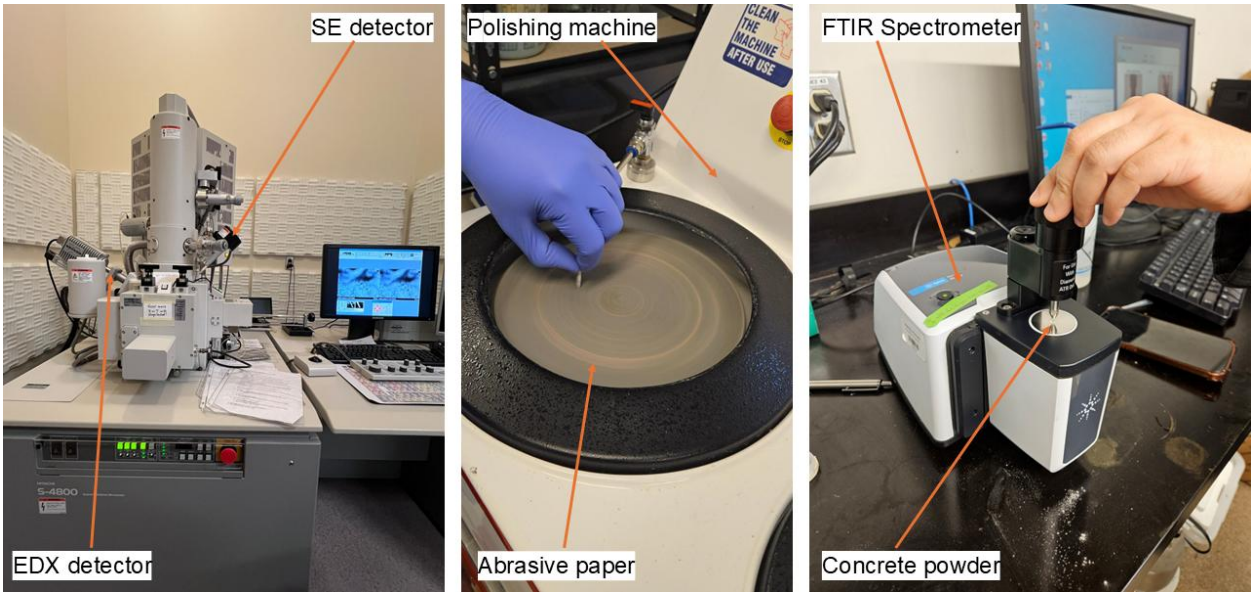

(a) (b) (c)

Figure 3.5 (a) Hitachi S-4800 SEM, (b) Polishing machine, (c) Agilent Cary 630 benchtop FTIR spectrometer

3.4.8 FTIR

FTIR spectroscopy was used in this study to compare the carbonate functional groups in CO_2-sequestered concrete samples with control concrete samples. Concrete samples, after 90 days of curing, from 0%, 0.25%, 0.5%, 0.75%, and 1% CO_2 dosages were prepared for FTIR analysis. The powdered samples were prepared using a procedure similar to that described in section 3.6 for thermal pyrolysis. The particle sizes of all powder specimens were less than 90 microns. The powders were dried in an oven at 110 ± 5 °C for 24 h before the test to ensure that all moisture was eliminated for FTIR characterization. All spectra were recorded from 4000-500 cm^{-1} using the Agilent Cary 630 benchtop FTIR spectrometer, as shown in Figure 3.5(c), equipped with a diamond attenuated total reflectance (ATR) sampling module. Each spectrum had a resolution of 2 cm^{-1}. The IR spectra were recorded and stored using MicroLab Expert spectroscopic software, focusing on the functional groups of interest.

3.5 Results and Discussions

3.5.1 Plastic Properties

Table 3.5 summarizes the plastic properties for each of the five 40 MPa concrete mixes, including slump, air content, temperature, fresh density, and pH of the mixing water with CO_2. While the 40 MPa grade concrete was intended to investigate plastic, mechanical, microstructure, and long-term durability, the 25 MPa grade concrete was utilized to comprehend the trend in the increase in compressive strength. The concrete samples with CO_2 addition seemed noticeably drier than those without CO_2 addition after the mixes were prepared. All four CO_2-injected mixes exhibited these workability changes, with mixes 4 and 5 exhibiting a slump reduction to nearly nil. The extra time spent mixing CO_2-injected concrete varied from 2 to 6 min, which would have caused some of the water content to evaporate and made the concrete drier. Additionally, when CO_2 was added, the formation of $CaCO_3$ may have consumed some free water and reduced the moisture content in the mix, further reducing the workability of concrete. The workability of the concrete mix before CO_2 addition and after 1% CO_2 dosage are shown in Figure A.1(a) and (b) in Appendix A.

Table 3.5 Plastic properties of concrete- slump, air content, temperature, fresh density, and pH

Mix	CO_2 dosage	Initial slump (mm)	Slump (mm) after CO_2 injection	Additional SP dosage (% bwc)	Slump (mm) after extra SP	Air Content (%) after CO_2 injection	Mix temperature after CO_2 addition (°C)	Wet density (kg/m^3)	pH of mixing water after CO_2 injection
Mix-01	0	150	N.A**	0	N.A**	7*	5*	2330	7.02*
Mix-02	0.25%	160	120	0.2	150	7	6	2332	4.1
Mix-03	0.50%	150	70	0.2	140	7.25	6	2325	4.05
Mix-04	0.75%	160	25	0.3	140	8	10	2335	3.95
Mix-05	1.00%	150	0	0.4	130	8.75	9	2330	3.9

Note: * Control concrete samples without CO_2 addition. **N.A-Not applicable.

The slump of the concrete significantly decreased after CO_2 injection. Initially, the slump was around 150±10 mm for all mixes, indicating good workability. However, post-CO_2 injection, the slump value dropped from 120 to almost zero for the CO_2-injected mixes with an increase in dosage. This drastic reduction in slump within the first 10 min of adding water is related to the formation of carbonic acid, $CaCO_3$ and the release of heat, as mentioned by Bukowski and Berger [64]. The pH of the mixing water blended with dosages of CO_2 from 0.25% to 1% indicated a pH range of 3.9-4.1, respectively, as shown in Table 3.5. The measurement of pH was done using a digital pH meter. As hydration progresses, the development of calcium hydroxide increases the pH of the concrete to between 12 and 13, when the phenolphthalein colour changes to purple, as mentioned by Lagerblad [65]. This was experimentally confirmed by treating the hardened concrete surface with a phenolphthalein indicator. This test was performed by cutting the concrete cylinder in half, spraying a 1% phenolphthalein solution on the concrete surface, and observing the colour change. The test was conducted on specimens of all CO_2 dosages ranging from 0% to 1% at 28 days and 90 days, and all specimens indicated a dark purple colour, as shown in Figure 3.6.

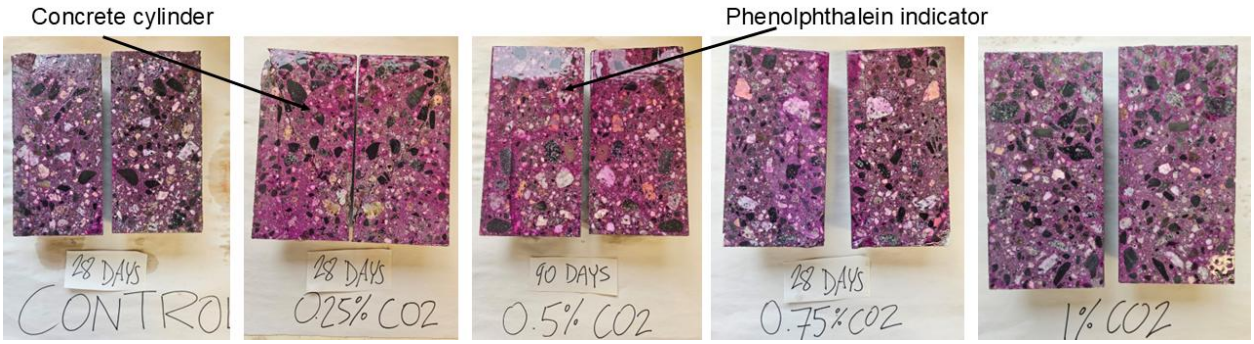

Figure 3.6 Concrete samples sprayed with phenolphthalein solution

An additional dose of the superplasticizer was added to the mixture to compensate for the reduction in workability and ensure that concrete could be properly mixed and placed into moulds. Table 3.5 shows the additional amount of superplasticizer added to the mix (% bwc). CO_2 sequestration in concrete provides enhanced mechanical properties and densification benefits. However, managing loss in workability as compared to control concrete needs further study. Although in this study, the loss of workability was resolved by adding an additional superplasticizer dosage, understanding that balancing the dosage and optimum mixing time is critical for its successful use in concrete production. In addition, a trade-off between increased strength and workability could also be explored.

3.5.2 Reaction Kinetics during early hydration of CO_2 sequestered concrete

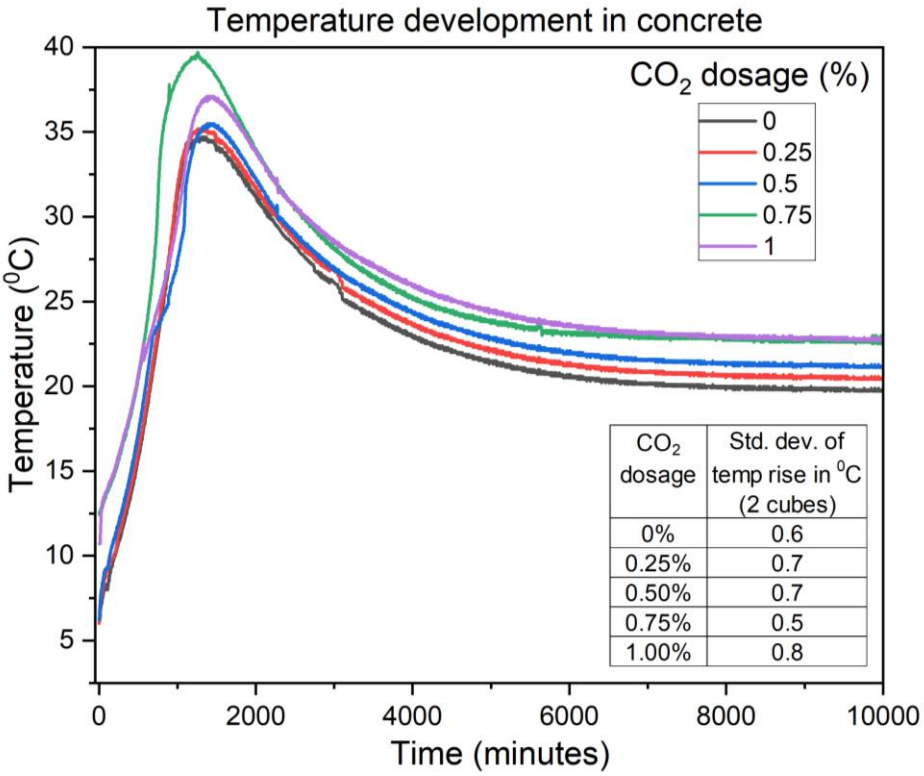

CO_2 dosage	Std. dev. of temp rise in ^{0}C (2 cubes)
0%	0.6
0.25%	0.7
0.50%	0.7
0.75%	0.5
1.00%	0.8

Figure 3.7 Representative temperature development in concrete with respect to time

A semi-adiabatic calorimeter developed in the laboratory was used to monitor the temperature rise in each mix during the early hydration of CO_2-sequestered and control concrete. This semi-adiabatic calorimeter allowed for some heat exchange with the environment during the mixing and casting process. The temperature measurement began approximately 30-45 min after adding the mixing water and continued for a duration of 7 days. Figure 3.7 is a graphical representation of temperature development in concrete with respect to time for various CO_2 dosages, including control concrete. The plots included are representative samples chosen to maintain brevity in this chapter. Of the two casted cubes for each CO_2 dosage used for temperature monitoring, data from one sample was selected for analysis, as the second sample exhibited low variance in test values. The corresponding standard deviation of the temperature of two cubes are displayed on the time-temperature curve in Figure 3.7. As shown in Figure 3.7, the control mix without CO_2 injection exhibited the lowest peak heat rate, serving as a baseline. Concrete mixes with CO_2 injections at 0.25%, 0.5%, 0.75%, and 1% showed varying degrees of hydration acceleration, reflected in higher peak temperatures. Peak heat rates for the 0.75% and 1% CO_2 mixes increased significantly and exceeded 37 °C, with the 0.75% CO_2 mix showing the greatest peak temperature. Every combination that received CO_2 injection had greater peak temperatures than the control, suggesting that CO_2 addition has an impact on hydration properties. This acceleration is explained by the creation of nanoscale calcium carbonate ($CaCO_3$), which is also reflected in an increase in the compressive strength of concrete.

Table 3.6 Effect of CO_2 dosage on thermal characteristics of concrete

CO_2 dosage	Max. temp. rise (°C)	Time to reach max temp. (min)	Area under the curve (h -°C)
Control-0%	34.7	1260	3768.60
0.25%	35.2	1261	3874.04
0.50%	35.5	1376	3957.94
0.75%	39.7	1256	4284.18
1.00%	37.1	1375	4248.36

Table 3.6 displays the maximum temperature rise, the time to reach the maximum temperature and the area under the curve, which has been calculated using Origin Pro-a data analysis and graphing software. The data reveals that 0.75% and 1.0% CO_2 dosages generally result in elevated peak temperatures, implying potentially more rapid or exothermic reactions within the concrete. Additionally, 0.75% and 1.0% CO_2 dosages indicate a higher initial rate of temperature rise increase, indicating greater initial heat release. With the exception of the 0.75% dosage, which reaches peak temperature quicker than the other dosages, there is a small variance in the amount of time required to reach peak temperature between dosages. Compared to other dosages and control concrete, the 0.75% CO_2 dosage shows a larger area under the temperature curve, indicating an increase in total heat release.

The findings suggest that CO_2 injection during mixing could be an effective technique for accelerating hydration in concrete and improving early-age strength. The observed increase in heat release and acceleration of hydration reactions, as compared to control concrete, confirms that adding CO_2 during the mixing stage of concrete results in the formation of nanoscale $CaCO_3$, which has also been verified from the microscopy and spectroscopy analysis. The study of time

vs. temperature curves highlights the influence of CO_2 addition during the mixing stage of concrete on its thermal characteristics, improvement in hydration properties and strength development.

3.5.3 Mechanical properties

3.5.3.1 Compressive strength and dry density- 25 MPa concrete

The compressive strength test results and dry density of the concrete cylinders for control concrete and CO_2-sequestered concrete for 25 MPa are shown in Figures 3.8(a) and 3.8(b), respectively. The strength values at each age are the mean of three cylinders, with the standard deviation indicated as error bars on the bar graph. The raw materials used for all the concrete mixes, which included cement, sand, aggregates, and admixtures, were from the same lot and were stored in separate bins for this test. Multiple control mix trials were conducted to check for any substantial variations in strength since the 25 MPa concrete trials for the different CO_2 dosages were cast over a period of one month. The standard deviation of the six control mixes was 1.9,3.5, and 2.3 MPa for 7, 28 and 90 days, respectively. As displayed in Figure 3.8(a), the average 7-day strength increased with CO_2 injection, particularly with 0.60% CO_2 and 0.75% CO_2, reaching 30.9 MPa. Continued improvement was observed at 28 days, with 0.75% CO_2 achieving 38.7 MPa, which was higher than the control mix. Lastly, at 90 days, mixes with 0.75% CO_2 showed higher compressive strength, reaching 40.1 MPa. The dry densities of the mixes with 0.5% CO_2 dosage and above have increased considerably as illustrated in Figure 3.8(b), as compared to the control mix. The rapid initial reaction rate, water loss from the concrete during mixing and densification of the matrix due to the formation of hydration products have led to an increase in the dry density of the mix, as observed for 0.5%, 0.6% and 0.75% CO_2 dosages.

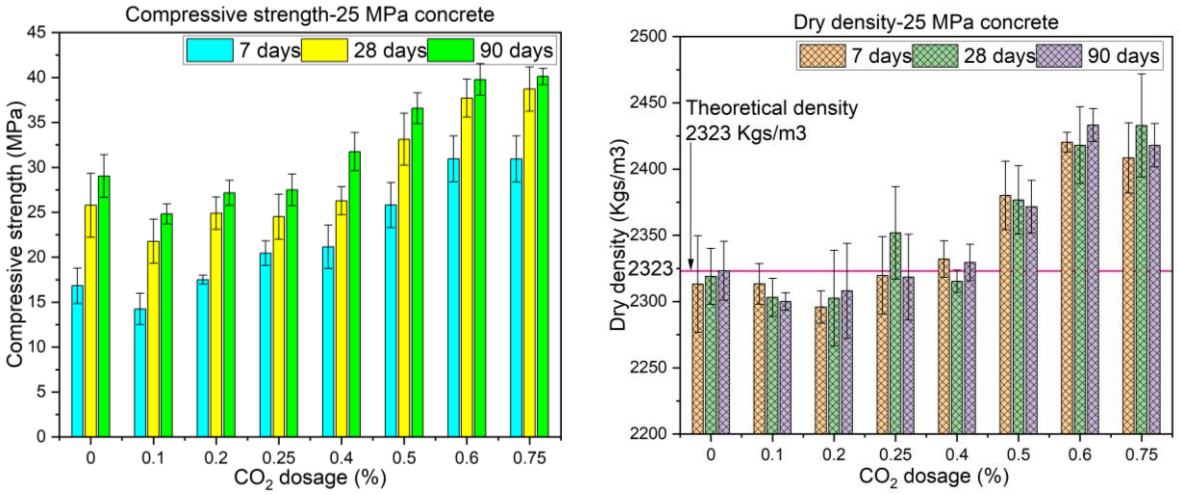

(a) (b)

Figure 3.8 (a) Average compressive strength, (b) average concrete density of 25 MPa concrete (Note: 0% (Control)-average of 6 mixes, 0.25%,0.4%,0.5%, 0.6% and 0.75%-average of 2 mixes)

3.5.3.2 Compressive strength and dry density- 40 MPa concrete

The compressive strength test and dry density results for the 40 MPa control and CO_2-sequestered concrete are shown in Figures 3.9(a) and 3.9(b), respectively. The strength values

at each age are the mean of three cylinders, with the standard deviation indicated as error bars on the bar graph. The control mix is indicated by 0% CO_2 dosage.

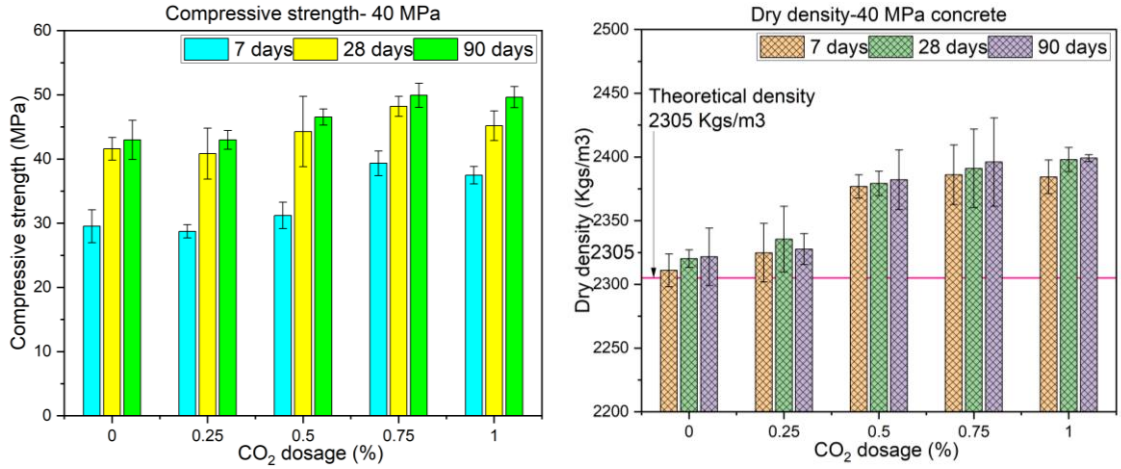

(a) (b)

Figure 3.9 (a). Average compressive strength (b) average concrete density of 40 MPa concrete

For the 40 MPa concrete, as illustrated in Figure 3.9(a), CO_2 injection showed an increase in early strength compared to the control mix at all ages, except for 0.25% CO_2 dosage. At 7 days, the mix with 0.75% and 1.0% CO_2 dosage displayed the highest compressive strengths at 39.3 MPa and 37.4 MPa, respectively. The trend continued at 28 days, with 0.5%, 0.75% and 1% CO_2-injected mixes maintaining higher compressive strengths, with 0.75% CO_2 dosage reaching 48.2 MPa. Furthermore, the CO_2-injected mixes also outperformed the control at 90 days, especially with 0.75% CO_2 dosage, achieving a compressive strength of 49.9 MPa. The density values, as illustrated in Figure 3.9(b), at each age are the mean of three cylinders used for the compression test, with the standard deviation indicated as error bars on the bar graph. The 0.5%, 0.75% and 1% CO_2 dosage mixes displayed higher densities at all curing ages as compared to control concrete. This has occurred mainly due to the mineralization and densification effect, water loss from the concrete during mixing and possibly the loss of air content from over-mixing. However, the air content of the mix measured using an air content meter did not show any significant reduction in the air content of the mix.

3.5.3.3 Modulus of rupture and split tensile strength of concrete

Figure 3.10 shows the flexural strength or modulus of rupture of concrete in relation to compressive strength for various CO_2 dosages in 40 MPa grade concrete. Similarly, Figure 3.11 presents the split tensile strength in relation to compressive strength for different CO_2 dosages in 40 MPa grade concrete. The flexural and split tensile strength values at each age are the mean of three cylinders, with the standard deviation indicated as error bars on the respective graphs. CO_2-injected mixes showed varied flexural strengths, with the 0.75% CO_2-injected mix having the highest value at 5.2 MPa. However, the control mix displayed a flexural strength of 5.0 MPa, indicating a minor improvement with CO_2 addition. The 0.5%, 0.75% and 1.0% CO_2-injected mixes also exhibited higher split tensile strengths as compared to the control and 0.25% CO_2 dosage. The 0.75% and 1.0% CO_2 injected mix achieved the highest value of 3.4 MPa compared to the control at 3.0 MPa, suggesting better tensile properties.

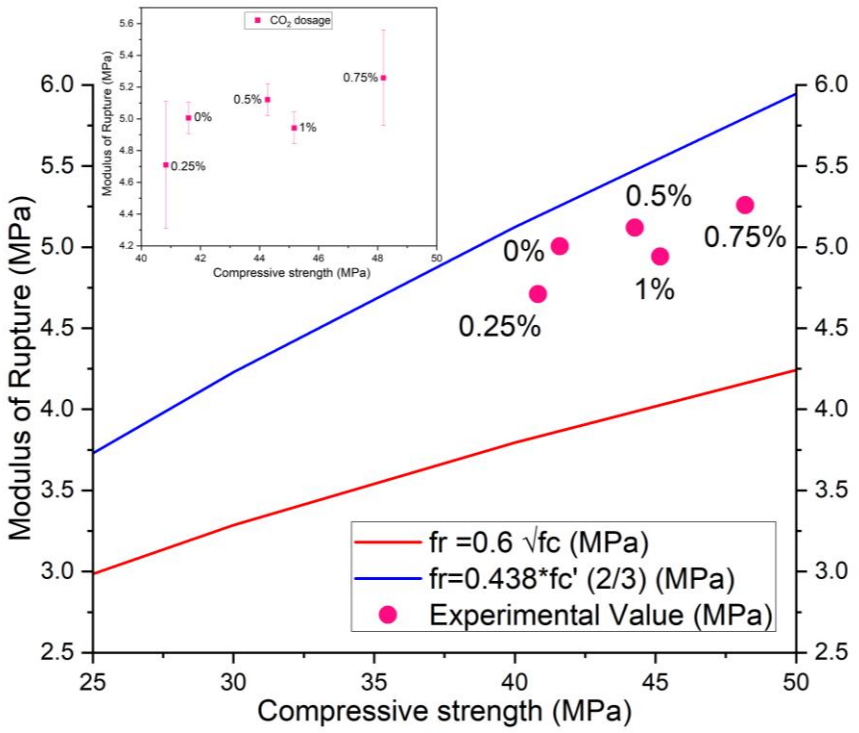

Figure 3.10 Modulus of rupture of concrete in relation to compressive strength for various CO_2 dosages

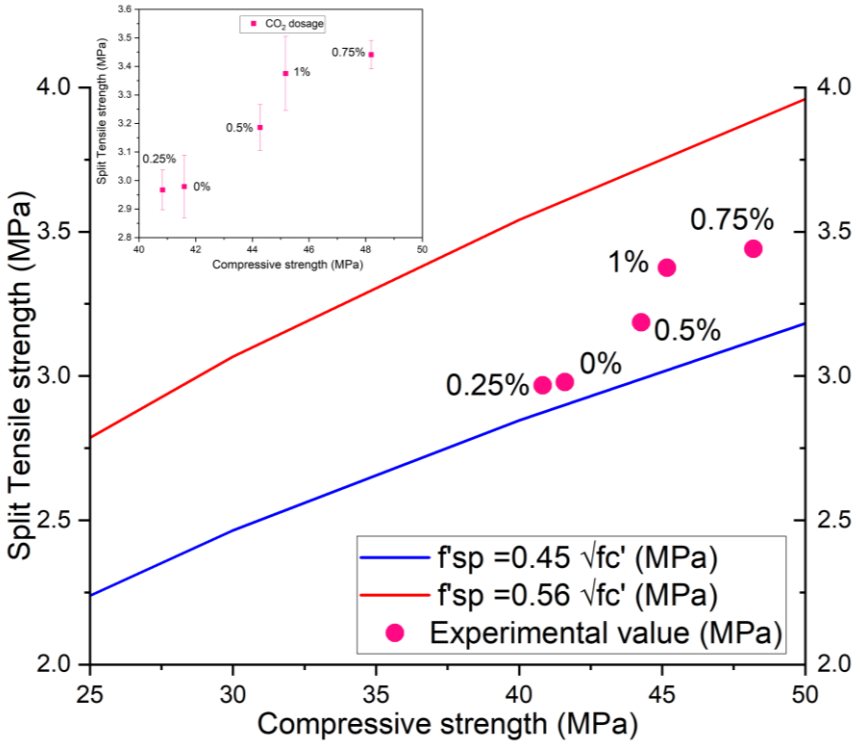

Figure 3.11 Split tensile strength of concrete in relation to compressive strength for various CO_2 dosages

These tests conclude that injecting CO_2 into concrete shows minor improvement in the modulus of rupture and split tensile strength of concrete. Monkman et al. [26] explained that this improvement is due to the formation of nanosized calcium carbonate ($CaCO_3$), which contributes to strength development. These experimental results confirm our hypothesis that CO_2 addition will improve the mechanical properties of concrete.

3.5.4 Correlation Between Flexural, Split Tensile, and Compressive Strength in CO_2 Sequestered Concrete

The correlations between the split tensile strength, modulus of rupture (flexural strength), and compressive strength of CO_2-sequestered concrete were examined using correlation analysis. The empirical models for the split tensile strength and modulus of rupture of concrete proposed by ACI 318-19(22) [105], Lee and Lee [106], and Mindess et al. [107] are summarized in Table 3.7, which was used to compare the projected values with the experimental results, as shown in Figures 3.10 and 3.11.

Table 3.7 Predictive equations for the Modulus of rupture and split tensile strength of concrete

Concrete property	Equation	Reference
Modulus of rupture (MPa)	$fr=0.6 * \sqrt{fc'}$	ACI-318-19(22) [105]
	$fr=0.438 * fc'^{(2/3)}$	Mindess et al. [107]
Split tensile strength (MPa)	$fr=0.45 * \sqrt{fc'}$	Lee and Lee [106]
	$fr=0.56 * \sqrt{fc'}$	ACI-318-19(22) [105]

Table 3.8 Correlation coefficients matrix

	Compressive strength	Flexural strength	Split tensile strength
Compressive strength	1.00		
Flexural strength	0.81	1.00	
Split tensile strength	0.96	0.65	1.00

The following relationships have been interpreted by referring to the article by Schober et al. [108].

a) Compressive Strength vs. Flexural Strength: Strong positive correlation (0.81).
b) Compressive Strength vs. Split Tensile Strength: Very strong positive correlation (0.96).
c) Flexural Strength vs. Split Tensile Strength: Moderate to strong positive correlation (0.65).

The correlation coefficients between compressive strength and flexural strength, compressive strength and split tensile strength, and flexural strength and split tensile strength were calculated using the data analysis tool in Microsoft Excel. The correlation coefficients matrix is provided in Table 3.8. The compressive strength, flexural strength, and split tensile strength in CO_2-sequestered concrete are shown to be positively correlated by these correlations mentioned above, with compressive strength and split tensile strength having the strongest association at 0.96. The experimental data also falls between the predicted values as per the empirical models by ACI 318-19(22), Lee and Lee, and Mindess et al. confirming the relationship. The experimental results and the correlational analysis demonstrate that the flexural and split tensile strength of concrete with CO_2 addition displays a comparable strength with a marginal improvement compared to a control mix.

3.5.5 Multiple Linear Regression Model for Predicting Compressive Strength of CO_2-Sequestered concrete

A multiple linear regression model was developed using the experimental data to predict the compressive strength of CO_2-sequestered concrete. This model considers CO_2 dosage and cement content as independent variables. The regression model was created using data from 23 distinct sets of samples, each consisting of the average of three cylinders with a varied CO_2 dosage. The maximum CO_2 dosage, by weight of cement, considered for this model is 1%. Microsoft Excel data analysis tool for regression was used to fit the regression model.

The multiple linear regression model can be expressed as shown in equation 15.

Compressive Strength (28 days) = Intercept + Coefficient (X1)× CO_2 Dosage + Coefficient (X2)× Cement Content + Coefficient (X3)× w/c ratio+ ϵ (15)

Where,

- CO_2 Dosage- Percentage of CO_2 injected into the concrete mix, expressed as a ratio by weight of cement
- Cement Content (C) -Amount of cement in the mix (kg/m³)
- w/c ratio- water-cement ratio in the mix
- X1, X2, X3 -Regression coefficients for CO_2 dosage, cement content and w/c, respectively
- ϵ\epsilon - Error term

Table 3.9 Summary of Regression Statistics

Regression Statistics	
Multiple R	0.92
R Square	0.84
Adjusted R Square	0.77
Standard Error	3.45
Observations	23

Table 3.10 Coefficients and Model Parameters for Compressive Strength Prediction

	Coefficients	Standard Error	P-value	Lower 95%	Upper 95%
Intercept	-10.81	5.71	0.07	-22.73	1.11
Dosage	14.10	2.50	0.00	8.88	19.31
Cement	0.12	0.02	0.00	0.08	0.16
W/C	0.00	0.00		0.00	0.00

Based on the coefficients provided in the regression analysis, as summarized in Tables 3.9 and 3.10, the multiple linear regression model has been formulated as shown in equation 16.

Compressive strength 28 days (MPa) = (−10.81) + (14.10× CO_2) + (0.12×C) + (0×W/C) + (±3.45) (16)

As shown in Tables 3.9 and 3.10, the model was fitted using least squares regression, and statistical measures, including R-squared, adjusted R-squared, and the p-values of the coefficients, were used to validate the performance of this model. As indicated by the Multiple R-values of 0.92, there is a positive relationship between the observed and anticipated values of the dependent variables. Furthermore, the model accounts for 84% of the variability in compressive strength, as indicated by the R-squared value of 0.84. A linear relationship was observed between the dependent and independent variables, and statistical significance was observed when the P-values for the coefficients were all less than 0.05. The water-to-cement ratio had a zero unstandardized coefficient, indicating that this independent variable had no bearing on the dependent one. This implies that it may be very collinear with other variables in the model and is statistically insignificant. The low standard error of ±3.45 indicates a low average distance that the observed values fall from the regression line. This model has also been validated by comparing the predicted compressive strength values with the experimentally measured values by other researchers, summarized in Table 3.11.

Table 3.11 Comparison of predicted compressive strength and experimental values from recent studies

Cement	CO_2 dosage	w/c	28 days Compressive strength (MPa)		
kg/m^3	% bwc		Experimental data	Reference	Regression Model
350	0.1	0.46	35.8	[109]	32.6 ± 3.45
300	0.05	0.42	27.6	[110]	25.8 ± 3.45
400	0.15	0.45	36.8	[111]	39.3 ± 3.45
400	0.2	0.45	35.0	[111]	40.0 ± 3.45

This regression model may be used as a tool for the preliminary design of concrete mixes mixed with CO_2 in dosages ranging from 0% to 1% by the weight of cement. The model adopts PLC and is applicable to a range of water-cement (w/c) ratios between 0.4 and 0.5. It predicts the compressive strength of CO_2-sequestered concrete and can be used by concrete technologists to design mixes using CO_2 for environmental sustainability.

3.5.6 Thermal Pyrolysis

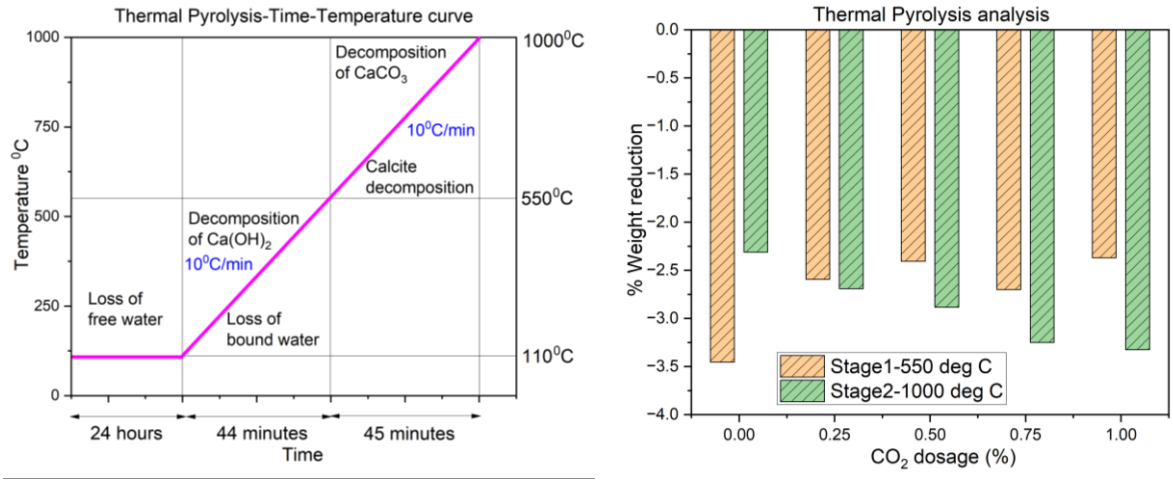

(a) (b)

Figure 3.12 (a). Time-Temperature curve of the Thermal Pyrolysis test, (b) Percentage weight loss at 550 °C and 1000 °C for concrete samples from the Thermal Pyrolysis test

Figure 3.12 (a) represents the time-temperature curve for the thermal pyrolysis test. Additionally, the percentage weight loss at 550 °C and 1000 °C from the thermal pyrolysis test of the five concrete samples are summarized in Figure 3.12 (b). Substantial mass reductions were seen in Stage 1 (550 °C) due to the dehydration and dehydroxylation processes. The percentage reductions ranged from 2.37% (for 1.0% CO_2) to 3.45% (Control), indicating the decomposition of $Ca(OH)_2$. The mass reduction was lower for CO_2-sequestered concrete, as carbonation results in the consumption of $Ca(OH)_2$ content to form $CaCO_3$, as explained by Wang et al. [63]. In Stage 2 (1000 °C), further mass reductions were noted, particularly in samples with higher CO_2 concentrations (0.75% and 1%). The percentage reductions ranged from 2.31% (Control) to 3.93% (1% CO_2), indicating the decomposition of calcite. The control concrete sample indicated a CO_2 absorption of 2.31% even without CO_2 sequestration. This may have come through the residual CO_2 in the raw materials used and exposure to the atmosphere during the handling, mixing, curing, and sample preparation processes. Suescum-Morales et al. [112] and Wang et al. [113] observed that CO_2 uptake could reach between 2% to 3.5% in their experiments, which also matches the findings from this test. The authors of this paper acknowledge the potential limitations of the thermal pyrolysis method due to the dilution effect of aggregates present in concrete. Nevertheless, this method remains one of the simplest approaches to evaluate CO_2 uptake in concrete, especially in concrete samples where separating aggregates is impractical and where a thermogravimetric analyzer is not available. The findings present an understanding of these limitations, and future studies may focus on using some advanced techniques to assess CO_2 uptake concretely.

3.5.7 Microstructural analysis

To assess microstructural changes in CO_2-sequestred concrete, a comparative study of control and CO_2-sequestered concrete was carried out using SEM and EDX to find variations in morphology and elemental composition. The SEM images of control concrete, displayed in Figures 3.13(a) and (b), show a poorly crystalline structure, namely C-S-H gel. Figures 3.14(a) and (b) show an amorphous and poorly crystalline structure of C-S-H gel for the CO_2-sequestered concrete sample. The morphological features of $CaCO_3$ could not be clearly identified and differentiated from the crystalline structure of C-S-H in both the control concrete and CO_2-sequestered concrete images. The EDX spectra were used to identify the presence of carbon and, thereby, $CaCO_3$, considering the limitations in distinguishing the morphological features through the SEM images.

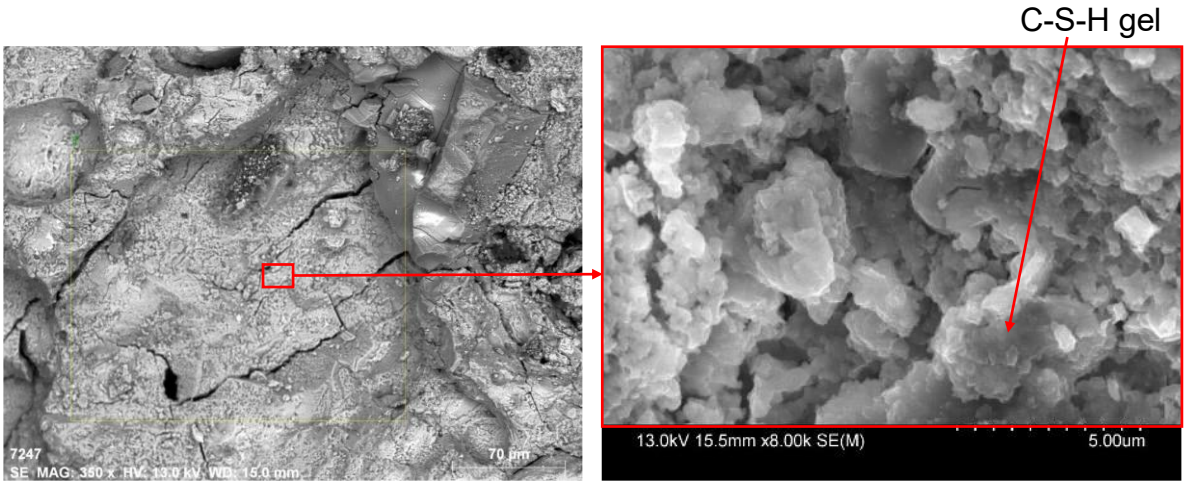

Figure 3.13 (a) and (b) SEM images of control concrete showing a poorly crystalline C-S-H gel structure

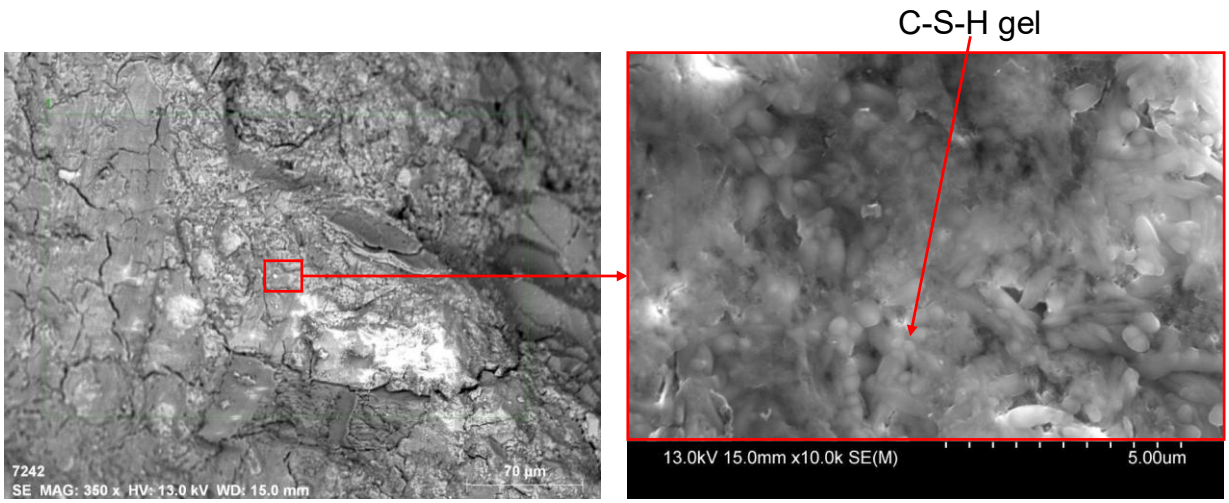

Figure 3.14 (a) and (b) SEM images of CO_2-sequestered concrete showing an amorphous and poorly crystalline structure of C-S-H gel

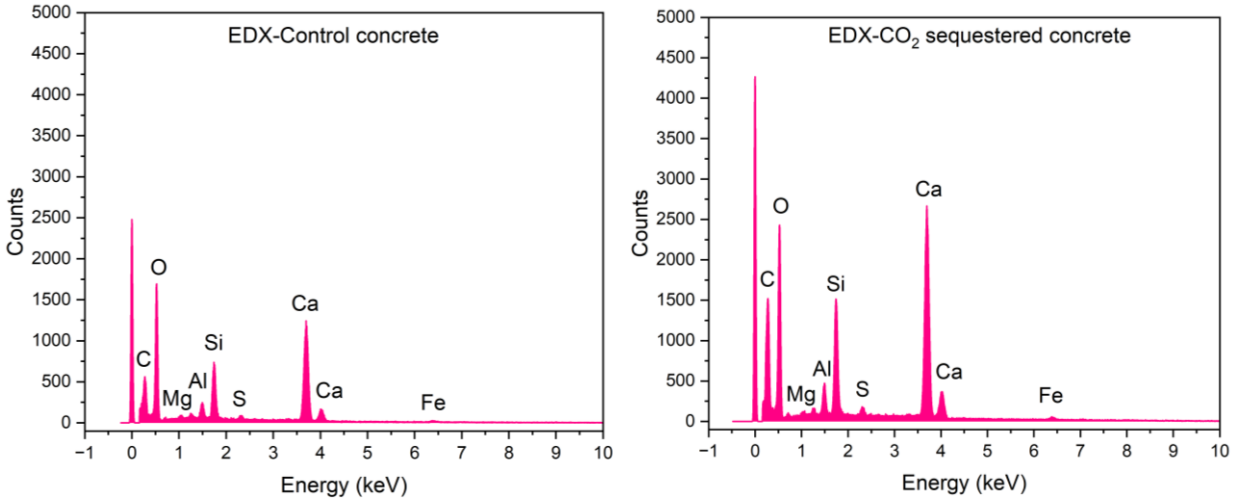

Figure 3.15 (a) EDX spectrum of control concrete sample showing higher calcium and oxygen, (b) EDX spectrum of CO_2-sequestered concrete sample showing enhanced carbon along with calcium and oxygen

The EDX spectra of the control and CO_2-sequestered samples are shown in Figures 3.15(a) and 3.15(b), respectively. A sizable amount of calcium and oxygen in the control specimen suggests the presence of $Ca(OH)_2$. Additionally, silica and aluminum indicate the presence of C-S-H and calcium aluminosilicate phases. A small amount of carbon suggests that the sample may have been exposed to the CO_2 from the surrounding environment during sample preparation. The EDX spectra of the CO_2-sequestered sample, illustrated in Figure 3.15(b), show a substantial presence of carbon, calcium, oxygen, and silica. This indicates the presence of C-S-H, $Ca(OH)_2$ and $CaCO_3$. Based on the comparative SEM and EDX examination of control and CO_2-sequestered concrete, it is clear that CO_2 sequestration substantially impacts the microstructural properties and elemental composition of concrete, mainly due to the formation of $CaCO_3$.

3.5.8 FTIR Spectroscopy

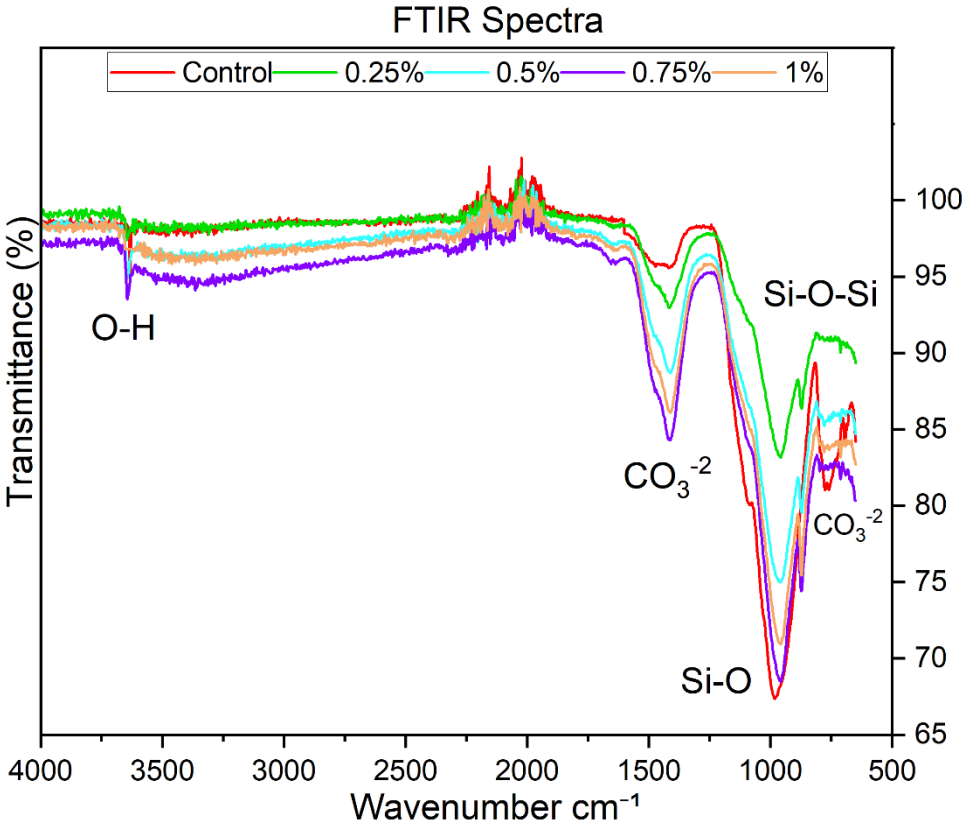

Figure 3.16 FTIR spectra of control and CO_2 sequestered concrete samples

As shown in Figure 3.16, the FTIR spectra of the CO_2-sequestered concrete samples showed absorption peaks around 1400 cm^{-1} and 870 cm^{-1} corresponding to out-of-plane bending vibrations of carbonate ions, which were more distinct as compared to the control concrete sample, indicating enhanced carbonate formation due to CO_2 sequestration. The control concrete sample indicated a slight out-of-plane bending between 1400 and 870 cm^{-1}, which may have resulted from the absorption of CO_2 from the air during sample preparation. The silicate-related Si-O-Si stretching bands around 950 cm^{-1} confirm the presence of C-S-H in all CO_2 mixes, suggesting that the hydration reactions occur normally even with CO_2 addition. Compared to control concrete, the intensity of OH^- related bands in CO_2-sequestered concrete decreased by around 3644 cm^{-1}. Although it has not been completely reduced, it is important for early-age carbonation reactions to take place. At the same time, its presence is necessary to maintain the high pH of concrete and improve its resistance to corrosion. The FTIR spectra shows higher carbonate (CO_3^{2-}) peaks around 1400 cm^{-1} and 870 cm^{-1} in the 0.75% and 1% CO_2 sequestered concrete samples, indicating a higher degree of carbonation compared to the control concrete sample. The 1% dosage displays slightly less absorption in the carbonate region compared to 0.75%. The authors hypothesize that this may be possibly due to saturation effects limiting the CO_2 reaction inside the concrete mix. Identifying the functional groups of $CaCO_3$, C-S-H, and $Ca(OH)_2$ from FTIR spectroscopy helps confirm the hydration reactions and microstructural changes taking place in CO_2-sequestered concrete.

3.6 Concluding Remarks

The aim of this study was to understand the impact of adding CO_2 during the mixing stage of concrete on its plastic, mechanical and microstructural properties. For the experimental analysis, two grades of concrete, 25 MPa and 40 MPa, were analyzed using PLC, natural aggregates and chemical admixtures. A simple CO_2 dosing system was set up, and comprehensive mechanical testing was conducted for 90 days to study the impact of CO_2 on plastic and mechanical properties and changes taking place at a microstructural level.

Within the scope of this research, the following conclusions can be drawn from this study:

- The addition of CO_2 to concrete reduced its workability and slump for dosages above 0.5%. This may be due to an increase in the heat of hydration resulting from a chemical process and longer mixing times during CO_2 addition. In order to maintain the desired workability of concrete, redosing of the superplasticizer was required, which added to the cost of the mix. In addition, a shorter CO_2 dosing and remixing time would have been beneficial.
- The semi-adiabatic calorimetry test results showed improved hydration with CO_2 addition, with a peak temperature rise observed at 0.75% CO_2 dosage.
- CO_2 injection led to higher compressive strength, especially for the 0.75% dosage, with minor improvements observed in the flexural and split tensile strength of CO_2-sequestered concrete.
- Thermal Pyrolysis test, microscopy and FTIR spectroscopy analysis indicated the formation of $CaCO_3$, mainly due to accelerated carbonation reactions.

The authors of this chapter hypothesize that the slight reduction in strength and carbonate formation in the 1% CO_2 mix compared to 0.75% may be attributed to an increased effective w/c ratio due to superplasticizer dosage which contains 30-40% solids and balance water. In addition CO_2 diffusion into the inner matrix due to early age pore clogging may have led to lower total carbonation. This emphasizes the importance of optimizing CO_2 dosage to enhance carbonation without compromising on concrete quality. Additionally, the lower compressive strength observed in the 0.25% CO_2 dosage mix may be attributed to partial carbonation. At this low dosage, the amount of injected CO_2 may have led to surface-level carbonation only, leaving the core of the matrix unreacted. This results in a weaker pore structure with limited densification benefits compared to higher CO_2 dosages (0.5%, 0.75%, and 1%).

Contributions from this study include a simplified CO_2 sequestration process and a predictive model developed to estimate the compressive strength of concrete, which a concrete manufacturer may use as a starting point to develop a CO_2-sequestered concrete mix. By sequestering CO_2 in concrete and permanently trapping this greenhouse gas, concrete manufacturers can promote a low-carbon construction material. With the global production of approximately 15 billion cubic metres of concrete annually [19], sequestering CO_2 in concrete presents a promising approach to reducing the construction industry's carbon footprint and advancing the goal of a net-zero emissions future.

The following limitations of this work should be noted:

- This study used pure CO_2 gas available in the market and not effluent CO_2 gas captured through carbon capture technologies.
- During the experiments, CO_2 gas was injected into the mix at a dosage ranging from 0.1% to 1% by weight of cement. However, the exact amount of CO_2 sequestered in concrete and the gas lost in the injection process could not be quantified.
- This study involved the addition of a small quantity of CO_2 into concrete, a maximum of 1% by weight of cement. Higher dosages had adverse effects on workability and strength.
- PLC was used in the study, as other types of cement were not readily available. The effect of different types of cement and cementitious materials, as well as a broad range of humidity and temperatures, was not explored.

This study does not focus on large-scale deployment of CO_2-sequestered concrete in the field, including material and equipment cost, equipment and batching plant modifications and operational challenges.

Recommendations for Future Work:

- Studies should explore methods to resolve workability issues resulting from CO_2 addition without increasing the cost per cubic meter of concrete.
- The effect of CO_2 addition on the different cement types and other cementitious materials available needs further experimental investigation.
- Further research is required to study the effect of CO_2 captured from industrial emissions.
- Long-term durability tests under various exposure conditions and lifecycle assessments need to be studied.
- Advanced analytical instruments and software tools can used for future research to assess carbon uptake in CO_2 sequestered concrete and quantification of losses during the injection process.

In conclusion, this experimental study has shown that CO_2 sequestration improves the mechanical properties of concrete and densifies its microstructure.

Chapter 4 : Effect of CO_2 Sequestration on Long-term Concrete Performance and Durability

Clinton Pereira [1,2,3,4] and Rishi Gupta [1,2,3,5]
[1] Department of Civil Engineering, University of Victoria (UVic), Canada.
[2] Facility for Innovative Materials and Infrastructure Monitoring (FIMIM) UVic, Canada.
[3] Centre for Advanced Materials and Related Technology (CAMTEC) UVic, Canada.
[4] clintonpereira@uvic.ca
[5] guptar@uvic.ca

This chapter has been adapted from a research paper that has been submitted to a journal and is currently under review. This paper is the outcome of a detailed investigation of the long-term effect of CO_2 sequestration on the performance and durability of concrete. This paper evaluates the impact of varying CO_2 dosage, introduced during the mixing stage of concrete, on the transport properties, resistance to freezing and thawing conditions and the corrosion resistance of embedded rebars subjected to alternative wetting and drying cycles under harsh environmental conditions. The study also adopts an existing model to predict the enhancement in the service life of CO_2-sequestered concrete over control concrete and assess its effectiveness.

4.1 Abstract

As global greenhouse gas emissions have increased, all industries have been exploring green and sustainable materials and technologies. Studies have shown that adding CO_2 to concrete while it is mixed improves its hardened properties. This experimental approach aims to understand the impact of adding CO_2 during the mixing stage on the transport properties, freeze-thaw (F-T) resistance and corrosion resistance of embedded rebars. Key parameters like water permeability, rapid chloride ion penetration, resistivity, dynamic modulus, corrosion potential and rate were measured to assess the long-term durability. For CO_2 dosages ranging from 0.25% to 1% by weight of cement, a 50-90% reduction in the permeability coefficient, a 25-40% decrease in chloride ion penetration values, and a 10-20% increase in resistivity were observed, in comparison to control. Additionally, CO_2 dosages between 0.5%-0.75% showed improved resistance to F-T cycles, as observed by lower mass loss, less surface scaling, and increased stiffness. ANOVA results and flattening P-curves between 0.5%-0.75% confirm that these CO_2 dosages would provide optimum resistance to F-T cycles. Concrete slab panels subjected to alternative wetting and drying cycles at elevated temperatures and salt-free environments showed improved corrosion resistance at CO_2 dosages between 0.5% and 0.75%. However, similar resistance could not be obtained in saline conditions, highlighting the need for supplementary protection to mitigate corrosion. This study also applies Tuutti's model to predict the service life of reinforced concrete to assess the effectiveness of CO_2 sequestration.

Keywords: CO_2 Sequestration, Accelerated carbonation, Dynamic modulus, Corrosion resistance, Service life, Corrosion rate, Corrosion potential.

4.2 Introduction

Global temperatures have risen due to increased heat-trapping greenhouse gases (GHGs) in the atmosphere brought on by the overuse of natural resources, burning of fossil fuels, and deforestation [55]. The most critical anthropogenic contributor to GHGs is CO_2, which is produced in massive quantities [16]. It is a need of the hour to find a long-term solution to minimize the impact of CO_2 emissions on our environment globally [114]. All sectors are working towards minimizing their carbon footprint, and the construction industry has also been adopting ways to decarbonize and sequester CO_2 during the life cycle of structures [19]. Adding CO_2 during the mixing or curing stage of concrete have shown to improve certain properties [11—14]. However, as the natural carbonation process has led to carbonation-induced corrosion, doubts remain regarding the long-term durability of CO_2-sequestered concrete [115]. The extensive use of CO_2 sequestration in concrete by the construction industry is currently limited due to a lack of regulatory and codal approvals, insufficient field application data, and concerns about carbonation-induced corrosion in reinforced concrete structures. Although several studies have explored the plastic, mechanical and microstructural properties of CO_2-sequestered concrete, minimal research has been conducted to understand the effects of accelerated carbonation on concrete subjected to varying environmental conditions. Understanding these long-term effects has been the primary motivation for this study.

This experimental study compares the impact of varying CO_2 dosages on the freeze-thaw resistance of concrete. It also studies its impact on the corrosion resistance of rebars in concrete when subjected to alternate wetting and drying cycles, with and without salts. This study experimentally evaluates the long-term effects of CO_2 sequestration in concrete by measuring pH levels, water permeability, rapid chloride penetration, resistivity, dynamic modulus, corrosion rate and corrosion potential of concrete under varying environmental conditions. The conclusions from this study will offer important guidance on implementing this technology without sacrificing the sustainability and structural soundness of concrete structures.

4.3 Literature Review

Researchers have highlighted that natural carbonation is a process by which concrete absorbs atmospheric CO_2 [15, 60, 107, 116, 117]. Marani et al. [118] explain that during this process, CO_2 enters the body of concrete through cracks and a network of interconnecting voids, drops the pH of the pore solution and destroys the passive protective layer leading to corrosion of the embedded rebars. Angst [40] describes that calcium hydroxide ($Ca(OH)_2$) formed in hydrated Portland cement pastes keeps the pH of concrete around 12.6, and the passive layer on the steel surface remains stable. When atmospheric CO_2 penetrates into concrete, calcium ions from hydrated cement paste react with aqueous CO_2 to form calcium carbonate ($CaCO_3$), as explained by Auroy et al. [12]. The pH of the pore solution can drop to around 9.0 when $Ca(OH)_2$ starts to reduce [117]. This is less than the de-passivation threshold of rebars which is around 9.5, as explained by Savija et al. [60], making the steel rebar vulnerable to corrosion. The corrosion process accelerates due to the presence of moisture and oxygen, which enter into the body of concrete through the network of cracks and interconnecting pores, which eventually lowers the life of the reinforced concrete structures [119]. Although the formation of $CaCO_3$ densifies the concrete microstructure, it generates additional crystal pressure on the concrete structure, as

detailed by Savija et al. [60], which leads to micro-cracks in the interfacial transition zone (ITZ). Because of this, concrete is generally designed for low permeability and fewer cracks to stop the entry of CO_2 into its microstructure and prevent carbonation-induced corrosion [61]. Alternatively, studies by Kamal et al. [13], Rostami et al. [46], Lagerblad [65], Shao [21], and Monkman et al. [27] have found that the strength and durability of concrete is increased when CO_2 is added during the mixing or curing process. Even though studies have demonstrated that CO_2 can be utilized to improve the properties of concrete, before implementing CO_2 sequestration as a sustainable building method, it is crucial to understand how it affects the long-term performance of concrete. To understand the long-term advantages and challenges of CO_2 sequestration in concrete, this literature review objectively examines transport characteristics, pH levels, freeze-thaw behaviour, and corrosion of steel in concrete based on prior studies.

4.3.1 Transport Properties of Concrete

Classie [120], highlights that the transport properties of concrete determine its long-term durability. Concrete microstructure generally comprises of the solid, liquid, and vapour phases [121]. As detailed by Azarsa and Gupta [122], as the liquid phase contains pore water, the resistivity of this phase can be as low as 10 Ω-m. The authors also highlight that the solid phase, comprising of aggregates and hydrated cement paste, exhibits high electrical resistivity as high as 10^6 Ω-m. According to Li et al. [123], these properties govern the movement of water, CO_2 and salts of chlorides and sulphates and other deleterious material within the concrete mass, which eventually plays a crucial role in corrosion and cracking. Studies by Garboczi [124], Li et al. [125], Julio-Betancourt et al. [126], Feldman et al. [127], Spragg et al. [128], and Ramezanianpour et al. [129] have shown that minimizing surface cracks, reducing porosity and permeability, enhancing resistivity, minimizing chloride ion penetration and limiting sulphate attack, in addition to high strength, can improve the longevity and service life of reinforced concrete structures. Studies by Gupta [130] and Kamal et al. [131] have found that accelerated carbonation densifies the concrete matrix and reduces permeability, while Elkhaldi et al. [132] observed lower electrical resistivity. Additionally a decrease in porosity of concrete was observed by Gil et al. [133] and Kazemian et al. [37] in concrete subjected to early-age carbonation. Although several studies have been conducted on the transport properties of CO_2-sequestered concrete, there is still a research gap on the impact of these properties on the long-term durability of concrete under varying environmental conditions. The impact of reduction in porosity, permeability and increased resistivity on freeze-thaw resistance of concrete also remains unexplored.

4.3.2 Freeze-Thaw Resistance of Concrete

Extensive research has been done to date to understand the resilience of concrete to Freeze-Thaw (F-T) cycles. According to Zhao et al. [134] and Cai and Liu [135], F-T damage of concrete takes place due to the freezing and thawing of water trapped within the pore structure of concrete. As per ACI Committee, 201.2R-16 [136], using air-entraining agents improves the F-T resistance of concrete by allowing the freezing water inside it a space to expand. According to Auroy et al. [12] and Monkman et al. [27], when concrete is sequestered with CO_2, the carbonation reactions decrease the porosity of concrete, which in turn reduces the freezable water in the pores and eventually minimizes the pressure build-up from inside. On the other hand, Kamal et al. [13] and Savija et al. [60] point out that the carbonation process might reduce porosity, which leaves

concrete vulnerable to F-T damage. The impact of adding CO_2 to concrete during the mixing stage on its F-T resistance needs to be better understood experimentally in order to answer the concerns expressed by some researchers.

4.3.3 pH of concrete

According to Fajardo et al. [137] and Shaheen and Pradhan [138] the passive layer formed on the surface of rebars remains stable due to the highly alkaline environment of concrete, and protects the steel bars against corrosion. The pore solution in concrete is usually between 12.5 to 13.5, as referenced in the research by Silva [139]. Concrete starts losing its alkalinity when $Ca(OH)_2$ starts reducing while getting converted to $CaCO_3$ during carbonation [117]. According to Savija et al. [60], the consumption of $Ca(OH)_2$ lowers its pH, which slowly removes the protective layer on the steel reinforcement and increases the likelihood of corrosion. Scholars like Guo et al. [140] and Steffens et al. [141] support the argument that this pH reduction can seriously jeopardize the durability of reinforced concrete. Conversely, Chi et al. [142] highlight that the concrete matrix becomes denser due to the formation of $CaCO_3$, which improves mechanical properties, decreases porosity and enhances durability. The contradictory conclusions by some researchers set the ground for additional work required to determine the impact of adding CO_2 during the mixing stage of concrete on its pH levels and understand its effects in protecting the steel reinforcement from carbonation-induced corrosion.

4.3.4 Corrosion of steel in concrete

Since steel reinforcement is used in most concrete constructions, Talukdar and Banthia [143] highlight the importance of understanding the effect of carbonation on steel rebars to assess the long-term durability and service life of reinforced concrete structures. Chlorides can break down the passive protective layer on the steel surface even at high pH, and the combination of carbonation and chloride penetration can accelerate corrosion [144]. Research by Gupta [130], Guo et al. [140], and Kamal et al. [131] has highlighted that when CO_2 is added to concrete during the mixing stage, the microstructure of concrete is densified, and durability is increased; however, their study does not analyze its impact on the corrosion of rebars. Furthermore, limited research has been done to study the impact of elevated temperatures and salt solution on embedded rebars in CO_2-sequestered concrete. To address this gap, this study has conducted a few expedited tests with harsh environmental conditions.

This overview of the literature review aligns with this experimental study on the long-term effects of CO_2 sequestration in concrete. Studies by several researchers have indicated that adding CO_2 to concrete during the mixing stage has provided benefits and some challenges. However, due to insufficient experimental data on the long-term effects of CO_2 sequestration in concrete, the construction industry is skeptical of the implementation of this technology. To fill in these gaps on this subject and assess the impact of early-age carbonation on long-term durability, this study first analyzes the impact of adding CO_2 during the mixing stage on the transport properties of concrete and the impact of densification on the concrete microstructure. It further studies its resistance to deterioration when subjected to 300 F-T cycles, with an aim to identify the effect of early-age carbonation on the frost action of concrete. Lastly, it aims to understand the effect of CO_2 addition on the resistance of concrete to carbonation and chloride-induced corrosion when subjected to harsh environmental conditions of alternative wetting and drying cycles at elevated temperatures,

with and without the presence of corrosive salts. By expanding on the work from previous researchers and filling some of the knowledge gaps, this experimental work aims to provide the concrete industry with helpful information which can be used for implementing CO_2 sequestration in concrete during the mixing stage.

4.4 Methodology

4.4.1. Raw materials and Concrete mix design

Portland Limestone Cement (PLC), conforming to the CSA A3001-03 GUL (General Use Limestone) standard [145] or ASTM C595 for Type IL [146] (PLC with up to 15% limestone content) was used. Natural sand and crushed granite locally sourced and meeting ASTM C33/C33M-18 [88] specifications were used. A superplasticizer meeting with Type F requirements of ASTM C494/C494M-19 [147] and an air-entraining admixture (AEA) meeting ASTM C260-10 [91] standards were utilized.

Table 4.1 Concrete mix design

Concrete Ingredients	Grade 40 MPa
Cement (kg/m^3)	400
Water (kg/m^3)	160
water/cement ratio	0.4
Fine aggregate (kg/m^3)	712
Coarse aggregate (9.5 mm) (kg/m^3)	464
Coarse aggregate (19 mm) (kg/m^3)	567
Superplasticizer (% bwc)	0.3
Air Entraining Admixture (% bwc)	0.3
Theoretical bulk density (kg/m^3)	2305

A 40 MPa concrete mix was designed following the ACI PRC-211.1-91 [93] guidelines for proportioning normal, heavyweight, and mass concrete. The mix was designed to meet C2, S2, and A2 class exposure conditions according to the Canadian Standards Association (CSA A23.1:24) [148]. Detailed mix proportions for the 40 MPa concrete are provided in Table 4.1. Sample preparation adhered to ASTM C192/C192M-19 [95] procedures using a tilting drum mechanical mixer. Dry ingredients were mixed for 2 min, followed by 3 min of wet mixing. Superplasticizer and AEA were added to the mixing water. For CO_2-sequestered concrete, CO_2 was injected after the initial wet mixing phase, with controlled flow in cubic feet per hour (CFH) and duration in minutes, using the flowmeter connected to the CO_2 cylinder. To introduce the desired percentage of CO_2 mass per cubic meter by the weight of cement, ranging from 0.25% to 1%, an additional dosing and mixing time ranged from 2 to 6 min. This was achieved by controlling the flow rate and injection time to ensure proper dosing and uniform distribution of CO_2 within the concrete.

As explained by Lagerblad [65], $Ca(OH)_2$ from the hydrating cement reacts directly with CO_2, leading to the formation of $CaCO_3$. The author highlights that water is needed in its transformation, which results in a drop in the workability of the concrete mix. To counteract the slump reduction due to CO_2 exposure, an additional dose of superplasticizer, ranging from 0.1-0.3% by weight of

cement (bwc), was added to maintain a slump of 125-150 mm during casting, with an additional one minute of mixing time. This additional CO_2 dosing and mixing time may have been one of the reasons for the reduction in the workability of concrete observed in the CO_2-sequestered concrete mixes. Lab conditions were at 15 ± 5 °C and 65 ± 5% relative humidity during the mixing and casting process. After 24 h of casting, the samples were cured in a tank at 23 ± 2 °C until testing. Compressive strength testing was conducted at 7, 28, and 90 days in accordance with ASTM C39-21 [101]. The tests utilized a compression testing machine with a 2000 kN load capacity, applying the load at a stress rate of 0.25 MPa/s ± 0.05 MPa/s.

Details about the CO_2 sequestration process, plastic and mechanical properties, and microstructural investigation, focusing on the hydration, structure, and strength of CO_2-sequestered concrete, can be found in Chapter 3 of this thesis [54].

4.4.2 Transport Properties of Concrete

4.4.2.1 Surface Electrical Resistivity Test

According to AASHTO 358-19 [149], the surface electrical resistivity test uses the four-probe (Wenner-Array) approach to measure the resistivity on the concrete surface. As shown in Figure 4.1(a), this test was conducted on the surface of a cylindrical specimen measuring 100 x 200 mm at 28 days. The test procedure, as explained in AASHTO 358-19, was followed. The specimens were kept submerged in water maintained at 23 ± 2 °C before the test and tested under SSD conditions after 28 days of casting. This instrument measured resistivity along the curved face of the cylindrical concrete specimen using four channels of a 4-probe array, positioned at 90° intervals from each other [150]. As per the manufacturer, it records the resistivity based on an average of eight sets of measurements. The measuring device, built with a data acquisition system (DAQ), passes a current between the outer two electrodes, while the voltage is measured between the inner two electrodes [151].

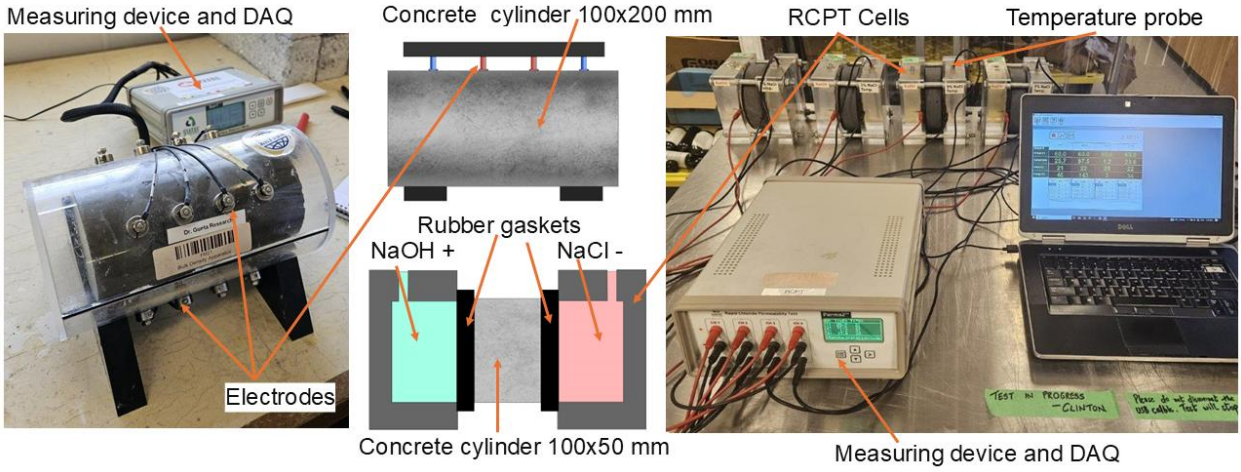

(a) (b)

Figure 4.1 (a) Surface Electrical Resistivity Test and (b) Rapid Chloride Permeability Test

4.4.2.2 Rapid Chloride Permeability Test

The Rapid Chloride Permeability Test (RCPT), an indirect measure of the durability of concrete under chloride attack, was used to measure the chloride ion penetration [127]. In compliance with ASTM C1202-22 [152], the test was carried out following 28 days of water curing; however, AASHTO T277 [153] or any other applicable standard may also be utilized. Following the procedure as explained in ASTM C1202-22, three samples of each CO_2-sequestered concrete mix were made for the test. Two specimens of 50 mm thickness were cut from each 100x200 mm cylinder, as shown in Figure A.4(a) in Appendix A. The curved faces of the cylindrical specimens were sealed with waterproof tape to prevent leakage of water, which could compromise the test results. The samples were submerged in water for 20 h after 3 h of low-pressure (less than 50 mm Hg) vacuum desiccator treatment. Each specimen was placed in a test cell, where one side was exposed to the sodium chloride (NaCl) solution (3% concentration) and the other to the sodium hydroxide (NaOH) solution (0.3 M concentration), as shown in Figure 1(b). Rubber gaskets and a sealant were used around the specimen-cell boundary to prevent leakage, and the setup was securely fastened with nuts, as shown in Figure A.4(b) in Appendix A. A constant 60V DC voltage was applied across the specimen, with the positive electrode in the NaOH solution and the negative electrode in the NaCl solution , as shown in Figure A.4(c) in Appendix A. Before starting the RCPT test, the instrument was calibrated using a verification kit provided by the manufacturer [154]. In accordance with the ASTM C1202-22 standard, the test runs for 6 h, and the device automatically recorded the current flowing through the material at regular intervals, using the measuring device inbuilt with a DAQ, as shown in Figure 4.1(b) [155]. This test links the total electrical charge that flows through the material, measured in Coulombs, to provide an indirect indicator of the permeability of concrete to chloride ions. The chloride ion penetration can be classified into the categories as provided in Table 4.2 in accordance with ASTM C 1202-22.

Table 4.2 Chloride Ion permeability based on charge passed

Charge passed (Coulombs)	Chloride ion penetrability
>4000	High
2000-4000	Moderate
1000-2000	Low
100-1000	Very low
<100	Negligible

4.4.2.3 Water Permeability Test

In order to measure the resistance of concrete to the movement of water, chemicals and salts within its pore structure, the water permeability test is usually conducted [107]. This test is typically conducted following the procedures outlined in BS EN 12390-8:2019, DIN 1048-5, or other relevant standards. For this particular test, BS EN 12390-8:2019 [156] standard was followed. Three cubic specimens with 150 mm sides that were cast and cured for 28 days in accordance with ASTM C192/C192M-19 [95]. The specimens were mounted on the water permeability apparatus, as shown in Figure A.5(a) in Appendix A, with the formed surface in contact with the water inlet at the bottom to prevent any water leakage. During the test, the pressure was maintained at 500 ± 50 kPa, creating a water head of 51 m (H). This pressure was maintained for

72 h (t), after which the specimens were split in half using a cube splitting jig as shown in Figure A.5(b) in Appendix A, and the depth of water penetration was immediately marked and measured as shown in Figure A.5(c) in Appendix A.

The coefficient of permeability (k) is generally calculated using the depth of water penetration, as explained by Mehta and Monterio [157]. The coefficient of permeability (k) is determined using Darcy's law, as shown in equation 17, where dq/dt is the rate of water flow, μ is the viscosity of water, ΔP is the pressure gradient, A is the surface area, and L is the thickness of concrete.

$$\frac{\mathrm{dq}}{\mathrm{dt}} = \mathrm{k}\,\frac{\Delta \mathrm{P}\,\mathrm{A}}{L\mu} \tag{17}$$

Equation 18 describes the model that Ibrahim and Issa [158] suggested to estimate the permeability coefficient based on the average depth of water penetration. In this model, C represents the ratio of the average to the maximum water penetration depth ($d_{average}$/ d_{max}), t is the test duration (seconds), and H is the hydrostatic head driving the water percolation (m).

$$\mathrm{k} = \mathrm{C}^2\,\frac{\mathrm{d}^2\mathrm{max}}{\mathrm{Ht}} \tag{18}$$

4.4.3 Freeze-Thaw testing of concrete

For each concrete batch, three 75 x 100 x 405 mm specimens were cast for different CO_2 dosages (0%,0.25%,0.5%,0.75% and 1%) and cured per ASTM C192-19 [95], for a period of 28 days after casting, as shown in Figure A.6(a) in Appendix A. These specimens were subjected to standard cyclic F-T testing up to 300 cycles as per ASTM C666-15 [159], Procedure A (Rapid Freezing and Thawing in Water) without de-icer salts. A Humboldt HC-3186S·4F freeze-thaw cabinet was used for the test, as shown in Figure A.6(b) in Appendix A. As summarized in the operation manual provided by Humboldt Mfg. Co [160], a 0.75 HP (0.6 KW) refrigeration unit and electric resistance heaters with fully automated controls were used to maintain the temperature of the concrete prisms. The specimens' temperatures were lowered from 4 °C to -18 °C and raised from -18 °C to 4 °C over the course of roughly 3.5 h in each F-T cycle, in accordance with the procedure explained in ASTM C666-15. As suggested by the manufacturer of the F-T cabinet, to ensure an automatic cyclic F-T temperature control by the machine, a thermocouple was placed in the middle of the control specimen. Additionally, using metallic spacers, the specimens in the F-T moulds were fully submerged in 1-3 mm of water during the test, ensuring water contact throughout the freezing-thawing cycles. As per the procedure explained in ASTM C666-15, non-destructive testing (NDT) methods were used to determine the fundamental transverse, longitudinal, and torsional frequencies, in addition to surface resistivity, and ultrasonic pulse velocity (UPV), including mass loss measurements at intervals of 0, 30, 60, 90, 120, 150, 180, 210, 240, 270, and 300 F-T cycles. All tests were performed on specimens in a saturated surface dry (SSD) condition at a room temperature of 23 ± 2 °C. Because the relative dynamic modulus of elasticity did not decrease below 60% of the initial modulus, the test continued up to 300 cycles as stipulated by ASTM C666-15.

4.4.3.1 Mass loss

The percent mass loss at various F-T cycles was recorded to assess the durability and resistance of the concrete to freeze-thaw damage. The mass loss rate is described in equation 19.

$$\Delta\mathrm{Wn} = \frac{(\mathrm{W0}-\mathrm{Wn})}{\mathrm{W0}}\ \mathrm{x100} \tag{19}$$

Where ΔW_n is the mass loss rate after n F-T cycles (%), W_0 is the mass at 0 F-T cycle (kg), and W_n is the mass after n F-T cycles (kg).

4.4.3.2 Resonance frequency

The longitudinal, transverse, and torsional fundamental frequencies were measured using resonance frequency testing as per the procedure explained in ASTM C215-19 [161] to determine the durability factor and dynamic modulus of CO_2-sequestered concrete and compare it with control concrete to observe changes in physical properties. This study utilized a resonance test gauge by Olson Instruments with a built-in data acquisition system and a PCB Piezotronics accelerometer. The manufacturer of this instrument provided a 110 g steel ball peen hammer that could produce resonance frequencies up to around 10 kHz when struck on a flat concrete surface with a light force. According to the procedure explained in ASTM C215-19 [161] for the impact resonance method, the accelerometer was placed intact on the concrete surface using a petroleum gel, and the concrete specimen was struck with a hammer to determine the fundamental longitudinal, transverse, and torsional frequencies. The test was repeated for each specimen after every 30 F-T cycles from 0 to 300 cycles, as shown in Figure A.7(a), (b) and (c) in Appendix A. ASTM C215-19 specifies the procedure to determine the dynamic elastic and rigidity modulus based on the resonant frequencies of the specimens. Equation 20 was used to calculate the dynamic Young's modulus of elasticity (E) from the fundamental transverse frequency; equation 21 was used to calculate the dynamic Young's modulus of elasticity (E) from the fundamental longitudinal frequency, and equation 22 was used to determine the dynamic modulus of rigidity (G) from the fundamental torsional frequency, as provided by ASTM C215-19. Furthermore, ASTM C666-15 specifies the determination of the relative dynamic modulus of elasticity (Pc) using equation 23 and the Durability Factor (DF) using equation 24, both based on the fundamental transverse frequency.

$$\text{Dynamic E} = \text{C x M x n}^2 \tag{20}$$

$$\text{Dynamic E} = \text{D x M x } (\text{n}^{\text{I}})^2 \tag{21}$$

$$\text{Dynamic G} = \text{B x M x } (\text{n}^{\text{II}})^2 \tag{22}$$

$$\text{Pc} = \frac{(n_c^2)}{(n_0^2)} \text{x} 100 \tag{23}$$

$$DF = \frac{\text{Px N}}{\text{T}} \tag{24}$$

Where C, D and B are dimensional factors of the specimen, M is the mass of the specimen, and n, n^{I}, n^{II} represent the fundamental transverse, longitudinal and torsional frequency, respectively, after c cycles of freezing and thawing. Additionally, Pc is the relative dynamic modulus of elasticity after c cycles of freezing and thawing, n_0 and n_c are the fundamental transverse frequency at 0 & n cycles, N is the number of cycles and, T is the specified number of cycles at which the exposure was terminated.

4.4.3.3 Ultrasonic Pulse Velocity

Concrete quality and consistency can be assessed non-destructively using Ultrasonic Pulse Velocity (UPV) testing ASTM C597-22 [162]. As explained by Mohana [163], this test is established using the pulse velocity method to obtain information regarding the uniformity of concrete and identify any cracks, cavities, and other defects. The author further explains that

because of these defects inside concrete, the travel path of the waves becomes blocked, increasing their travel time and decreasing their velocity. A Proceq Pundit Lab UPV test apparatus, which included two 50 mm diameter transducers and an electrical pulse generator operating at 54 kHz, was utilized to test the concrete prisms for UPV. To ensure adequate contact between the transducers and the concrete surface, cellulose gel was applied to the surface of the transducers in contact with the concrete surface. Following the procedure outlined in ASTM C597-22 [162], the UPV testing was carried out. The test was carried out on the formed surface of the concrete prisms in both longitudinal and transverse directions for each specimen utilizing a direct transmission mechanism, as shown in Figure A.8(a) and (b) in Appendix A. The pulse velocity in m/s is given by equation 25.

$$V = L/T \tag{25}$$

Where, V is the longitudinal pulse velocity, L is the path length, and T is the time taken by the pulse to traverse that length.

The dynamic modulus of elasticity (Ed) was derived from the UPV test, which was calculated using the velocity of the ultrasonic pulse passing through the concrete and its density, as explained by IAEA guidelines [164]. The relationship between the pulse velocity, density and dynamic Poisson's ratio is given by equation 26.

$$Ed = (\rho\, V\text{^}2\ [((1+\upsilon)(1-2\upsilon))/(1-\upsilon)]) \tag{26}$$

Where, Ed is the dynamic elastic modulus, ρ is the density of concrete, V is the pulse velocity, and υ is the dynamic Poisson's ratio. A Poisson's ratio of 0.2 was used for the calculation of dynamic modulus referring to the study by Swamy [165]

4.4.3.4 Resistivity

The resistivity of concrete was measured in accordance with AASTHO T358-19 [149], this test makes use of a Wenner 4 probe to provide the surface electrical resistivity of concrete.

4.4.4 pH of concrete

To determine if there were any changes to the alkalinity of concrete after CO_2 sequestration, pH measurements were done. The indirect pH measurement was done by mixing powdered concrete samples with distilled water. After testing the cylindrical specimens for 90-day strength, one cylinder was broken into smaller pieces using a hammer and placed in an oven at 110 ± 5 °C for 24 h to dry free water. The concrete samples were then crushed into a fine powder using an automatic Marshall impact compactor, and the powder was sieved by a 90-micron sieve. As per the procedure detailed by Robayo-Salazar et al. [117], 15 g of the concrete powder was mixed with 150 g of distilled water and mixed on a magnetic plate for 20 min, as shown in Figure A.9(a) in Appendix A. After mixing, the pH values of each suspension were measured three times using a digital pH meter, as shown in Figure A.9(b) in Appendix A. The qualitative analysis was experimentally done by splitting the concrete cylinders in half, spraying a 1% phenolphthalein solution on the concrete surface, and observing the colour change.

4.4.5 Evaluation of corrosion resistance of reinforced concrete

The alternate wetting and drying cycle test was conducted to check the resistance of CO_2-sequestered concrete to withstand corrosion. The test was performed both with and without the

addition of chloride salts. In order to estimate the service life and provide information about its long-term performance, the Tuutti Model [166] was also utilized. Concrete slab panels measuring 300 x 300 x 100 mm were cast, each containing four deformed low-carbon steel reinforcement bars of 10 mm diameter, conforming to CSA G30.18 [170]. The bars were arranged in a crosswise pattern in a wooden mould, as illustrated in Figure 4.2(a), to simulate typical reinforced concrete slab conditions. As shown in the schematic sketch in Figure 4.2(b), four bars, each 240 mm in length, were placed crosswise with a 60 mm spacing between the four nodes. The ICOR (instantaneous corrosion) rate measurement equipment of Giatec Scientific Inc. was used, which has an electrode influence area with a diameter of 180 mm. The rebar mesh spacing was designed in such a way that the four nodes of the rebars aligned with the electrodes of the ICOR device. A clear cover of 30 mm was provided to the bottom steel, in accordance with CSA A 23.1 requirements, by using plastic spacers as indicated in Figure 4.2(a). The rebars were designed with a length that ensured a minimum concrete cover of 30 mm in all directions within the slab. To conduct half-cell potential measurements, an electrical copper wire was connected to one rebar, which was also in contact with the other three rebars. Panels were cast for each of the five mixes, with CO_2 dosages ranging from 0% to 1%. After the concrete was poured into the wooden moulds, it was compacted by placing them on a vibrating table. After 24 h of casting, the slab panels were demoulded and cured for 28 days in a controlled lab environment at 23 ± 2 °C by covering the panels with moist hessian cloth.

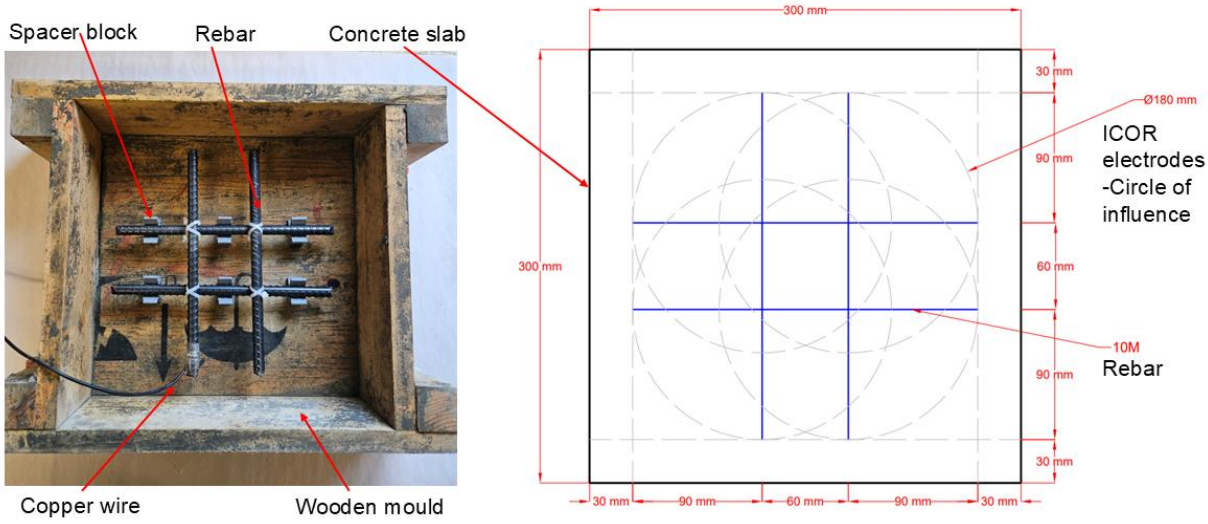

(a) (b)

Figure 4.2 (a) Rebar layout for corrosion testing, and (b) Schematic sketch of rebar design in the slab

After 28 days of water curing, each slab panel was tested under alternating wetting and drying conditions following the procedure outlined by Elbakari and Shehata [167]. The wetting-drying cycle for this test consisted of 50 cycles over 100 days. Rangel et al. [168] implemented 50 wetting-drying cycles over a 100-day period to replicate conditions, such as heavy rainfall and hot summers, in the laboratory. This approach ensured that the impact of alternating wetting and drying conditions could be evaluated across the different slab panels with varying CO_2 dosages. The test was performed manually with the use of water tubs and laboratory ovens, as shown in

Figure A.10(a) and (b) in Appendix A. Sets A, B and C comprised of five slab panels each, with CO_2 dosages ranging from 0% to 1%, subjected to wetting and drying exposure conditions as detailed in Table 4.3. Each cycle lasted for 24 h, ensuring both complete drying of water present in the concrete pores in the drying cycle and saturation of concrete in the wetting cycle. The slab panels in set A were placed in the oven set at to 50 °C, and panels in sets B and C were subjected to 60 °C. Sets A and C had their wetting cycle in potable water, whereas Set B had the wetting cycle in potable water with 5% NaCl concentration. All tests were conducted at the 0th and at the end of the 25th and 50th, as per the timelines indicated in Figure 4.3. An ICOR device, a half-cell potential copper-copper sulphate electrode, and a Wenner four-probe resistivity measurement equipment were used to measure the corrosion rate, corrosion potential and the resistivity of concrete, respectively. The ICOR device was used to record the concrete resistivity and corrosion rate readings at each node in both horizontal and vertical locations. Additionally, a Wenner four-probe instrument was used to test resistivity in each of the four quadrants in the slab.

Table 4.3 Wetting and drying exposure conditions

Category	Wetting cycle (Water temp- 23 ± 2 °C)	Drying cycle (Oven temp)
Set A	Potable water	50 °C
Set B	Potable Water+ 5% NaCl	60 °C
Set C	Potable water	60 °C

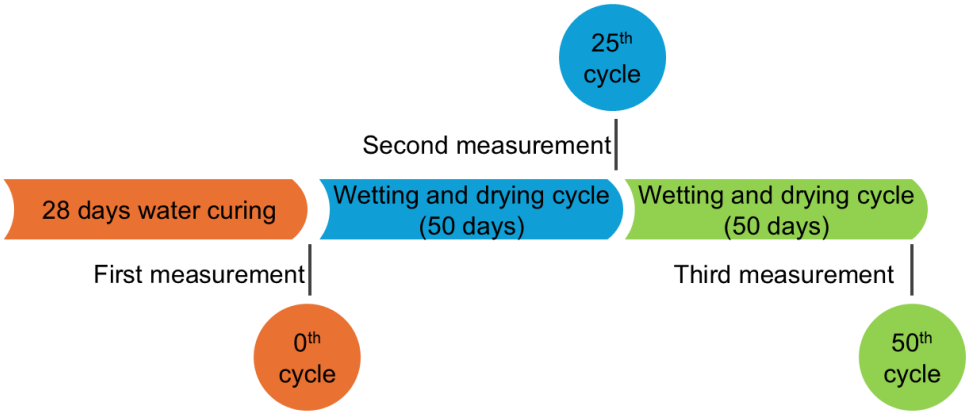

Figure 4.3 Wetting and drying cycle testing regime

4.4.5.1 Corrosion rate measurement

In this test, the corrosion rate of the steel rebar in concrete was measured using the non-destructive ICOR instrument by Giatec Scientific Inc. [169]. It functions according to the linear polarization resistance (LPR) concept. As explained by the manufacturer [170], the device has a four-probe Wenner array design, where a steady AC current is delivered between the outer probes and voltage measurements are obtained between the inner probes. The rebars in the samples were identified and marked using a rebar locator to pinpoint the four nodes, as shown in Figure 4.4(a). Furthermore, Figure 4.4(b) shows the positioning of the ICOR device at the nodes on the concrete slab for corrosion rate measurements and resistivity. These measurements were taken every 30 min at each of the four nodes, as recommended by the manufacturer. As the circle of

influence for the four nodes overlaps, repeated measurements can cause residual polarization effects to occur at the rebar surface, which can lead to inaccurate results of corrosion rate or current density. The instrument was calibrated to provide the corrosion rate of rebar in micro-Amps per square centimetre (μA/cm²) and the corrosion penetration rate in μm/year.

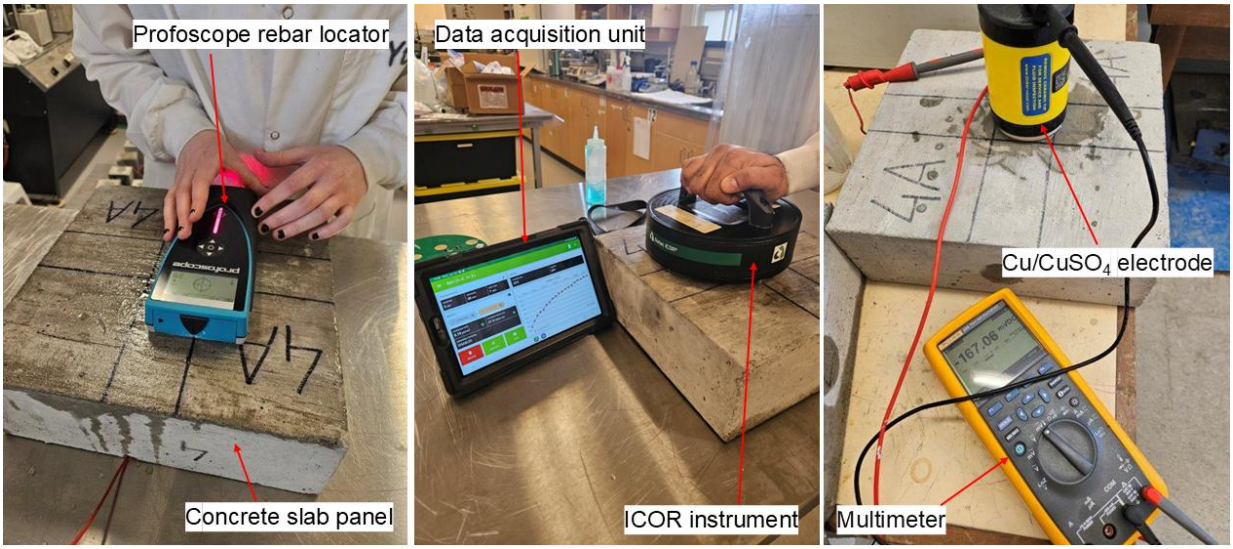

Figure 4.4 (a) Rebar locator, (b) ICOR measuring device and (c) Half cell potential test set-up

4.4.5.2 Half-Cell Potential Test

To measure the corrosion potential of steel rebars embedded in the 300×300×100 mm concrete slab panels, a copper-copper sulphate (Cu-$CuSO_4$) electrode, a digital multimeter and a wire connected to the rebar mesh were used as shown in Figure 4.4(c), following the procedure as described in ASTM C876-15 [171]. The voltage readings for each slab panel in sets A, B and C were recorded at the 0th cycle and at the end of the 25th and 50th cycle. To ensure proper coverage of the electrode base over all four overlapping bars at the center of the slab, where the bar spacing is 60 mm center-to-center, a 75 mm diameter waffle-patterned, pre-calibrated electrode was used. The concrete surface in contact with the electrode was made moist with water to ensure good conductivity. The voltage value was recorded once the reading stabilized to within ±0.02 V, as per ASTM C876-15.

4.5 Results and Discussions

4.5.1 Transport Properties of Concrete

4.5.1.1 Surface electrical resistivity, RCPT and water permeability

The surface electrical resistivity and RCPT test results are graphically represented in Figures 4.5(a) and 4.5(b), and the water permeability test results and computed coefficient of permeability are compiled in Table 4.4. The RCPT values are the average of three cylindrical specimens, while the resistivity test data are the mean of six cylinders. The error bars on the bar graphs indicate the standard deviation.

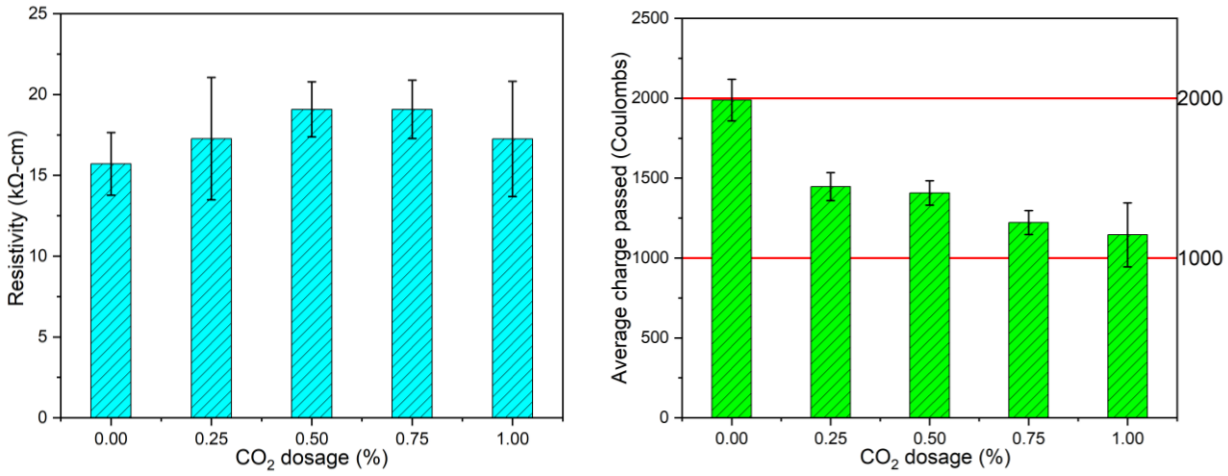

(a) (b)

Figure 4.5 (a) Average surface electrical resistivity, and (b) RCPT-Average charge passed in Coulombs

Table 4.4 Coefficient of permeability (k) m/s

Water permeability test					
Particulars	Control	0.25%	0.50%	0.75%	1.00%
$d_{average}$ (m)	0.02	0.01	0.01	0.01	0.01
$d_{std.dev}$ (m)	0.0015	0.0015	0.0026	0.0010	0.0006
d_{max} (m)	0.02	0.02	0.01	0.01	0.01
C	0.92	0.91	0.70	0.83	0.95
2 HT (m.s)	26438400				
k (m/s)	1.41×10^{-11}	7.06×10^{-12}	1.85×10^{-12}	9.46×10^{-13}	1.68×10^{-12}

From Figure 4.5 and Table 4.4, it can be observed that the control concrete sample shows the highest permeability and RCPT values and comparatively lower resistivity than other dosages of CO_2 addition. Further reduction in permeability was observed at 0.50% CO_2 dosage, indicating better resistance to the flow of water and other deleterious materials. At 0.75% the permeability and RCPT were comparatively low, and the resistivity was higher as compared to other CO_2 dosages, indicating improvement in durability due to the densification of the matrix. At 1% CO_2 dosage, the resistivity and permeability values were lower as compared to the 0.75% CO_2 dosage indicating a threshold in early age carbonation benefits. All the concrete samples indicate a low chloride ion permeability value in accordance with ASTM C1202-22 criteria, as summarized in Table 4.2.

4.5.1.2 SEM imaging analysis

The decrease in porosity was visually observed under a desktop SEM at 30x magnification, which confirms the densification. The air voids appear dark in the SEM images due to low atomic density. Figures 4.6(a), 4.6(b) and 4.6(c) show the SEM images of 0%, 0.5% and 1% CO_2 dosage samples, respectively, after 90 days of curing. The SEM imaging of the three samples indicates a reduction of voids in the concrete microstructure for the CO_2-sequestered concrete samples as compared to the control concrete sample.

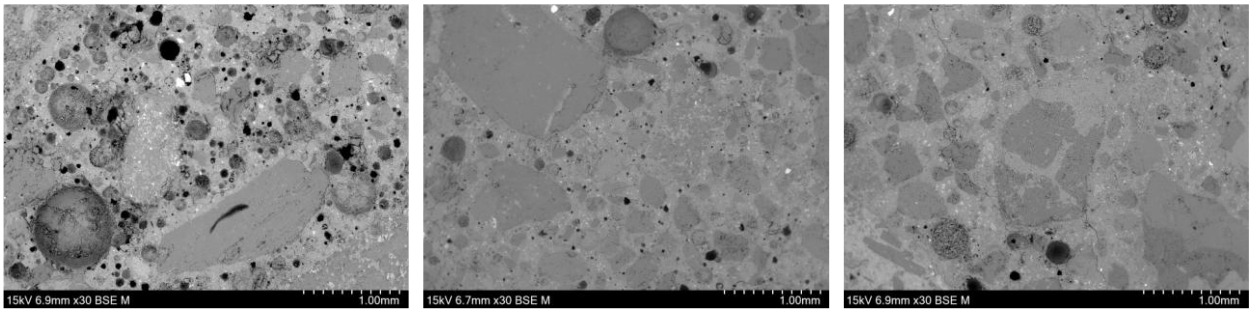

(a) (b) (c)

Figure 4.6 SEM images (a) Control concrete, (b) 0.5% CO_2 dosage and (c) 1% CO_2 dosage

Table 4.5 Analysis of air voids in SEM images using ImageJ

Specimen	Count	Area (mm^2)	% Area	Mean
Control	274	0.238	1.813	255
0.5% CO_2	23	0.048	0.359	255
1% CO_2	24	0.048	0.366	255

A Java-based image processing software, ImageJ, was used to measure the percentage of air voids from the SEM images shown in Figure 4.6. The data from ImageJ, summarized in Table 4.5, for the three CO_2 dosages (0%, 0.5%, and 1%) provides insights into the void distribution in concrete at the microstructural level. 274 voids were identified in the control concrete specimen as compared to 23 and 24 voids, respectively, in the concrete specimens with 0.5% and 1% dosage. This reduction in the void count results from the densification of the microstructure due to early-age carbonation. Furthermore, the void area has been found to decrease with 0.048 mm^2 for 0.5% and 1% dosage, compared to 0.238 mm^2 for control concrete. Additionally, the void region accounts for 1.813% of the entire picture area for the control concrete specimen, as compared to 0.359% and 0.366%, respectively, for 0.5% and 1% CO_2 dosage, indicating a reduction in porosity. This analysis strengthens our hypothesis that adding CO_2 to concrete during the mixing stage leads to the densification of its microstructure.

4.5.1.3 Statistical analysis of transport properties

To determine if a correlation exists between permeability, RCPT charge passed, and concrete resistivity, a statistical analysis was conducted. The test outcomes are shown in Table 4.6, along with the Pearson correlation coefficient values for the above-mentioned pairs, determined using the Microsoft Excel data analysis tool. The Pearson correlation coefficients have been interpreted by referring to the article by Schober et.al [172]. The very strong positive linear relationship between the coefficient of permeability and chloride ion penetration from RCPT indicates that adding CO_2 to concrete helps to minimize both these parameters and eventually enhances durability. The moderately strong to strong negative linear connections between RCPT and resistivity and the coefficient of permeability and resistivity, respectively, indicate that the resistivity of concrete is influenced by some other factors. Both the experimental data and the Pearson coefficients support the hypothesis that adding CO_2 to concrete during the mixing process improves its durability.

Table 4.6 Statistical analysis of permeability coefficients, RCPT charge passed and concrete resistivity

Mix (CO_2 dosage)	k (m/s)	RCPT (Coulombs)	Resistivity (kΩ-cm)
Control	1.41×10^{-11}	1989	15.71
0.25%	7.06×10^{-12}	1447	17.27
0.50%	1.85×10^{-12}	1407	19.09
0.75%	9.46×10^{-13}	1222	19.09
1.00%	1.68×10^{-12}	1146	17.26
Pearson correlation coefficient	k and RCPT	RCPT and Resistivity	k and Resistivity
	0.95	-0.69	-0.86
	Very strong positive linear relationship	Moderate negative linear relationship	Strong negative linear relationship

4.5.2 Freeze-thaw test

4.5.2.1 Mass loss

The mass loss was tested using the test procedure explained in ASTM C666-15, which is graphically represented in Figure 4.7(a). The control concrete specimens indicated a larger mass loss of up to 0.25%, as compared to other specimens with CO_2 addition, suggesting lower resistance under F-T conditions. The test results show that 0.75% CO_2 dosage indicated the least mass loss, and it appears that the resistance of concrete to surface scaling and cracking under F-T conditions seems to improve with the addition of CO_2 during the mixing process.

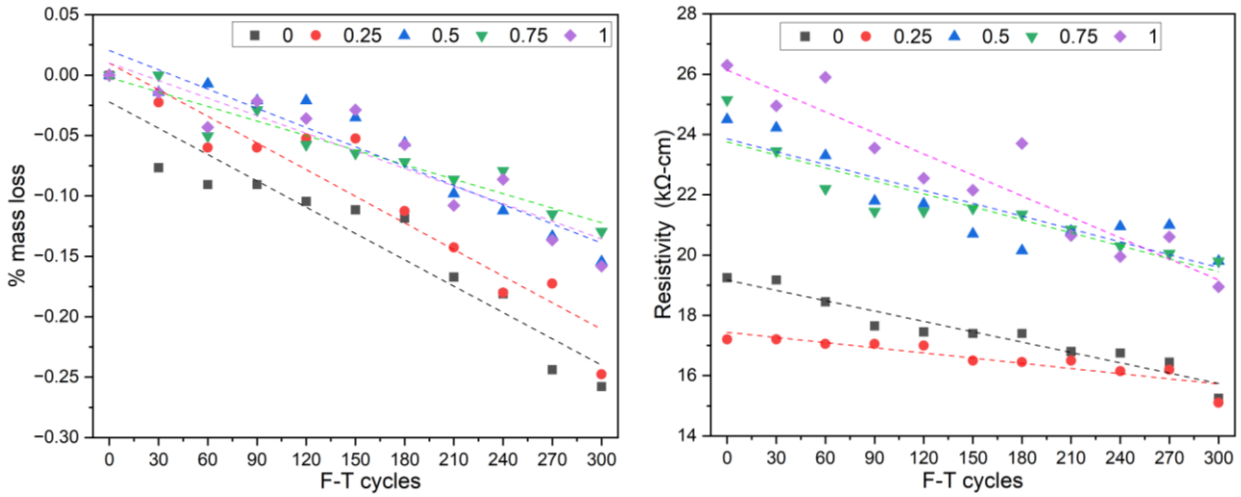

(a) (b)

Figure 4.7 (a) Percent mass loss and (b) Concrete Resistivity (kΩ-cm) at various F-T cycles

4.5.2.2 Concrete Resistivity

Figure 4.7(b) graphically displays the surface resistivity of concrete measured using a Wenner probe. The concrete specimens with 0% and 0.25% CO_2 dosages indicated a lower resistivity of 18-20 kΩ-cm, which decreased with time, suggesting a higher permeability as compared to other

dosages. The 0.5% and 0.75% CO_2 dosage mix shows a higher resistivity of 24-25 kΩ-cm at the start of the test and uniformly declines to 19.8 kΩ-cm after 300 cycles. The mix containing 1% of the CO_2 showed the highest initial resistivity of 26.3 kΩ-cm and ended at 18.95 kΩ-cm after 300 cycles, suggesting lower permeability in comparison with other dosages. From the test results, it appears that a CO_2 dose of between 0.50% and 0.75% may provide optimum resistance to freeze-thaw resistance based on the resistivity test.

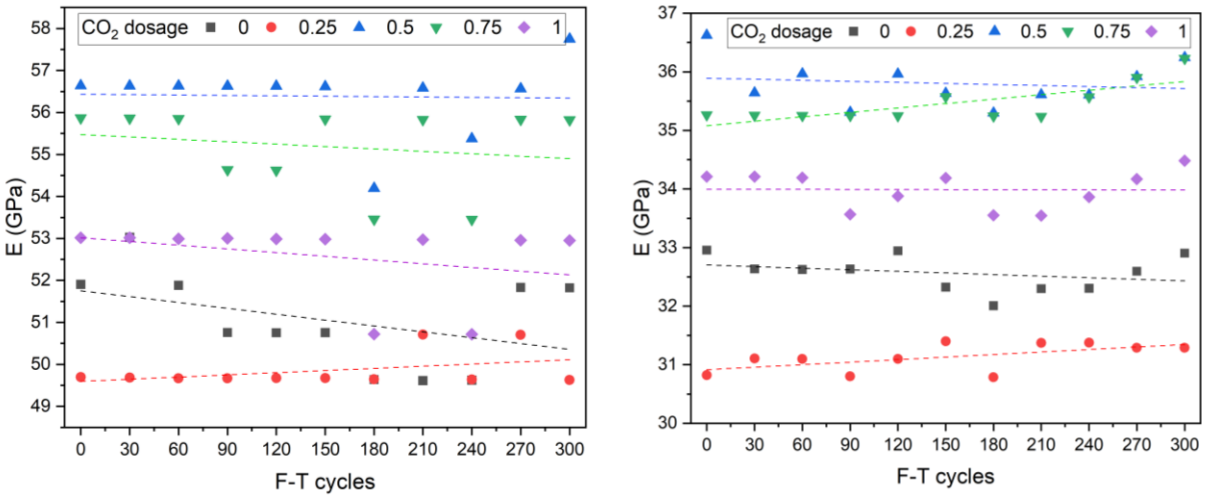

Figure 4.8 Young's modulus of elasticity E (GPa) from (a) fundamental transverse frequency and (b) fundamental longitudinal frequency

4.5.2.3 Young's modulus of elasticity and Dynamic modulus of rigidity

Figures 4.8(a) and 4.8(b) show Young's modulus of elasticity calculated from the fundamental transverse and longitudinal frequency for control concrete and mixes with varying CO_2 dosages. Additionally, the dynamic modulus of rigidity, calculated from fundamental torsional frequency, is illustrated in Figure 4.9(a). The test results of the mix with 0.25% CO_2 dose indicate the lowest elastic modulus and modulus of rigidity. The mix with 0.50% CO_2 dosage shows the highest stiffness, with values between 56-57 GPa for transverse frequency, 36-37 GPa for longitudinal frequency and 8.6-8.6 GPa for torsional frequency. The mix with 0.75% indicates stiffness values close to 0.50% CO_2 dose mixes in all three cases. Higher dosages at 1% CO_2 show a reduction in stiffness, indicating a threshold for CO_2 addition. This test suggests a dosage between 0.5% and 0.75% CO_2 addition provides an optimum stiffness and rigidity to concrete when subjected to F-T cycles, over control concrete mixes.

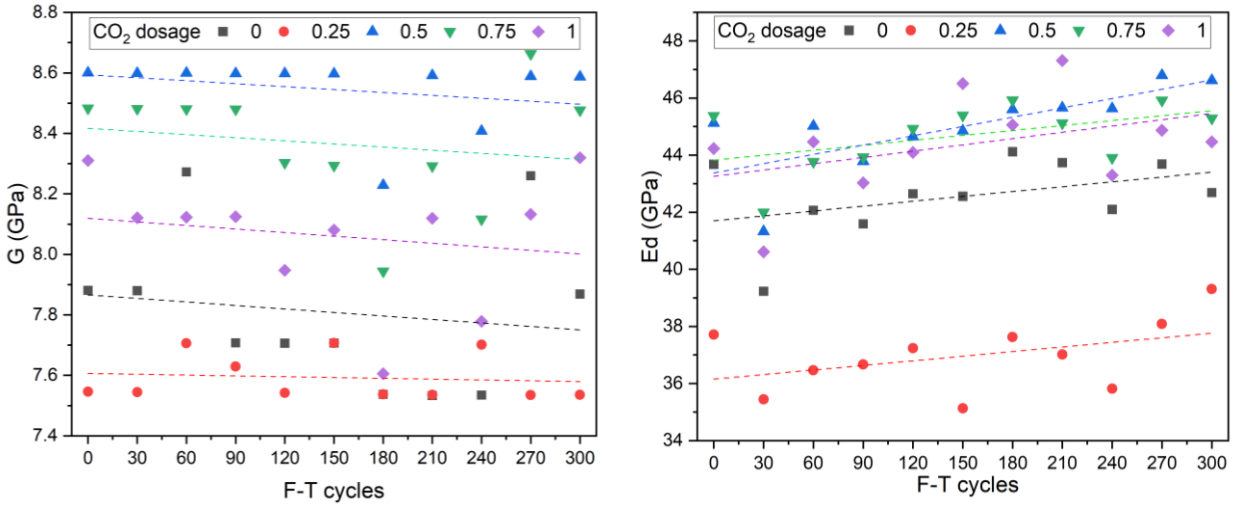

(a) (b)

Figure 4.9 (a) Dynamic modulus of rigidity from fundamental torsional frequency and (b) Dynamic modulus of elasticity from UPV

4.5.2.4 Dynamic modulus of elasticity from UPV

The dynamic modulus of elasticity calculated from the UPV wave velocity from equation 26 in 300 F-T cycles has been graphically displayed in Figure 4.9(b). The control mix shows a minor decrease in dynamic modulus of around 42 GPa, as compared to the other dosages, with 0.25% CO_2 dosage indicating the least stiffness. The dynamic modulus values of the mixes containing 0.50%, 0.75% and 1% CO_2 dosage indicate an improvement over control, between 44-46 GPa, with an increase in the number of F-T cycles and progress of hydration.

All the above test results for the F-T test show that the dynamic modulus of elasticity, dynamic modulus of rigidity, and resistivity values generally increase with CO_2 dosage, except at the 0.25% dosage level. The stiffness values were highest in the CO_2 dosage range of 0.50% to 0.75%, with a marginal improvement with the increase in F-T cycles suggesting improved bonding between the concrete particles. However, 1% CO_2 dosages did not show a proportional increase in stiffness; instead, a decrease in elastic properties was observed, as seen in the test results displayed graphically. Visual observations from the Dynamic Modulus, UPV, and resistivity test results on concrete subjected to 300 F-T cycles suggest that the optimal CO_2 dosage range lies between 0.50% and 0.75%. However, statistical analysis would also be beneficial to predict the optimal dosage range.

4.5.2.5 Statistical analysis of Dynamic Modulus of concrete

To analyze the experimental data of dynamic modulus obtained from transverse, longitudinal and torsional frequencies and UPV of concrete, a one-way ANOVA (Analysis of Variance) was calculated using the Microsoft Excel data analysis tool. The independent variables include the F-T cycles, whereas the dependent variables comprise of the dynamic modulus of elasticity and dynamic modulus of rigidity for the respective test across different CO_2 dosages. Andrade [173] explains that a P-value less than 0.05 means that the null hypothesis is not true and there exists a linear relationship between the variables. Based on the ANOVA results graphically illustrated in Figure 4.10(a), the P-values calculated across the five CO_2 dosages (0%,0.25%,0.5%, 0.75% and

1%) show a value below 0.05, indicating a linear relationship between F-T cycles and dynamic modulus making the relationship statistically significant. As seen in the graph, the P curves tend to flatten or decrease between 0.5% and 0.75%, indicating that a dosage between these values would provide an optimum resistance to freezing and thawing. This dosage range also aligns with the values obtained from the calculations of dynamic modulus from the experimental data.

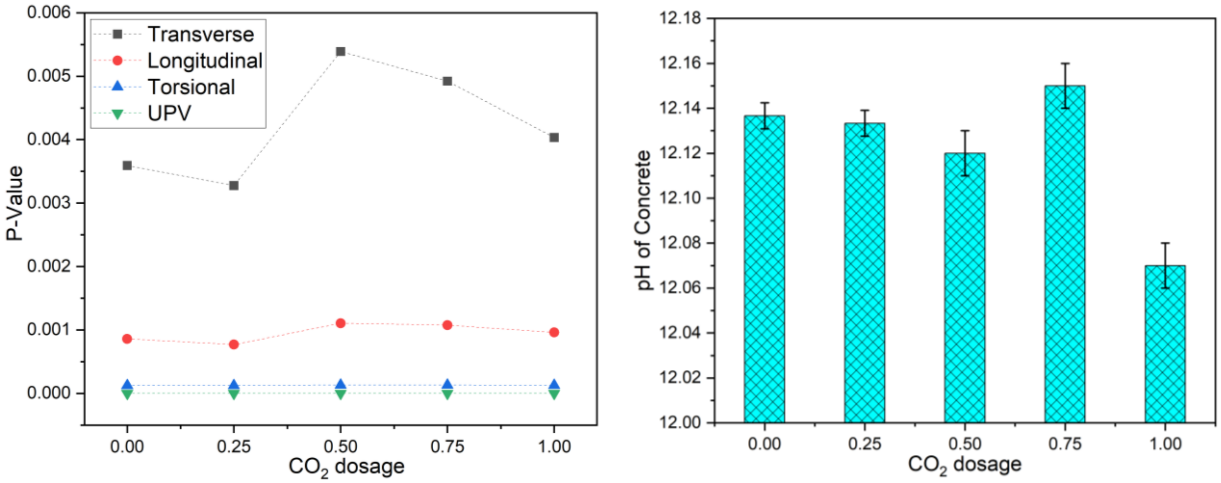

(a) (b)

Figure 4.10 (a) ANOVA P-values of dynamic modulus and (b) pH of concrete

4.5.3 Evaluation of pH of concrete

The pH of the powdered concrete samples extracted from specimens with CO_2 dosages ranging from 0.25% to 1%, including control concrete, at 90 days indicated a pH value between 12.05 and 12.16, as graphically represented in Figure 4.10(b). Additionally, the phenolphthalein indicator test conducted on specimens at 90 days indicated a dark purple colour in all specimens, as shown in Figure 4.11. These test results indicate that although the concrete samples were subjected to early-age carbonation, the alkalinity of the concrete remained sufficiently high, comparable to that of the control concrete. This ensures an environment inside concrete where the steel remains passivated.

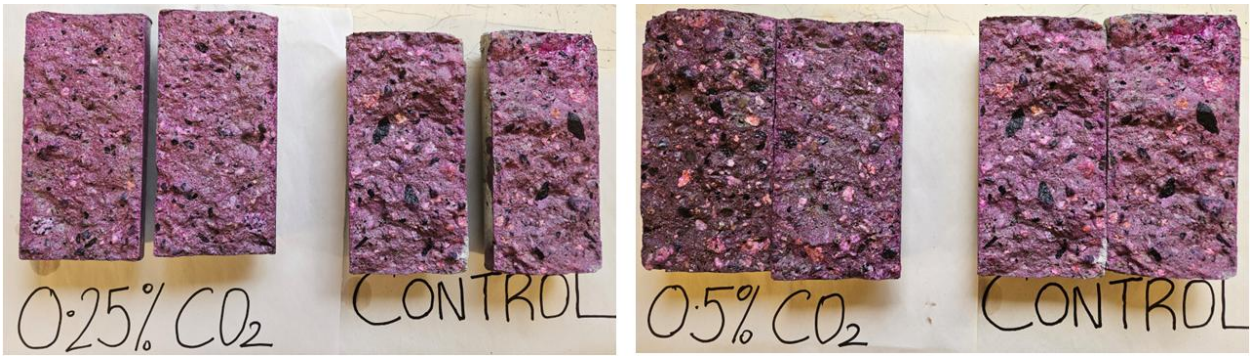

(a) (b)

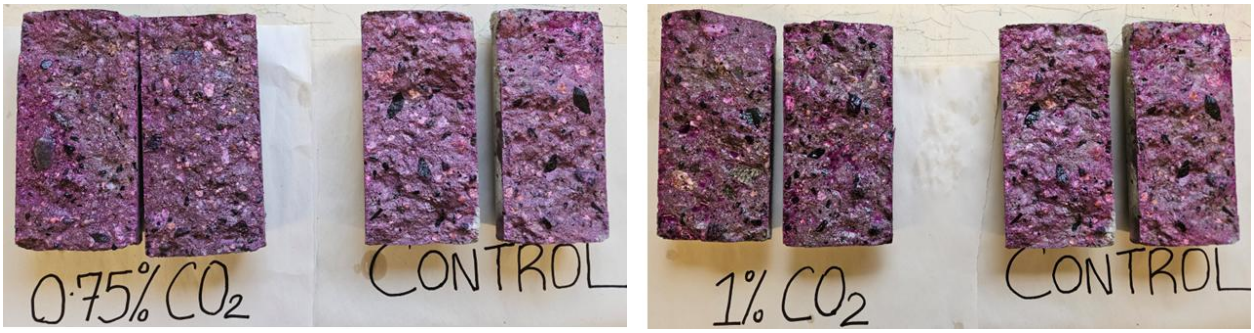

(c) (d)

Figure 4.11 Comparison of CO_2-sequestered concrete and control samples sprayed with phenolphthalein: (a) Control vs. 0.25% CO_2, (b) Control vs. 0.5% CO_2, (c) Control vs. 0.75% CO_2, and (d) Control vs. 1.00% CO_2

4.5.4 Alternate Wetting and Drying Cycles

4.5.4.1 Corrosion Rate Analysis

The average corrosion rate measured using the ICOR device for the concrete slab panels in sets A, C and B for different CO_2 dosages and environmental conditions at the 0th and at the end of the 25th & 50th wetting and drying cycles are shown in Figures 4.12(a), 4.12(b) & 4.12(c) respectively. The standard deviation of the average corrosion rate (average of 8 readings), measured by the ICOR device at each of the four nodes, in the horizontal and vertical positions for the respective slab panels are indicated as error bars on the bar graph. The authors of this chapter acknowledge the high error observed in set B after 50 cycles, which may be due to a potential testing error caused by high corrosion of the embedded rebars.

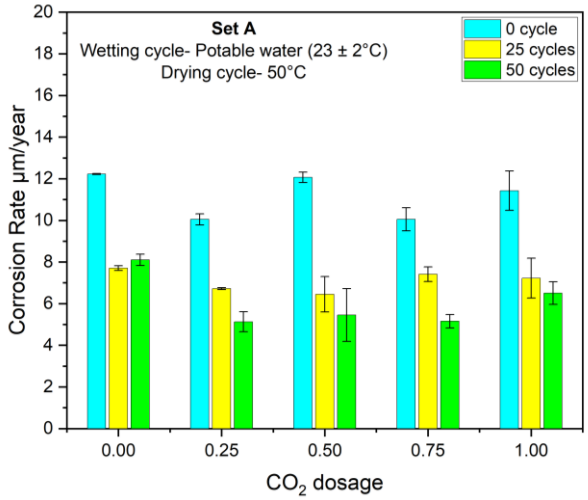

(a)

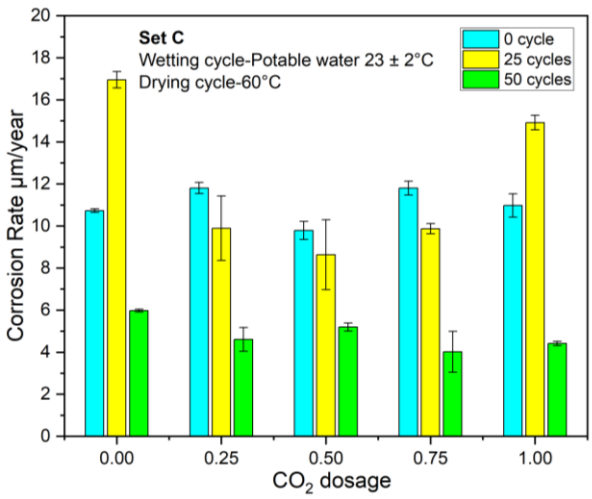

(b)

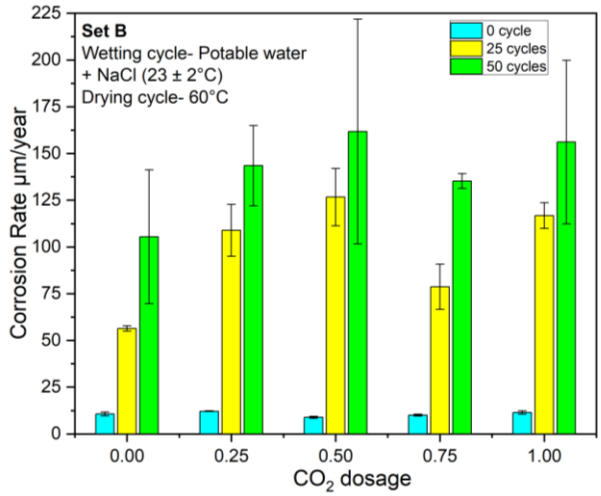

(c)

Figure 4.12 Corrosion rate for concrete slab panels in (a) set A, (b) set C and (c) set B for different CO_2 dosages

In control concrete, as observed in all three sets, the initial corrosion rate was between 10-12 µm/year, measured after 28 days of curing immediately before starting the wetting and drying cycles. A study by Ali et al. [174] highlights that moisture in concrete and oxygen near the steel surface after 28 days of curing results in mild oxidation on the surface of the rebar. This activity takes place even in the highly alkaline environment of concrete, causing mild corrosion. The corrosion rate for the control concrete slab panel in set A drops at 25 cycles from 12.22 µm/year to 7.70 µm/year. However, by the 50th cycle, it increases marginally to 8.10 µm/year, suggesting that corrosion protection decreases with time due to environmental conditions. A rise in the corrosion rate was seen for the control concrete slab panel in set B throughout all cycles, especially between 25 and 50 cycles, when it increased from 56.40 µm/year to 105.40 µm/year. This suggests that the saline environmental conditions and a high temperature of 60 °C resulted in a high degree of corrosion. The control concrete slab panel in set C showed a moderate corrosion rate of 16.95 µm/year by the end of the 25th cycle and dropped to 5.97 µm/year by the end of the 50th cycle. The authors of this article hypothesize that this phenomenon may be attributed to the self-healing properties of concrete and ongoing hydration.

For the CO_2 sequestered concrete slab panels with 0.25%, 0.5% and 0.75% CO_2 dosage, a decline in corrosion rate over time was observed for the slab panels in sets A and C, as compared to the control concrete slab panels, suggesting better performance with moderate CO_2 dosage and indicating the progress of hydration over time. For the 1% CO_2 dosage, a reduction in corrosion rate over time was observed for set A. However, in the case of set C, the corrosion rate increased after 25 cycles from 10.98 µm/year to 14.92 µm/year and decreased by the 50th cycle to 4.42 µm/year. The authors of this article hypothesize that although corrosion protection mechanisms may initially be compromised due to environmental factors, self-healing properties and ongoing hydration in the concrete may help to mitigate some of the corrosion effects. Set B showed an increase in corrosion rate for all dosages from 0.25% to 1% CO_2 addition due to the high temperature of 60 °C during the drying cycle and immersion in water with a 5% NaCl concentration during the wetting cycles, indicating chloride-induced corrosion. This suggests that

adding CO_2 alone cannot enhance the durability of concrete under harsh and saline environmental conditions.

This corrosion analysis indicated that CO_2-sequestered concrete at dosages between 0.25% to 0.75% exhibited a reduction in corrosion rates over time when subjected to high temperatures but in chloride-free environments (Sets A and C). Control concrete samples in sets A and C experienced varying corrosion rates influenced by environmental factors. However, neither control nor CO_2-sequestered concrete could withstand the harsh saline conditions (Set B), which led to increased corrosion rates. This highlights the limitations of early age carbonation in enhancing the durability of concrete, over control, under harsh saline environmental exposures.

4.5.4.2 Concrete Resistivity Analysis

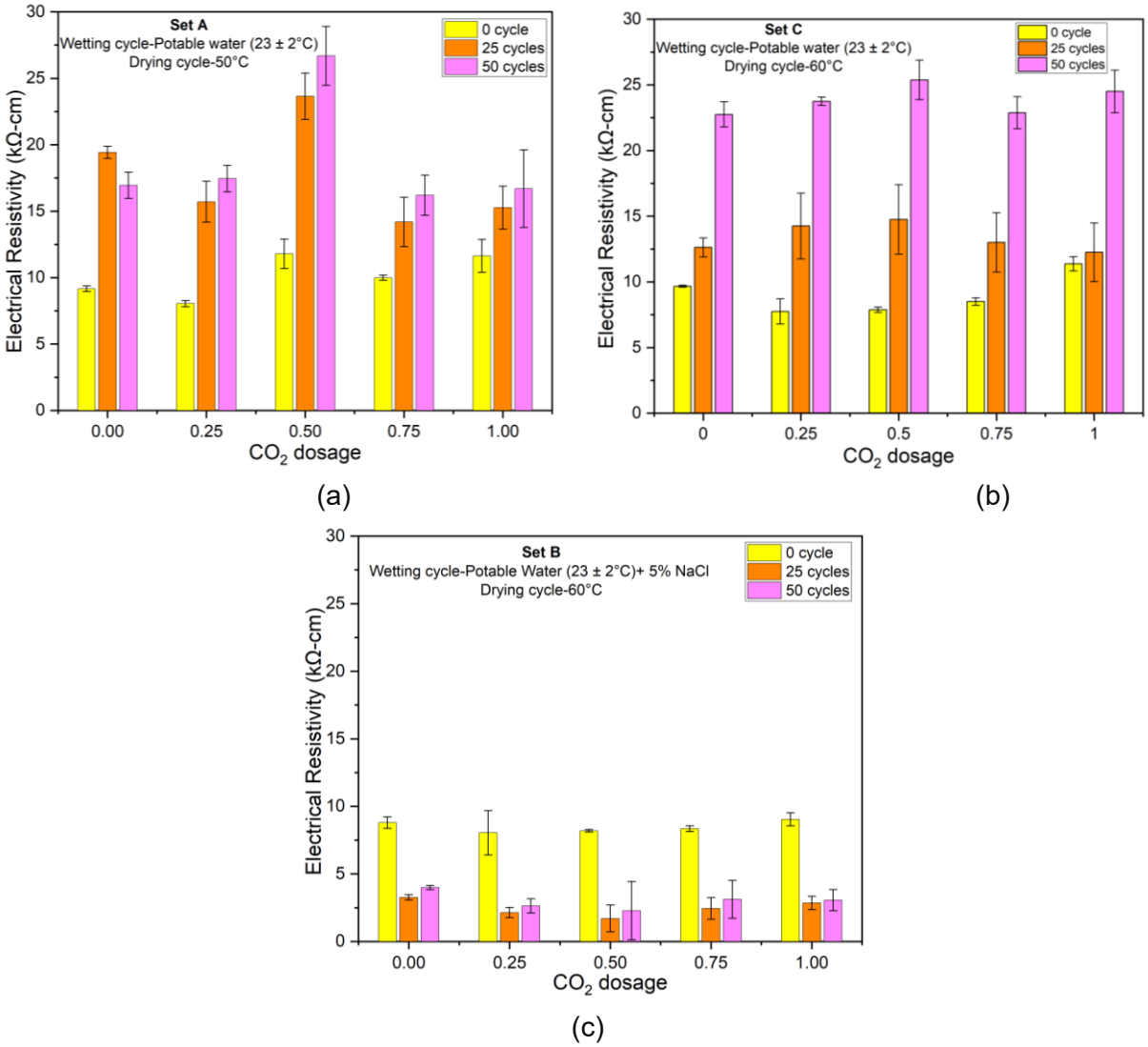

Figure 4.13 Concrete resistivity for concrete slab panels in (a) set A,(b) set C and (c) set B for different CO_2 dosages

The average resistivity measured by the ICOR device and the Wenner probe for the concrete slab panels in sets A, C and B for different CO_2 dosages are illustrated in Figures 4.13(a), 4.13(b) &

4.13(c) the 0th, and at the end of the 25th & 50th wetting and drying cycles. The standard deviation of the average resistivity readings for the respective slab panels are indicated as error bars on the bar graph. The average resistivity is calculated using eight measurements taken by the ICOR device at four nodes (in both horizontal and vertical positions) and four measurements obtained using the Wenner probe in the four quadrants of the respective slab panels. Resistivity measured by both devices indicates that control and CO_2-sequestered concrete show an improvement in resistivity as hydration progresses. For the 0.5% CO_2 dosage, there has been an improvement in resistivity values from 11.78 kΩ-cm to 26.69 kΩ-cm in set A and from 7.88 kΩ-cm and 25.38 kΩ-cm in set C. These values are higher compared to other dosages, indicating that CO_2 dosing at a particular threshold improves the resistivity of concrete and thereby enhances its long-term durability. The electrical resistivity for all the slab panels in set B decreased for all dosages, including control concrete. This suggests that adding CO_2 alone to concrete is insufficient to resist the risk of chloride-induced corrosion when exposed to extreme weather conditions and corrosive salts.

4.5.4.3 Half-Cell Potential Analysis

The half-cell potential or voltages measured using a copper-copper sulphate half-cell and a digital multimeter for the concrete slab panels in sets A and C for different CO_2 dosages are illustrated in Figures 4.14(a) and 4.14(b), respectively. These values are measured at the 0th cycle and at the end of the 25th & 50th wetting and drying cycles. The concrete slab panels in set B did not show any potential difference or voltage readings on the multimeter at the end of the 25th and 50th cycles, indicating severe corrosion for all CO_2 dosages, including control concrete. This may have been due to the formation of rust, which is generally non-conductive and creates a discontinuity in the electrical contact with the rebar. The voltage readings at the 0 cycle were in line with the readings for samples A and C; however, as there were no readings on the multimeter for the 25th and 50th cycle, the data of the 0th cycle for sample B has not been plotted. As per the criteria provided in ASTM C876-15 [171] for a Cu-$CuSO_4$ electrode, which has been detailed in Table 4.7, the probability of corrosion up to 10% was observed in all concrete slab panels. The concrete slab panels with 0.25% CO_2 dosage, in both sets A and C, indicate a lower probability of corrosion as compared to other CO_2 dosages. This test also indicates that mineralization, through CO_2 alone, cannot provide resistance to corrosion under harsh environmental conditions.

Table 4.7 Half Cell Potential criteria according to ASTM C876-15

Half-cell potential (mV)	Probability of corrosion
>−200	Less than 10%
−200 to −350	Uncertain
<−350	More than 90%

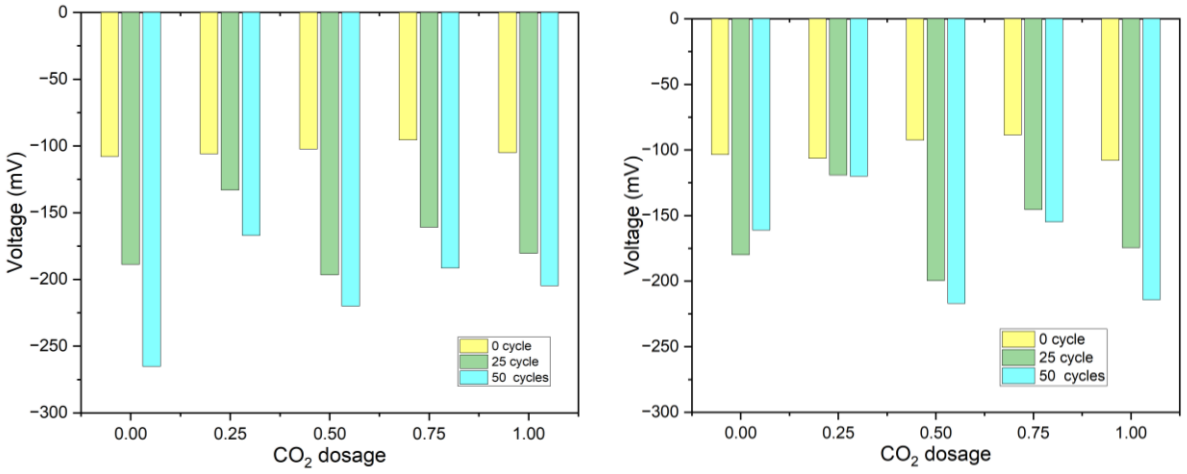

Figure 4.14 (a) Half-cell potential for concrete slab panels in (a) set A and (b) set C for different CO_2 dosages

The alternative wetting and drying cycles test demonstrates improved corrosion rate, resistivity and half-cell potential for concrete slab panels in sets A and C for dosages between 0.5% and 0.75% as compared to control concrete, which were subjected to high temperatures without chloride salt exposure. However, the harsh environmental conditions of high temperature and salt solution (5% NaCl) for concrete slab panels in set B potentially led to corrosion for all CO_2 dosages including control concrete, as indicated by the test data. The authors feel that when concrete is exposed to chloride salts and high temperatures, CO_2 sequestration alone cannot provide corrosion resistance, and supplementary techniques will have to be adopted.

4.5.5 Predicting the service life of reinforced concrete subjected to accelerated corrosion

Literature has documented well-established corrosion models that can be used to understand the behaviour of reinforced concrete under different environmental conditions. As part of this study, the authors have adopted the Tuutti model to estimate the service life of reinforced concrete subjected to accelerated corrosion. As explained by Tuutti [166], this model divides the corrosion process into two main phases: the Initiation phase and the Propagation phase. The initiation phase is the time taken for chlorides to penetrate the concrete cover and reach the rebar at a critical concentration. Tuutti explains that the steel reinforcement becomes de-passivated during this time due to the deterioration of the passive protective oxide coating. The author also describes how corrosion begins during the propagation phase, causing damage to the concrete and possibly structural failure. The service life model, as described by Tuutti, has been shown in equation 27, and the progress of the corrosion of steel in concrete has been schematically illustrated in Figure 4.15. Based on the test results from RCPT, corrosion rate and resistivity data under the two exposure conditions for alternative wetting and drying conditions, for the five CO_2 dosages varying from 0% to 1%, the Tuutti model has been referred to estimate the service life of concrete. This analysis aims to compare the corrosion resistance of CO_2-sequestered concrete over control and check if early-age carbonation helps to enhance the service life of reinforced concrete structures.

$$T_{service} = T_{initial} + T_{propagation} \quad (27)$$

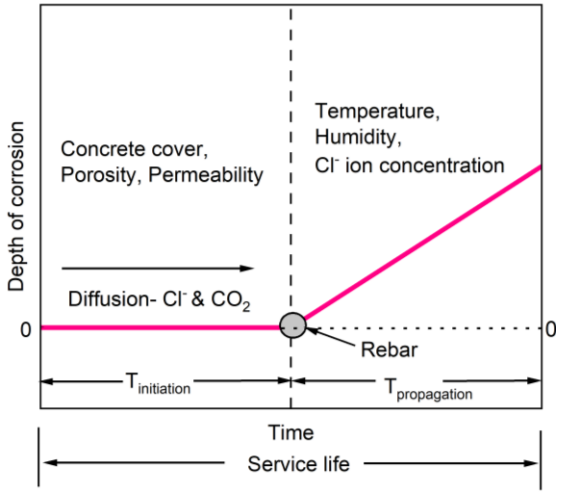

Figure 4.15 Schematic sketch of steel corrosion in concrete (Tuutti 1982) *[166]*

4.5.5.1 Initiation Time ($T_{initiation}$)

As explained by Tuutti [166], the initiation time indicates the period during which the chloride ions from the concrete surface penetrate the clear concrete cover to reach the rebars and to start the onset of corrosion. The factors affecting the initiation time include the porosity and permeability of concrete, the chloride ion diffusion coefficient, the clear concrete cover, the critical chloride threshold and the surface ion concentration, which mainly depends upon the environmental conditions. As described by Justnes et al. [175], equation 28 illustrates how Fick's Second Law of Diffusion is typically used to determine the onset time for chloride ion penetration.

$$\frac{\Delta C}{\Delta t} = D\frac{\Delta^2 C}{\Delta x^2} \tag{28}$$

Where, $\frac{\Delta C}{\Delta t}$ represents the rate of change of concentration (C) with respect to time (t). $\frac{\Delta^2 C}{\Delta x^2}$ represents the second spatial derivative of concentration (C) with respect to the spatial position from the surface (x), indicating the rate of change of concentration over distance.

In order to determine the initiation time in this study, equation 29 has referred to the article by Dinh [176], who used Fick's second law of diffusion to obtain the concentration at a specific depth from the surface.

$$\mathrm{Ct} = \mathrm{Cs}\,[1 - \mathrm{erf}\left(\frac{x}{2\sqrt{Dt}}\right)] \tag{29}$$

Where, Ct is the concentration as a depth x from the surface at time t, Cs is the surface concentration, x is the depth within concrete, and D is the diffusion coefficient for concrete.

To determine the initiation time ($T_{initiation}$ in seconds), Justnes et al. [175] have modified equation 29 in terms of the clear concrete cover, diffusion coefficient (D, in m^2/s) and the error function, as shown in equation 30.

$$\mathrm{Tinitiation} = \frac{\mathrm{x}^2}{4\mathrm{D}}\,\frac{1}{[\mathrm{erf}^{-1}\,(1-\left(\frac{\mathrm{Ct}}{\mathrm{Cs}}\right)]^2} \tag{30}$$

Where x is the clear cover depth (m), which is 30 mm for this test, Ct is the critical chloride

threshold, and Cs is the surface ion concentration. The value of Ct/Cs has been taken as 0.6, as provided in ACI 365.1R00, assuming Ct to be 0.4% by mass of cement [177].

The diffusion coefficient has been determined using the Nernst-Einstein equation, as described by Konecny et al. [178] as shown in equation 31.

$$D = \frac{R\,T\,t_i}{Z^2\,F^2\,\gamma_i\,Ci\,\rho_{BR}} \tag{31}$$

Where R universal gas constant (8.31446 J/mol.K), T absolute temperature (296.15 K- as the test is conducted at 23 °C), and the Faraday's constant (F) is 96500 C/mol. The Z valence of ions [-], the transport number (t_i) of chloride ions [-] and γ_i activity coefficient of chloride ions [-] is assumed to be 1, as described by Konecny et al. Ci represents the molar weight of the solution in mol/m^3. The molar concentration of chloride ions for a 3% NaCl solution, with the molar weight of NaCl being 58.44 g/mol, is 513.3 mol/m^3.

The volumetric electrical resistivity ρ_{BR} (Ω-m) which is described by Konecny et al. and obtained from the RCPT in equation 32.

$$\rho_{BR} = \frac{VtA}{QL} \tag{32}$$

Where V represents the electrical potential applied during the test (60 V), t is the test duration (6 h or 21,600 s), A is the cross-sectional area of the specimen (m²) for a sample with a 100 mm diameter, Q is the total electrical charge in coulombs that passed through the specimen, and L is the sample thickness, which was 50 mm. These parameters comply with the requirements outlined in ASTM C1202-22.

4.5.5.2 Propagation Time ($T_{propogation}$)

As explained by Tuutti [166], the propagation time indicates the period between the initiation of corrosion of rebars in concrete and until complete degradation takes place. The author further explains that the time to corrosion propagation depends on the critical steel loss ($d_{critical}$ in μm) and corrosion rate (ν_{corr} in $\mu m/year$), as summarized in equation 33. The corrosion rate for this study was obtained directly from the ICOR device, and it can also be derived from Faraday's law if the corrosion current is known. Broomfield [119] highlights that cracking is induced by less than 100 μm of steel section loss for structural deterioration to begin. For the calculation of propagation time, $d_{critical}$ has been assumed to be 100 μm.

$$T_{propogation} = \frac{d_{critical}}{\nu_{corr}} \tag{33}$$

4.5.5.3 Service Life Prediction

Tuutti's model has been used in this study to determine the service life of the structure by combining the corrosion initiation and progression time relationships. Table 4.8 provides an analysis of the estimated service life of concrete mixes with different CO_2 dosages during mixing. The parameters include RCPT values, resistivity (ρBR), diffusion coefficient, initiation time, corrosion rate, and propagation time, which have been used to estimate the overall service life. The accelerated corrosion test, by subjecting the reinforced concrete slabs to alternative wetting and drying cycles, has been used to speed up the natural corrosion process. The authors of this

chapter believe that service life estimations in Table 4.8 might be conservative, as the data is based on accelerated tests. However, the intention is to use these estimations for comparing CO_2-sequestered concrete with control concrete. Additionally, Broomfield [119] explains that the propagation period in actual structures is expected to be longer than the propagation time observed in accelerated tests, assuming the structure is in a moderate or controlled environment.

Table 4.8 Assessment of the estimated service life of reinforced concrete

Mix (CO_2 dosage)	RCPT (Coulombs)	ρ_{BR} (kΩ-cm)	Diffusion coefficient (m/s^2*10^{-12})	$T_{initiation}$ (years)	Average ν_{corr} ($\mu m/year$)	Average $T_{propogation}$ (years)	*$T_{service}$ (years)
Control	1989	10.24	5.03	10.3	7.04	14.2	24.6
0.25%	1447	14.07	3.66	14.2	4.87	20.5	34.8
0.50%	1407	14.47	3.56	14.6	5.32	18.8	33.4
0.75%	1222	16.66	3.09	16.8	4.59	21.8	38.6
1.00%	1146	17.76	2.90	18.0	5.46	18.3	36.3

Note: * calculated under accelerated conditions. Average ν_{corr} corresponds to the average corrosion rate of concrete slab panels in sets A & C at the end of 50 wetting and drying cycles

Table 4.8 shows that the control mix has the shortest service life. The high RCPT, low resistivity and high corrosion rate of control concrete, compared to the mixes with CO_2 addition, led to a shorter initiation and propagation phase and decreased overall service life. The 0.25%, 0.50% and 0.75% CO_2 dosage provided improvements as compared to the control mix, with 0.75% CO_2 dosage indicating the most extended service life. Although the 1.00% CO_2 mix had the maximum resistance to chloride ingress, its higher corrosion rate as compared to 0.75% reduced its service life to 36.3 years as compared to 38.6 years observed with 0.75% CO_2 dosage, indicating a threshold of CO_2 benefits to corrosion resistance. This analysis demonstrates that a CO_2 dosage between 0.5%- 0.75% would provide optimum performance during the initiation and propagation phase.

4.6 Concluding Remarks

This study investigated the long-term effects of early-age carbonation on the durability of CO_2-sequestered concrete by evaluating its transport properties, freeze-thaw resistance and corrosion behaviour under varying environmental conditions. The experimental approach adopted in this study focussed on resistivity, chloride ion penetration, water permeability, dynamic modulus under freeze-thaw cycles, corrosion rate and corrosion potential of reinforced concrete subjected to alternative wetting and drying conditions. The test results shed light on the benefits of early-age carbonation on the long-term durability of concrete in terms of lowered permeability and chloride ion penetration, enhanced resistivity, and improved freeze-thaw and corrosion resistance. The findings from this study reveal that CO_2 dosages between 0.5% and 0.75% provided optimal results in terms of resistivity, stiffness and corrosion resistance compared to control concrete. However, the test results also revealed a threshold in CO_2 addition at 1%, as observed in reducing these parameters.

Conclusions:

1. The test result indicates an overall improvement in the durability of CO_2 sequestered concrete, which has been observed with lower RCPT and permeability values and higher resistivity readings between 0.5% to 1% dosage.
2. CO_2 dosages between 0.5% and 0.75% showed improved performance to F-T cycles, as compared to control concrete, observed by lower mass loss and surface scaling and increased stiffness. Higher dosages can reduce the F-T resistance due to the densification effect.
3. Even though the concrete was subjected to accelerated carbonation, the alkalinity of the concrete was sufficiently high to resist the onset of corrosion, as observed by the pH of the concrete.
4. Reinforced concrete panels with 0.5%-0.75% CO_2 dosage showed improved corrosion resistance under high temperatures in salt-free environments. However, all panels, including the control, experienced increased corrosion rates in saline conditions. This highlights the need for adding supplementary materials and rebar coatings, in addition to CO_2 sequestration, to enhance durability in aggressive environments.
5. Predicting the service life by applying Tuutti's model to the experimental results indicates that a CO_2 dosage between 0.5% and 0.75% provides an enhanced service life of reinforced concrete.

The authors of this chapter hypothesize that a possible reason for the 0.75% CO_2 dosage outperforming the 1% dosage in multiple durability and mechanical tests—such as surface electrical resistivity, water permeability, freeze-thaw resistance, modulus of elasticity, dynamic rigidity, and corrosion performance may be attributed to the optimum level of CO_2 reacting efficiently with hydrated cement compounds, particularly calcium hydroxide, to form calcium carbonate and an increased effective w/c ratio due to additional superplasticizer dosage in the 1% dosage. Early age carbonation results in densification and capillary pore refinement at a microstructural level which improves resistance to ion migration, prevents corrosion risk and enhances mechanical interlocking which improves stiffness and strength enhancing the freeze thaw resistance of concrete. However, at 1% CO_2 dosage, the excess CO_2 results in a drop in workability and the increased superplasticizer content to obtain a placing slump might have altered the w/c ratio which may have resulted in the formation of more porous microstructure and an incomplete or less efficient carbonation, which was observed in the thermal pyrolysis test, FTIR and EDX spectroscopy.

These conclusions reinforce the hypothesis that concrete specimens subjected to early-age carbonation will maintain the alkalinity of concrete, decrease permeability and chloride ion ingress, enhance resistance to F-T cycles and protect embedded rebars from corrosion. The improvement in concrete properties is limited to the specific mixes evaluated in this study. The authors suggest that further research should be conducted across a broader range of concrete mix designs with different cement and cementitious materials under varying environmental conditions. Additionally, the issue of loss of workability of concrete after CO_2 addition also needs to be addressed.

This research contributes to the body of knowledge on the long-term impact of CO_2 sequestration on concrete performance and durability. As natural carbonation has had sufficient evidence to prove corrosion of rebars and deterioration to surrounding concrete, there are apprehensions within the engineering community to adopt CO_2 sequestering in concrete during the mixing stage. The results from this study would provide valuable insights for decision-makers to explore the implementation of CO_2 sequestering in concrete in the ready-mix concrete industry across the globe.

Limitations of this study:

- This study used commercially available pure CO_2 gas, as effluent CO_2 captured through carbon capture technologies was not readily available. As a result, the potential environmental benefits of using CO_2 captured from industrial effluent gases, its impact on concrete properties in both plastic and hardened stage and lowering its impact on the atmosphere, could not be fully assessed.
- The durability performance was evaluated under accelerated conditions, and long-term performance data for CO_2-sequestered concrete under natural exposure conditions is not unavailable.
- The study focused on a maximum CO_2 dosage of 1% by weight of cement, as increasing the dosage had an adverse impact on the workability of the concrete mix. The impact of higher dosages of durability has not been studied.
- The effects of different cement types and supplementary cementitious materials were not explored in this study.

Recommendations for Future Work:

- Experimental research on the use of CO_2 sourced from carbon capture technologies is required to assess the impact of industrial-grade effluent gases on fresh and hardened properties of concrete.
- Effect of CO_2-sequestration on the durability of concrete under natural environmental exposures over extended periods is required to validate the findings from the accelerated tests.
- Studies should focus on improving the workability of concrete at higher CO_2 dosages, and further exploration is needed to assess its impact on durability.
- The effect of different cement types and supplementary cementitious materials, along with their compatibility with CO_2 sequestration, should be studied to understand their impact on concrete performance in fresh and hardened stages.
- A life cycle assessment needs to be done to assess the environmental impacts of CO_2-sequestered concrete across all stages of its life cycle, including raw material extraction, production, usage, and end-of-life.

In a nutshell, the authors feel that sequestering CO_2 in concrete would help the concrete industry develop a green and sustainable building material.

Chapter 5 : Life Cycle Assessment (LCA) of CO_2 sequestered concrete

With a growing concern for the fast depletion of natural resources, the environmental impact of products needs to be assessed over their life cycle to determine whether the system remains productive indefinitely [179]. Hence, from the raw material extraction stage to the ultimate disposal end-of-life stage, an environmentally sustainable design has to be adopted. For this purpose, a Life Cycle Analysis (LCA) has to be adopted which assesses the possible impact the product has on the environment during its life cycle [180]. In the case of CO_2-sequestered concrete, LCA has been done to evaluate its environmental impact right from the raw material extraction stage to its final disposal, by offsetting the carbon added to concrete and taking into account the enhancement obtained in its durability and service life over control concrete.

To perform the LCA for CO_2-sequestered concrete with different CO_2 dosages (0.25%, 0.5%, 0.75%, and 1%) and compare it with control concrete for 40 MPa strength, ISO 14040:2006 [181] guidelines have been adopted in this study. This LCA study has been limited to calculating the Global Warming Potential (GWP) for CO_2-Sequestered concrete mixes and comparing them with the control concrete mix, mainly to focus on the carbon emissions and understand their impact on climate change. GWP is a direct measure of calculating GHGs in terms of their CO_2 equivalence [182]. As CO_2-sequestered concrete is specifically designed to permanently trap CO_2 by converting it to crystalline $CaCO_3$, GWP allows us to assess the impact of these mixes in mitigating climate change. A detailed LCA involves assessing the acidification potential, eutrophication potential, ozone layer depletion potential, smog potential, primary, non-renewal energy and fossil fuel consumption [181]. Limiting the scope of this study to the GWP allows for a focused evaluation of carbon emissions, simplifies data collection, and provides carbon footprint reduction values, before expanding it to broader environmental impacts [183].

5.1 Goal and Scope Definition

- **Objective**: Adding CO_2 to concrete offers twin benefits of mitigating climate change by trapping CO_2 permanently in concrete through the mineralization effect and enhancing microstructural and mechanical properties. This LCA aimed to assess the environmental impacts of CO_2-sequestered concrete with varying CO_2 dosages against control concrete for a compressive strength of 40 MPa.
- **Functional Unit**: In this study, a functional unit was defined as one cubic meter of 40 MPa concrete.
- **System Boundaries**: Cradle-to-grave analysis (from raw material extraction to the end-of-life disposal) approach was used to assess and compare the environmental impact of CO_2-sequestered concrete with control concrete.
- **Impact Categories**: GWP, energy consumption, water use, and resource depletion were estimated to understand the potential environmental benefits of CO_2-sequestered concrete over control concrete, if any.

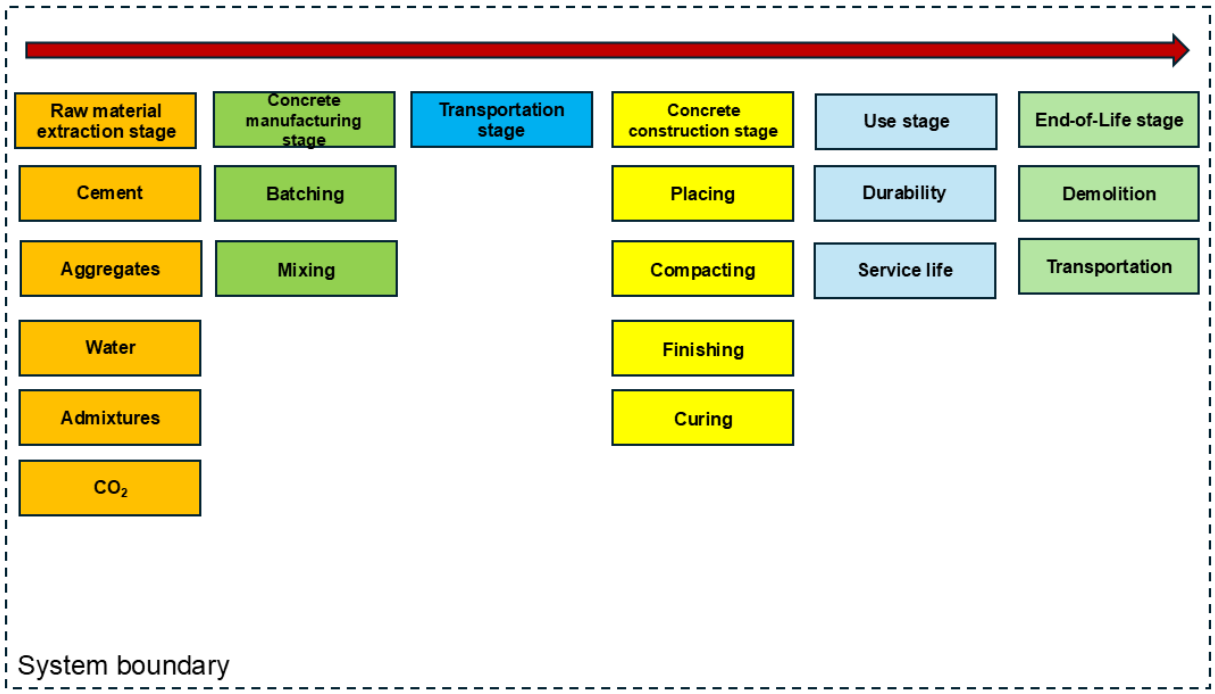

Figure 5.1 System boundary and process flow

System Boundaries Definitions

The cradle-to-grave system boundaries are defined according to the various raw materials and processes involved in the life cycle of both CO_2-sequestered concrete and control concrete, as are illustrated in Figure 5.1 and summarized below:

Raw material extraction stage (cradle)

- Cement- The manufacturing of cement is presently a high-carbon-intensive process. CO_2 emissions in cement production primarily stem from three sources- approximately 50% arises from the calcination or decomposition of limestone of $CaCO_3$, around 40% is generated from the fuel combustion in kilns, which is generally pulverized coal or PET coke and the balance 10% from manufacturing operation, transportation and electricity usage [30].
- Aggregates- The aggregates used may be extracted from a mine or a riverbed, crushed and washed, if necessary. The environmental considerations include energy usage, land disturbance, water consumption, and emissions from transportation to a concrete batching plant or construction site.
- Water- Water sourced for batching concrete has an environmental impact when extracted and treated. This excludes the footprint of the water used for other batching plant operations like washing transit mixers and maintenance of other plant machinery.
- Chemical admixtures- Superplasticizers, air-entraining agents, and some other admixtures are used to enhance the workability of concrete. Although they help to reduce the energy required to place concrete in its final position, a considerable amount of energy is used in manufacturing and emissions during transportation to the batching plant..

Concrete manufacturing stage- This stage involves batching and mixing of concrete ingredients and CO_2 sequestration. This stage has an environmental consideration with respect to the energy consumption for batching and mixing and the process for incorporating CO_2 in the mix.

Transportation of concrete to the construction site- Transportation of ready-mixed concrete from the batching plant to the construction site involves fuel usage and emissions from the concrete transit mixers or dump trucks.

Concrete construction at the site- Placing, vibrating, compaction, finishing, and curing involve energy and fuel usage for machinery, water usage for curing, and other emissions from on-site activities.

Use stage of the structure- The extended service life and durability and lowered maintenance of CO_2-sequestered concrete over control concrete reduces the frequency and the extent of maintenance or repairs, lowering the environmental impact.

End-of-Life (Grave)-The breaking down of concrete structures at the end of their useful life involves energy use, dust generation, and emissions from demolition machinery. As CO_2 is permanently captured in concrete through carbonation reactions, forming $CaCO_3$, it would remain embodied carbon, offering advantages over control concrete in terms of carbon retention.

Although CO_2 is injected into the concrete mix during the mixing stage, some environmental considerations are associated with the manufacturing or capturing process. If industrial CO_2 is captured as a byproduct from the industrial process, which is already being generated, it does not significantly add to overall emissions. Therefore, its impact is not accounted for in this study.

5.2 Life cycle Inventory analysis phase

In any LCA, the Life Cycle Inventory (LCI) analysis is an important step. This phase involves quantifying the input parameters related to energy consumption for manufacturing or extracting raw concrete materials and proportioning them to the mix design and energy consumption for various concreting processes. This phase also includes the end-of-life emissions associated with the life cycle of concrete. This study focuses on the LCI phase for 40 MPa concrete with varying CO_2 dosages (0.25%, 0.5%, 0.75%, and 1%), comparing it to a control concrete mix. This inventory analysis phase serves as the basis for calculating the GWP of the different concrete mixes. According to the experiments carried out and as detailed in Chapter 3, Table 5.1 summarizes the concrete mix design for 40 MPa concrete and various CO2 dosages.

Table 5.1 Concrete mix design for 40 MPa concrete and CO_2 dosage

Concrete Ingredients	**Grade 40 MPa**
Cement GUL (kg/m^3)	400
Water (kg/m^3)	160
Fine aggregate- Natural sand (kg/m^3)	712
Coarse aggregate (9.5 mm) (kg/m^3)	464
Coarse aggregate (19 mm) (kg/m^3)	567
Superplasticizer (kg/m^3)	1.2
Air Entraining Admixture (kg/m^3)	1.2
Theoretical bulk density (kg/m^3)	2305
Mass (kg) of CO_2 for 1 m^3 of concrete	
CO_2 Dosage	Weight (kg/m^3)
Control	0
0.25%	1
0.50%	2
0.75%	3
1%	4

Based on experimental data from various organizations and researchers, Table 5.2 outlines the energy flows into the system and output emissions. All concrete raw materials such as cement, water, aggregates and admixtures have been assumed to be sourced locally from Vancouver within a distance of 50 km from the batching plant and concrete is supplied within a distance of 50 km from the batching plant; this includes to and fro distances. Vazquez-Calle et al.[184] estimates the energy use in concrete production to be around 120 kWh/m^3. The emission factor for electricity used in Vancouver as provided by BC Building Code 2024 [185] is 0.011 kg CO_2 e/kWh. Energy consumed in construction activities at the site for concrete generally includes transporting and placing using concrete pumps or crane buckets, compaction using needle vibrators or surface vibrators, finishing using power trowels, and curing by water or membranes using appropriate equipment requires between 5 to 10 kWh/m^3 of energy, as obtained from Athena Sustainable Materials Institute LCI database. [186]. Furthermore, Athena's LCI database for construction, demolition and transportation indicates 15 to 30 kWh/m^3 of energy required. The energy consumed for manufacturing concrete, transporting, placing, vibrating, and finishing are referred to the LCI databases for the Vancouver location. Also, the emission factor for the energy consumed has been considered for the Vancouver location in this LCA calculation. Table 5.3 provides a calculation of the total GHG emissions of control concrete before CO_2 sequestration. Additionally, Table 5.4 indicates the net GHG emissions after CO_2 sequestration.

Table 5.2 Energy flows into the system and outputs emissions.

Material	Process	Mix Quantity / Production energy	Emission Factor (kg CO_2e/unit)	Reference
Cement	Cement Production	400 kg/m^3	0.75 kg CO_2e/kg cement	[187]
Water	Water extraction and treatment	160 kg/m^3	0.00032 kg CO_2e/kg water	[188]
Fine Aggregates (Natural)	Fine Aggregate Extraction and washing	712 kg/m^3	0.01 kg CO_2e/kg aggregate	[189]
Coarse Aggregates	Coarse Aggregate Extraction and crushing	1031 kg/m^3	0.01 kg CO_2e/kg aggregate	[189]
Superplasticizer	Superplasticizer Production	1.2 kg/m^3	1.02 kg CO_2e/kg admixture	[190]
Air Entraining Admixture	Air Entraining Admixture Production	1.2 kg/m^3	0.537 kg CO_2e/kg admixture	[190]
Concrete raw materials	Transportation of raw materials to plant	2305 kg/m^3	0.25 kg CO_2e/km per ton	[188]
Concrete	Batching and Mixing Energy	120 kWh/m^3	0.011 kg CO_2e/kWh	[184], [185]
Concrete	Transportation of concrete to site	2305 kg/m^3	0.25 kg CO_2e/km per ton	[188]
Concrete	On-Site-Placing, Vibration and Curing Energy	10 kWh/m^3	0.011 kg CO_2e/kWh	[185], [186]
Concrete	Demolition and transportation Energy	25 kWh/m^3	0.011 kg CO_2e/kWh	[185], [186]

5.3 Life cycle impact assessment phase

This phase involves calculating the CO_2 emissions for 1 m^3 of concrete based on the material extraction, manufacturing, transportation, construction, maintenance and end-of-life stages. Table 5.3 indicates the total GHG emissions of control concrete before CO_2 sequestration, calculated from Table 5.2. Defining the functional unit and system boundaries, identifying the emission sources across the life cycle stages and calculating the emissions provided a baseline emission of 379 CO_2e/m^3. These GHG emissions are calculated based on the cradle-to-grave life cycle assessment of concrete.

Table 5.3 Total GHG Emissions before CO_2 sequestration

Cradle-to-grave emissions	**Emissions CO_2e/m^3**
Cement production emissions	300
Water extraction emissions	0.05
Fine Aggregate production emissions	7.12
Coarse Aggregate production emissions	10.31
Superplasticizer production emissions	1.22
AEA production emissions	0.64
CO_2 dosing emissions	0.11
Concrete raw material transportation emissions	28.81
Batching and Mixing emissions	1.32
Transportation of concrete to site emissions	28.81
On-Site-Placing, Vibration and Curing emissions	0.11
Concrete demolition emissions	0.275
Total emissions	**379 CO_2e/m^3**

The same 40 MPa concrete mix design was fed into the carbon calculator of the National Ready Mixed Concrete Association (NRMCA) for a location near Vancouver, BC, in Washington State, USA (this calculator is designed for concrete manufactured in the US for a cradle-gate assessment). This calculator provided an emission of 355 kg CO_2e/m^3 as compared to our calculated value of 349 kg CO_2e/m^3 for a cradle-to-gate LCA. The difference of 6 kg CO_2e/m^3 has been mainly due to the different LCI values used in the calculations for the respective concrete manufacturing locations. The Tuutti model used to estimate the service life of concrete, as explained in Chapter 4, revealed that early-age carbonation helps to enhance the service life of reinforced concrete structures under aggressive environmental conditions. This extended service life and durability help to lower the frequency of maintenance of CO_2-sequestered concrete over control concrete, thereby reducing the environmental impact. ISO 14044:2020 [191] suggests normalizing accounting service life differences to a reference value. In the present case, the normalization of GWP can be used for lifecycle assessments of CO_2-sequestered concrete to compare it with control concrete to understand the sustainability performance over time. Table 5.4 indicates the net GHG emissions after CO_2 sequestration and the normalized GWP emissions estimated from the service life of concrete using the Tuutti model.

Table 5.4 Net GHG emissions and normalized GWP emissions

Dosage (% CO_2)	Sequestered CO_2 (kg/m^3)	Net GWP (kg CO_2e/m^3)	Service life ($T_{service}$ years)	Normalized GWP (kg CO_2e/m^3/year)
0% (Control)	0	379	24.6	15.4
0.25%	1	378	34.8	10.9
0.50%	2	377	33.4	11.3
0.75%	3	376	38.6	9.7
1%	4	375	36.3	10.3

5.4 Interpretation phase

Based on the LCA analysis for the concrete raw materials and the energy flows associated with raw material extraction, concrete production, transportation, and concreting operations at the site, which ranges from placement to curing, service life and maintenance during the use phase and end-of-life phase indicates that sequestering CO_2 into concrete helps reduce the carbon footprint to a small extent. Table 4 shows that the 0.75% CO_2 dosage mix shows the lowest normalized GWP value of 9.7 kg CO_2e/m³/year, indicating that this dosage provides optimal environmental performance. This has been due to a combination of CO_2 sequestration of 3 kg/m³ and the longest projected service life of 38.6 years compared to all the other mixes. In contrast, the control mix has the highest normalized GWP at 15.4 kg CO_2e/m³/year, making it less sustainable. Although the 1% mix achieves slightly higher sequestration of 4 kg/m³, in comparison with 0.75% CO_2 dosage, its shorter service life of 36.3 years diminishes its relative environmental benefit. Therefore, optimal sequestration efficiency was observed at 0.75%, with declining returns observed beyond 0.75% due to the reduction in the service life beyond this dosage.

5.5 Conclusions

This LCA, from raw material extraction to end-of-life disposal, with a primary focus on GWP, provides an overview of the potential environmental benefits of integrating CO2 during the manufacturing stage of concrete. The results highlight that adding CO_2 leads to a permanent trapping of CO_2 by converting it to $CaCO_3$ and enhancing the service life of structures thereby minimizing its environmental impact by reducing the resources involved in maintenance and repair.

This LCA accounted for the emissions associated with concrete raw material extraction and manufacturing, concrete batching, transporting, placing, vibrating, finishing and demolition at the end of its service life. The calculated baseline emissions for control concrete was 379 kg CO_2e/m³, while the CO_2-sequestered concrete indicated a net reduction in emissions with respect to the dosage. These results also closely align with the values obtained from the Concrete Carbon Calculator of NRMCA, which validates the calculations. Additionally, the net GHG emissions after the normalized GWP emissions estimated from the service life of concrete using the Tuutti model were lower for the CO_2-sequestered concrete in comparison to control concrete. The 0.75% CO_2-sequestered concrete mix achieved the lowest normalized global warming potential, a 37% reduction compared to the control mix, highlighting substantial environmental performance

Due to a higher initial investment and transportation cost, the cost of CO_2 from flu gases captured from the Carbon Capture, Utilization, and Storage (CCUS) technology is presently very high, approximately $100 USD/MT [53], which has been one of the setbacks. Additionally, the use of commercially available, industrial-grade CO_2 is also very expensive. However, the industrial carbon pricing in Canada, which is around $80 CAD/MT [192], could help to offset some of the material costs. While CO_2 sequestration improves sustainability, practical challenges like initial investment and CO_2 capturing and transportation cost needs be addressed. While this study primarily focused on GWP, future research should focus on other LCA indicators, such as acidification potential, eutrophication potential, ozone depletion, and resource depletion, to provide a more detailed sustainability assessment.

In conclusion, even though CO_2-sequestered concrete demonstrates a small reduction in the net GWP in comparison to control concrete, adoption of this technology in concrete production can provide the construction industry with an eco-friendly material to minimize the industry's carbon footprint, gain carbon credits and enhance the durability of concrete thereby minimizing maintenance and repair costs.

Chapter 6 : Concluding Remarks

Summary

Global warming is having an adverse effect on both human life and living organisms across the globe, which is endangering both health and safety. Climate change has been mainly due to rampant industrialization. As highlighted in the Paris Agreement 2015 on climate change, by the end of the 21st century, anthropogenic CO_2 emissions in all sectors, including construction, must be reduced to keep the global temperature rise below 2 °C [4]. As the cement and concrete industry is responsible for approximately 7% of global CO_2 emissions [9], the construction industry must take drastic steps to minimize its environmental impact. Research has shown that CO_2 can be added to concrete during the mixing or curing stage to enhance its mechanical properties. This study aimed to understand the impact of adding CO_2 during the mixing stage of concrete on the plastic, mechanical and microstructural properties, eventually minimizing the impact of CO_2 on the environment. In addition, it investigates the long-term effects of early-age carbonation on the durability of CO_2-sequestered concrete by evaluating its transport properties, freeze-thaw resistance, and corrosion behaviour under varying environmental conditions. For the experimental analysis, two grades of concrete, 25 MPa and 40 MPa, were analyzed using PLC, natural aggregates and chemical admixtures. A simple CO_2 dosing system was set up, and comprehensive mechanical testing was conducted for 90 days to study the impact of CO_2 on plastic properties, compressive strength, tensile strength and changes taking place at a microstructural level. To assess the impact of CO_2 added during the mixing stage on the long-term durability of concrete, permeability, chloride ion penetration, resistivity, freeze-thaw, and corrosion resistance were experimentally analyzed. The findings from this study reveal that CO2 dosages between 0.5% and 0.75% provided optimal results for compressive, flexural and split tensile strength, resistivity, stiffness and corrosion resistance compared to control concrete. However, the test results also revealed a threshold at 1% CO_2 addition, as observed in reducing these parameters.

Findings

Within the scope of this research, the following findings can be drawn from this study:

1. **Plastic properties**: Adding CO_2 to concrete reduced its workability and slump for dosages above 0.5%. This may be due to an increase in the heat of hydration resulting from a chemical process and longer mixing times during CO_2 addition. This issue was rectified with the addition of an extra dosage of the superplasticizer. However, a shorter CO_2 dosing and mixing time would help to minimize the slump issue. The semi-adiabatic calorimetry test results showed improved hydration with CO_2 addition, indicating a higher initial reaction rate. A peak temperature rise was observed at 0.75% CO_2 dosage, with all other dosages showing a higher reaction rate compared to control concrete.
2. **Mechanical properties:** Early-age carbonation showed a positive improvement in the mechanical properties of concrete. A higher compressive strength was observed, especially for the 0.75% dosage, with minor improvements in the flexural and split tensile strength of CO_2-sequestered concrete.

3. **Microstructure:** Thermal Pyrolysis test, microscopy and FTIR spectroscopy analysis indicated the formation of $CaCO_3$, mainly due to accelerated carbonation, thereby confirming the carbonation process. The reduction in porosity was also observed in the SEM images, which confirmed mineralization with the filling up of pores.

4. **Durability:** Adding CO_2 to concrete at the mixing stage densified the matrix, thereby enhancing its durability. This improvement was reflected in lower RCPT and permeability values and higher resistivity readings for dosages between 0.5% and 1%. A statistical analysis also indicated an improvement in the resistance of concrete to the transport of water and ions. The Pearson correlation coefficient for the coefficient of permeability and RCPT values indicate a strong positive correlation, suggesting that early-age carbonation reduces both parameters.

5. **Freeze-thaw resistance:** An enhancement in the resistance of concrete to freezing and thawing cycles was observed when concrete was subjected to early-age carbonation. CO_2 dosages between 0.5% and 0.75% showed improved performance to F-T cycles, as compared to control concrete, observed by lower mass loss, less surface scaling and increased stiffness. Higher dosages, 1% and above, could possibly reduce the F-T resistance due to the reduction in concrete porosity resulting from the mineralization and densification effect. The ANOVA results for the dynamic modulus calculated from the longitudinal, transverse, and torsional vibration frequency and UPV test values indicate a statistically significant relationship ($P < 0.05$). Additionally, the P curves tend to flatten or decrease between 0.5% and 0.75%, confirming that CO_2 dosages between 0.5% and 0.75% provide optimal performance when subjected to F-T cycles.

6. **Alternative wetting & drying cycles:** In the case of the accelerated corrosion test subjected to harsh environmental conditions and alternative wetting and drying cycles to accelerate corrosion, an improvement in resistance against corrosion was observed in samples subjected to CO_2 addition. Concrete slab panels in sets A and C were subjected to accelerated corrosion and showed enhanced resistance for dosages between 0.5% and 0.75% compared to control concrete and other dosages. In the case of concrete slab panels in set B, which was subjected to a highly aggressive environment, with high temperature during the drying cycle and 5% NaCl concentration during the wetting cycle, the corrosion rates increased significantly for all CO_2 dosages. This indicates that CO_2 alone cannot provide corrosion resistance in highly aggressive environmental conditions. In addition to high-grade concretes, supplementary cementitious materials and coatings on the rebars would be required to enhance the resistance of reinforced concrete to corrosion.

7. **pH of concrete**: Studies have revealed that natural carbonation causes the pH of concrete to fall below 9, which is indicated by the phenolphthalein colour changing to white when sprayed on the concrete surface. Conversely, though the concrete was subjected to accelerated carbonation, the alkalinity of the concrete was sufficiently high to resist the onset of corrosion, as observed by the pH of the concrete ($pH>12$), tested by the phenolphthalein indicator and the pH of the powdered concrete samples. A minor drop in the pH to 12.07 at 1% CO_2 dosage was observed, indicating a threshold in the dosage.

8. **Service life modelling**: Based on the experimental test results, Tuutti's model predicted the service life of concrete subjected to accelerated corrosion. The experimental results indicate that a CO_2 dosage between 0.5% and 0.75% enhanced the service life of reinforced concrete over control concrete.

9. **LCA:** The calculated baseline emissions for control concrete was 379 kg CO_2e/m^3, while the CO_2-sequestered concrete indicated a net reduction in emissions with respect to the dosage per cubic meter. Based on the LCA analysis, the mix with 0.75% CO_2 dosage showed the lowest normalized GWP value of 9.7 kg CO_2e/m^3/year, providing optimal environmental benefits. Conversely, the control mix has the highest normalized GWP at 15.4 kg CO_2e/m^3/year, making it less sustainable.

These findings reinforce our hypothesis that concrete specimens subjected to early-age carbonation will enhance the compressive and flexural strength by densifying the matrix due to the mineralization effect, maintain the alkalinity of concrete, decrease permeability and chloride ion ingress, enhance resistance to F-T cycles, and protect embedded rebars from corrosion.

Contributions to the body of knowledge

1. This study has laid a foundation for manufacturers to develop eco-friendly mixes by establishing a simplified CO2 sequestration process and developing a predictive model to estimate the compressive strength of concrete.

2. This research promotes a low-carbon construction material by permanently trapping CO_2 in concrete.

3. The test results from this study will help industry experts further advance the use of this innovative technique of sequestering CO_2 into concrete to make it green and sustainable.

4. This study eventually aims at an industrial-scale integration of CO_2 sequestration and maximizing its benefits in the ready-mix concrete business across the globe.

5. This study shows how CO_2 sequestration can lower the carbon footprint of concrete while also supporting the global sustainable development goals.

Limitations

The following limitations, which have been observed in this study, need further research:

1. This study used pure CO_2 gas available commercially, as effluent CO_2 gas captured through carbon capture technologies was not readily available. The effect of CO_2 captured from industrial emissions on the properties of concrete in plastic and hardened stages could not be determined.

2. During the experiments, CO_2 gas was injected into the mix at a dosage ranging from 0.1% to 1% by weight of cement. However, the amount of CO_2 lost in the injection process could not be quantified.

3. The loss in workability of concrete after CO_2 injection was rectified by an extra dose of the superplasticizer, which resulted in an increase in the overall mix cost.

4. This study could not explore CO_2 dosages above 1% (bwc) as it had an adverse effect on the workability of concrete.
5. PLC was used in the study, as other types of cement were not readily available. The effect of different types of cement and cementitious materials, as well as a broad range of humidity and temperatures, was not explored.
6. This study does not focus on large-scale deployment of CO_2-sequestered concrete in the field, including material and equipment cost, equipment and batching plant modifications and operational challenges.

Recommendations for Future Work

1. Further investigation is required to understand the effect of CO_2 captured from industrial emissions on concrete properties, as this would help to utilize effluent CO_2.
2. Studies should explore methods to resolve workability issues resulting from CO_2 addition without increasing the cost per cubic meter of concrete.
3. The effect of CO_2 addition on the different cement types and other cementitious materials available commercially needs to be analyzed.
4. Advanced analytical instruments and software tools can used for future research to assess carbon uptake in CO_2 sequestered concrete and quantification of losses during the injection process.
5. Future research needs to focus on field deployment and efficient implementation techniques for CO_2 sequestration in concrete across diverse engineering projects.
6. In order to validate the findings of this study which were adopted from the accelerated tests, future studies may focus on the effect of CO_2-sequestration on the durability of concrete under natural environmental conditions over an extended period of time.

Author's Final Reflections

With the global production of approximately 15 billion cubic metres of concrete annually [19], sequestering CO_2 in concrete can help the construction industry minimize its carbon footprint. This experimental approach and previous studies have shown that CO_2 addition per cubic meter of concrete is very small, with typical dosages ranging from 1-2 kg/m^3, without adversely hampering the plastic properties of concrete. While this dosage may seem very small, when expanded to economies of scale, the cumulative benefits can result in substantial reductions in minimizing the GHGs from the atmosphere.

However, certain challenges have hindered its widespread adoption in the construction industry. Presently, the energy costs associated with CO_2 capture, storage, and transportation exceed the economic cost of utilization in concrete, even when accounting for carbon credits to offset investment costs. Furthermore, concrete manufacturers do not find this technology lucrative as, presently, there are no government incentives or subsidies for producing low-carbon concrete. In addition, existing construction codes do not permit the addition of CO_2 during the mixing or curing

stage, making it difficult to comply with regulatory requirements. Additionally, higher CO_2 dosages (>0.75%) may alter the pore structure, marginally reduce alkalinity, and may cause localized microcracking due to ongoing $CaCO_3$ formation, leading to declining benefits.

To leverage the potential of CO_2 sequestration in concrete cost-effective carbon capture, storage and transportation systems, changes to construction codes and specifications and rewarding government policies are crucial for its widespread adoption. Addressing these challenges would help the construction industry adopt this sustainable and innovative technology to address the burning issue of climate change.

Bibliography

[1] "Industrial Revolution," *Wikipedia*. Oct. 11, 2024. Accessed: Oct. 15, 2024. [Online]. Available: https://en.wikipedia.org/w/index.php?title=Industrial_Revolution&oldid=1250691377

[2] "Since 1850, these historical events have accelerated climate change," World Economic Forum. Accessed: Jun. 13, 2024. [Online]. Available: https://www.weforum.org/agenda/2021/02/global-warming-climate-change-historical-human-development-industrial-revolution/

[3] "Global CO2 emissions by year 1940-2023," Statista. Accessed: Jun. 13, 2024. [Online]. Available: https://www.statista.com/statistics/276629/global-co2-emissions/

[4] "The Paris Agreement | UNFCCC." Accessed: Oct. 17, 2023. [Online]. Available: https://unfccc.int/process-and-meetings/the-paris-agreement

[5] "Carbon capture, utilization and storage – How it works and benefits | Alberta.ca." Accessed: Jun. 13, 2024. [Online]. Available: https://www.alberta.ca/carbon-capture-utilization-and-storage-how-it-works-and-benefits

[6] N. R. Canada, "Canada's Carbon Management Strategy." Accessed: Jun. 13, 2024. [Online]. Available: https://natural-resources.canada.ca/climate-change/canadas-green-future/capturing-the-opportunity-carbon-management-strategy-for-canada/canadas-carbon-management-strategy/25337

[7] O. Guirdham, "Global Ready Mix Concrete Market Forecast 2024-2033 – Market Size, Drivers, Trends, And Competitors," EIN Presswire. Accessed: Jun. 18, 2024. [Online]. Available: https://www.einpresswire.com/article/676256777/global-ready-mix-concrete-market-forecast-2024-2033-market-size-drivers-trends-and-competitors

[8] "Cement production global 2023," Statista. Accessed: Jun. 14, 2024. [Online]. Available: https://www.statista.com/statistics/1087115/global-cement-production-volume/

[9] S. and E. D. C. Innovation, "Government of Canada and Cement Association of Canada launch Roadmap to Net-Zero Carbon Concrete by 2050." Accessed: Dec. 19, 2023. [Online]. Available: https://www.canada.ca/en/innovation-science-economic-development/news/2022/11/government-of-canada-and-cement-association-of-canada-launch-roadmap-to-net-zero-carbon-concrete-by-2050.html

[10] F. Winnefeld, A. Leemann, A. German, and B. Lothenbach, "CO2 storage in cement and concrete by mineral carbonation," *Current Opinion in Green and Sustainable Chemistry*, vol. 38, p. 100672, Dec. 2022, doi: 10.1016/j.cogsc.2022.100672.

[11] M. Fernández Bertos, S. J. R. Simons, C. D. Hills, and P. J. Carey, "A review of accelerated carbonation technology in the treatment of cement-based materials and sequestration of CO2," *Journal of Hazardous Materials*, vol. 112, no. 3, pp. 193–205, Aug. 2004, doi: 10.1016/j.jhazmat.2004.04.019.

[12] M. Auroy *et al.*, "Comparison between natural and accelerated carbonation (3% CO2): Impact on mineralogy, microstructure, water retention and cracking," *Cement and Concrete Research*, vol. 109, pp. 64–80, Jul. 2018, doi: 10.1016/j.cemconres.2018.04.012.

[13] N. L. M. Kamal, Z. Itam, Y. Sivaganese, and S. Beddu, "Carbon dioxide sequestration in concrete and its effects on concrete compressive strength," *Materials Today: Proceedings*, vol. 31, pp. A18–A21, Jan. 2020, doi: 10.1016/j.matpr.2020.11.185.

[14] J. Zhu, S. Liu, L. Song, Z. Qu, and H. Wang, "Influence of Carbon Dioxide Curing on the Corrosion Resistance of Reinforced Cement Mortar under the External Erosion of NaCl Freeze–Thaw Cycle," *Applied Sciences*, vol. 12, no. 10, Art. no. 10, Jan. 2022, doi: 10.3390/app12105061.

[15] W. Ashraf, “Carbonation of cement-based materials: Challenges and opportunities,” *Construction and Building Materials*, vol. 120, pp. 558–570, Sep. 2016, doi: 10.1016/j.conbuildmat.2016.05.080.
[16] K. Ahmed Ali, M. Ahmad, and Y. Yusup, “Issues, Impacts, and Mitigations of Carbon Dioxide Emissions in the Building Sector,” *Sustainability*, vol. 12, p. 7427, Sep. 2020, doi: 10.3390/su12187427.
[17] O. US EPA, “Greenhouse Gases.” Accessed: Dec. 19, 2023. [Online]. Available: https://www.epa.gov/report-environment/greenhouse-gases
[18] “Global CO2 emissions by year 1940-2022,” Statista. Accessed: Oct. 17, 2023. [Online]. Available: https://www.statista.com/statistics/276629/global-co2-emissions/
[19] “Global cement and concrete industry announces roadmap to achieve groundbreaking ‘net zero’ co2 emissions by 2050,” GCCA. Accessed: Dec. 19, 2023. [Online]. Available: https://gccassociation.org/news/global-cement-and-concrete-industry-announces-roadmap-to-achieve-groundbreaking-net-zero-co2-emissions-by-2050/
[20] M. Kazemian and B. Shafei, “Carbon sequestration and storage in concrete: A state-of-the-art review of compositions, methods, and developments,” *Journal of CO2 Utilization*, vol. 70, p. 102443, Apr. 2023, doi: 10.1016/j.jcou.2023.102443.
[21] Y. Shao, “Beneficial Use of Carbon Dioxide in Precast Concrete Production,” 1155035, Jun. 2014. doi: 10.2172/1155035.
[22] S. Monkman, M. MacDonald, and L. Sutter, “Beneficiation of concrete wash water with carbon dioxide,” *Materials and Structures*, vol. 54, p. 64, Mar. 2021, doi: 10.1617/s11527-021-01642-9.
[23] R. Wang and Y. X. Zhang, “Recycling fresh concrete waste: A review,” *Structural Concrete*, vol. 19, no. 6, pp. 1939–1955, 2018, doi: 10.1002/suco.201800057.
[24] A. D’Alessandro, C. Fabiani, A. L. Pisello, F. Ubertini, A. Materazzi, and F. Cotana, “Innovative concretes for low carbon constructions: a review,” *International Journal of Low-Carbon Technologies*, May 2016, doi: 10.1093/ijlct/ctw013.
[25] “Carbon Capture, Utilisation and Storage - Energy System,” IEA. Accessed: Oct. 17, 2023. [Online]. Available: https://www.iea.org/energy-system/carbon-capture-utilisation-and-storage
[26] S. Monkman, P. A. Kenward, G. Dipple, M. MacDonald, and M. Raudsepp, “Activation of cement hydration with carbon dioxide,” *Journal of Sustainable Cement-Based Materials*, vol. 7, no. 3, pp. 160–181, May 2018, doi: 10.1080/21650373.2018.1443854.
[27] S. Monkman, M. MacDonald, R. D. Hooton, and P. Sandberg, “Properties and durability of concrete produced using CO2 as an accelerating admixture,” *Cement and Concrete Composites*, vol. 74, pp. 218–224, Nov. 2016, doi: 10.1016/j.cemconcomp.2016.10.007.
[28] “Cement production global 2022,” Statista. Accessed: Dec. 26, 2023. [Online]. Available: https://www.statista.com/statistics/1087115/global-cement-production-volume/
[29] “Cement-International Energy Agency (IEA),” IEA. Accessed: Dec. 26, 2023. [Online]. Available: https://www.iea.org/energy-system/industry/cement
[30] M. Hanifa, R. Agarwal, U. Sharma, P. C. Thapliyal, and L. P. Singh, “A review on CO2 capture and sequestration in the construction industry: Emerging approaches and commercialised technologies,” *Journal of CO2 Utilization*, vol. 67, p. 102292, Jan. 2023, doi: 10.1016/j.jcou.2022.102292.
[31] S. Gupta, B. N. Mohapatra, and M. Bansal, “A review on development of Portland limestone cement: A step towards low carbon economy for Indian cement industry,” *Current Research in Green and Sustainable Chemistry*, vol. 3, p. 100019, Jun. 2020, doi: 10.1016/j.crgsc.2020.100019.
[32] N. Voglis, G. Kakali, E. Chaniotakis, and S. Tsivilis, “Portland-limestone cements. Their properties and hydration compared to those of other composite cements,” *Cement and*

Concrete Composites, vol. 27, no. 2, pp. 191–196, Feb. 2005, doi: 10.1016/j.cemconcomp.2004.02.006.
[33] H. Mikulčić, J. J. Klemeš, M. Vujanović, K. Urbaniec, and N. Duić, “Reducing greenhouse gasses emissions by fostering the deployment of alternative raw materials and energy sources in the cleaner cement manufacturing process,” *Journal of Cleaner Production*, vol. 136, pp. 119–132, Nov. 2016, doi: 10.1016/j.jclepro.2016.04.145.
[34] “LC3 – Limestone Calcined Clay Cement.” Accessed: Jan. 16, 2024. [Online]. Available: https://lc3.ch/
[35] K. Scrivener, F. Martirena, S. Bishnoi, and S. Maity, “Calcined clay limestone cements (LC3),” *Cement and Concrete Research*, vol. 114, pp. 49–56, Dec. 2018, doi: 10.1016/j.cemconres.2017.08.017.
[36] D. Zhang, Z. Ghouleh, and Y. Shao, “Review on carbonation curing of cement-based materials,” *Journal of CO2 Utilization*, vol. 21, pp. 119–131, Oct. 2017, doi: 10.1016/j.jcou.2017.07.003.
[37] M. Achternboscha and P. Stemmermannb, “The carbon uptake by carbonation of concrete structures – some remarks by perspective of TA,” 2021. Accessed: Apr. 09, 2024. [Online]. Available: https://www.semanticscholar.org/paper/The-carbon-uptake-by-carbonation-of-concrete-%E2%80%93-some-Achternboscha-Stemmermannb/9ddd70738a85cd7b1b428f667e943e167c43a332
[38] Z. Huang *et al.*, “Global carbon uptake of cement carbonation accounts 1930–2021,” *Earth System Science Data*, vol. 15, no. 11, pp. 4947–4958, Nov. 2023, doi: 10.5194/essd-15-4947-2023.
[39] I. Odler, “6 - Hydration, Setting and Hardening of Portland Cement,” in *Lea’s Chemistry of Cement and Concrete (Fourth Edition)*, P. C. Hewlett, Ed., Oxford: Butterworth-Heinemann, 1998, pp. 241–297. doi: 10.1016/B978-075066256-7/50018-7.
[40] U. M. Angst, “Steel corrosion in concrete – Achilles’ heel for sustainable concrete?,” *Cement and Concrete Research*, vol. 172, p. 107239, Oct. 2023, doi: 10.1016/j.cemconres.2023.107239.
[41] X. Jia, T.-C. Ling (Bill), H. Mehdizadeh, and K. H. Mo, “Impact of CO2 curing on the microhardness and strength of 0.35 w/c cement paste: Comparative study of internal/surface layers,” *Journal of Materials Research and Technology*, vol. 9, pp. 11849–11860, Sep. 2020, doi: 10.1016/j.jmrt.2020.08.051.
[42] N. Li, L. Mo, and C. Unluer, “Emerging CO2 utilization technologies for construction materials: A review,” *Journal of CO2 Utilization*, vol. 65, p. 102237, Nov. 2022, doi: 10.1016/j.jcou.2022.102237.
[43] “CarbonCure’s Sustainable Concrete Solution,” CarbonCure Technologies Inc. Accessed: Dec. 30, 2023. [Online]. Available: https://www.carboncure.com/
[44] G. S. Monkman, K. Cail, P. J. Sandberg, M. MacDonald, J. J. Brown, and D. P. Forgeron, “Methods and compositions for concrete production,” US10927042B2, Feb. 23, 2021 Accessed: Jan. 02, 2024. [Online]. Available: https://patents.google.com/patent/US10927042B2/en?assignee=Carboncure&oq=Carboncure
[45] H. M. de Paula, M. S. de Oliveira Ilha, and L. S. Andrade, “Concrete plant wastewater treatment process by coagulation combining aluminum sulfate and Moringa oleifera powder,” *Journal of Cleaner Production*, vol. 76, pp. 125–130, Aug. 2014, doi: 10.1016/j.jclepro.2014.04.031.
[46] V. Rostami, Y. Shao, and A. J. Boyd, “Durability of concrete pipes subjected to combined steam and carbonation curing,” *Construction and Building Materials*, vol. 25, no. 8, pp. 3345–3355, Aug. 2011, doi: 10.1016/j.conbuildmat.2011.03.025.
[47] M. Mahoutian and M. Venditti, “Systems and methods for curing a precast concrete product,” EP4051474A1, Sep. 07, 2022 Accessed: Jan. 03, 2024. [Online]. Available:

https://patents.google.com/patent/EP4051474A1/en?q=(CO2)&assignee=Carbicrete&oq=Carbicrete+CO2
[48] “CarbonBuilt Ultra-Low Carbon Concrete for Green Construction.” Accessed: Jan. 03, 2024. [Online]. Available: https://carbonbuilt.com/
[49] Castro-Alonso, L. Montañez-Hernandez, M. Muñoz, M. Franco, R. Narayanasamy, and N. Balagurusamy, “Microbially Induced Calcium Carbonate Precipitation (MICP) and Its Potential in Bioconcrete: Microbiological and Molecular Concepts,” *Frontiers in Materials*, vol. 6, p. 126, Jun. 2019, doi: 10.3389/fmats.2019.00126.
[50] A. Alshalif, J. M. Irwan, N. Othman, E. Ing. A. Al-Gheethi, and S. Shamsudin, “A systematic review on bio-sequestration of carbon dioxide in bio-concrete systems: a future direction,” *European Journal of Environmental and Civil Engineering*, vol. 26, pp. 1–20, Feb. 2020, doi: 10.1080/19648189.2020.1713899.
[51] W. Mwandira, M. Mavroulidou, M. Gunn, D. Purchase, H. Garelick, and J. Garelick, “Concurrent Carbon Capture and Biocementation through the Carbonic Anhydrase (CA) Activity of Microorganisms -a Review and Outlook,” *Environmental Processes*, vol. 10, Sep. 2023, doi: 10.1007/s40710-023-00667-2.
[52] S. Kashef-Haghighi and S. Ghoshal, “CO2 Sequestration in Concrete through Accelerated Carbonation Curing in a Flow-through Reactor,” *Ind. Eng. Chem. Res.*, vol. 49, no. 3, pp. 1143–1149, Feb. 2010, doi: 10.1021/ie900703d.
[53] “Is carbon capture too expensive? – Analysis,” IEA. Accessed: Jan. 04, 2024. [Online]. Available: https://www.iea.org/commentaries/is-carbon-capture-too-expensive
[54] C. Pereira and R. Gupta, “Exploring the impact of CO2 sequestration on plastic properties, mechanical performance, and microstructure of concrete,” *Discov Civ Eng*, vol. 1, no. 1, p. 144, Dec. 2024, doi: 10.1007/s44290-024-00151-2.
[55] E. and C. C. Canada, “Causes of climate change.” Accessed: Jun. 13, 2024. [Online]. Available: https://www.canada.ca/en/environment-climate-change/services/climate-change/causes.html
[56] D. Narita, “Managing uncertainties: The making of the IPCC’s Special Report on Carbon Dioxide Capture and Storage,” *Public Underst Sci*, vol. 21, no. 1, pp. 84–100, Jan. 2012, doi: 10.1177/0963662510367710.
[57] “Atmospheric CO2 ppm by year 1959-2023,” Statista. Accessed: Jun. 13, 2024. [Online]. Available: https://www.statista.com/statistics/1091926/atmospheric-concentration-of-co2-historic/
[58] B. Lei, W. Yang, Y. Yan, S. Zaland, Z. Tang, and W. Dong, “Carbon-saving benefits of various end-of-life strategies for different types of building structures,” *Developments in the Built Environment*, vol. 16, p. 100264, Dec. 2023, doi: 10.1016/j.dibe.2023.100264.
[59] B. Lei, W. Yang, Y. Yan, Z. Tang, and W. Dong, “Carbon Emission Reduction Evaluation of End-of-Life Buildings Based on Multiple Recycling Strategies,” *Sustainability*, vol. 15, no. 22, Art. no. 22, Jan. 2023, doi: 10.3390/su152215711.
[60] B. Šavija and M. Luković, “Carbonation of cement paste: Understanding, challenges, and opportunities,” *Construction and Building Materials*, vol. 117, pp. 285–301, Aug. 2016, doi: 10.1016/j.conbuildmat.2016.04.138.
[61] M. Basheer, D. P. Russell, and G. I. B. Rankin, “Design of concrete to resist carbonation: 8th International Conference on Durability of Building Materials and Components (8dbmc),” May 1999, pp. 423–435.
[62] X. Qian, J. Wang, Y. Fang, and L. Wang, “Carbon dioxide as an admixture for better performance of OPC-based concrete,” *Journal of CO2 Utilization*, vol. 25, pp. 31–38, May 2018, doi: 10.1016/j.jcou.2018.03.007.
[63] M. Wang, S. Luo, B. T. Pham, and T.-C. Ling, “Effect of CO2-mixing dose and prolonged mixing time on fresh and hardened properties of cement pastes,” *J. Zhejiang Univ. Sci. A*, vol. 24, no. 10, pp. 886–897, Oct. 2023, doi: 10.1631/jzus.A2200571.

[64] J. M. Bukowski and R. L. Berger, “Reactivity and strength development of CO2 activated non-hydraulic calcium silicates,” *Cement and Concrete Research*, vol. 9, no. 1, pp. 57–68, Jan. 1979, doi: 10.1016/0008-8846(79)90095-4.
[65] B. Lagerblad, “Carbon dioxide uptake during concrete life cycle - State of the art,” *Swedish Cement and Concrete Research Institute*, Jan. 2005.
[66] M. A. Peter, A. Muntean, S. A. Meier, and M. Böhm, “Competition of several carbonation reactions in concrete: A parametric study,” *Cement and Concrete Research*, vol. 38, no. 12, pp. 1385–1393, Dec. 2008, doi: 10.1016/j.cemconres.2008.09.003.
[67] D. Adedokun, J. Ndambuki, and W. Salim, “Improving Carbon Sequestration in Concrete: A Literature Review,” Apr. 2013.
[68] N. C. Collier, “Transition and decomposition temperatures of cement phases - A collection of thermal analysis data,” *Ceramics - Silikaty*, pp. 338–343, Sep. 2016, doi: 10.13168/cs.2016.0050.
[69] D. Zhang and Y. Shao, “Early age carbonation curing for precast reinforced concretes,” *Construction and Building Materials*, vol. 113, pp. 134–143, Jun. 2016, doi: 10.1016/j.conbuildmat.2016.03.048.
[70] D. P. Bentz and P. E. Stutzman, “Curing, Hydration, and Microstructure of Cement Paste,” *NIST*, vol. 103, no. No. 5, pp. 348–356, Sep. 2006.
[71] K. Scrivener, “A practical guide to microstructural analysis of cementitious materials,” *(No Title)*, Accessed: Jul. 05, 2024. [Online]. Available: https://cir.nii.ac.jp/crid/1130282271270586240
[72] L. Alarcon-Ruiz, G. Platret, E. Massieu, and A. Ehrlacher, “The use of thermal analysis in assessing the effect of temperature on a cement paste,” *Cement and Concrete Research*, vol. 35, no. 3, pp. 609–613, Mar. 2005, doi: 10.1016/j.cemconres.2004.06.015.
[73] Q. Zhang *et al.*, “Utilization of solid wastes to sequestrate carbon dioxide in cement-based materials and methods to improve carbonation degree: A review,” *Journal of CO2 Utilization*, vol. 72, p. 102502, Jun. 2023, doi: 10.1016/j.jcou.2023.102502.
[74] G. Villain, M. Thiery, and G. Platret, “Measurement methods of carbonation profiles in concrete: Thermogravimetry, chemical analysis and gammadensimetry,” *Cement and Concrete Research*, vol. 37, no. 8, pp. 1182–1192, Aug. 2007, doi: 10.1016/j.cemconres.2007.04.015.
[75] F. Kaddah, E. Roziere, H. Ranaivomanana, and O. Amiri, “Complementary use of thermogravimetric analysis and oven to assess the composition and bound CO2 content of recycled concrete aggregates,” *Developments in the Built Environment*, vol. 15, p. 100184, Oct. 2023, doi: 10.1016/j.dibe.2023.100184.
[76] P. E. Stutzman, “Scanning Electron Microscopy in Concrete Petrography,” *NIST*, Nov. 2000, Accessed: Jan. 19, 2024. [Online]. Available: https://www.nist.gov/publications/scanning-electron-microscopy-concrete-petrography
[77] M.-G. Parvan, G. Voicu, A.-I. Badanoiu, A.-I. Nicoara, and E. Vasile, “CO2 Sequestration in the Production of Portland Cement Mortars with Calcium Carbonate Additions,” *Nanomaterials*, vol. 11, no. 4, Art. no. 4, Apr. 2021, doi: 10.3390/nano11040875.
[78] B. Liu, J. Qin, J. Shi, J. Jiang, X. Wu, and Z. He, “New perspectives on utilization of CO2 sequestration technologies in cement-based materials,” *Construction and Building Materials*, vol. 272, p. 121660, Feb. 2021, doi: 10.1016/j.conbuildmat.2020.121660.
[79] R. L. Berger, J. F. Young, and K. Leung, “Acceleration of Hydration of Calcium Silicates by Carbon Dioxide Treatment,” *Nature Physical Science*, vol. 240, no. 97, pp. 16–18, Nov. 1972, doi: 10.1038/physci240016a0.
[80] J. Kalkreuth, A. Ullrich, K. Garbev, D. Merz, P. Stemmermann, and D. Stapf, “Accelerated carbonation of hardened cement paste: Quantification of calcium carbonate via ATR infrared spectroscopy,” *Journal of the American Ceramic Society*, vol. 107, no. 4, pp. 2627–2640, 2024, doi: 10.1111/jace.19546.

[81] V. H. J. M. dos Santos *et al.*, “Application of Fourier Transform infrared spectroscopy (FTIR) coupled with multivariate regression for calcium carbonate (CaCO3) quantification in cement,” *Construction and Building Materials*, vol. 313, p. 125413, Dec. 2021, doi: 10.1016/j.conbuildmat.2021.125413.
[82] S. Nasrazadani, R. Eghtesad, E. Sudoi, S. Vupputuri, J. D. Ramsey, and M. T. Ley, “Application of Fourier transform infrared spectroscopy to study concrete degradation induced by biogenic sulfuric acid,” *Mater Struct*, vol. 49, no. 5, pp. 2025–2034, May 2016, doi: 10.1617/s11527-015-0631-5.
[83] R. Choudhary, R. Gupta, and R. Nagar, “Impact on fresh, mechanical, and microstructural properties of high strength self-compacting concrete by marble cutting slurry waste, fly ash, and silica fume,” *Construction and Building Materials*, vol. 239, p. 117888, Apr. 2020, doi: 10.1016/j.conbuildmat.2019.117888.
[84] J. Kalkreuth, A. Ullrich, K. Garbev, D. Merz, P. Stemmermann, and D. Stapf, “Accelerated carbonation of hardened cement paste: Quantification of calcium carbonate via ATR infrared spectroscopy,” *Journal of the American Ceramic Society*, vol. 107, Nov. 2023, doi: 10.1111/jace.19546.
[85] I. García Lodeiro, D. E. Macphee, A. Palomo, and A. Fernández-Jiménez, “Effect of alkalis on fresh C–S–H gels. FTIR analysis,” *Cement and Concrete Research*, vol. 39, no. 3, pp. 147–153, Mar. 2009, doi: 10.1016/j.cemconres.2009.01.003.
[86] P. Yu, R. J. Kirkpatrick, B. Poe, P. F. McMillan, and X. Cong, “Structure of Calcium Silicate Hydrate (C-S-H): Near-, Mid-, and Far-Infrared Spectroscopy,” *Journal of the American Ceramic Society*, vol. 82, no. 3, pp. 742–748, 1999, doi: 10.1111/j.1151-2916.1999.tb01826.x.
[87] S. Abd.El.Aleem, M. Heikal, and W. M. Morsi, “Hydration characteristic, thermal expansion and microstructure of cement containing nano-silica,” *Construction and Building Materials*, vol. 59, pp. 151–160, May 2014, doi: 10.1016/j.conbuildmat.2014.02.039.
[88] ASTM International, “ASTM C33/C33M-18 Standard Specification for Concrete Aggregates.” Accessed: Aug. 26, 2023. [Online]. Available: https://www.astm.org/c0033_c0033m-18.html
[89] ASTM International, “ASTM C136-06 Standard Test Method for Sieve Analysis of Fine and Coarse Aggregates.” Accessed: Aug. 26, 2023. [Online]. Available: https://www.astm.org/c0136-06.html
[90] “ASTM C494-Standard Specification for Chemical Admixtures for Concrete.” Accessed: Apr. 05, 2024. [Online]. Available: https://www.astm.org/c0494_c0494m-17.html
[91] “ASTM C260-10-Standard Specification for Air-Entraining Admixtures for Concrete.” Accessed: Jul. 07, 2024. [Online]. Available: https://www.astm.org/c0260-10.html
[92] “Sika Construction chemicals.” Accessed: Nov. 18, 2024. [Online]. Available: https://can.sika.com/en/download-center.html
[93] “ACI PRC-211.1-91: Standard Practice for Selecting Proportions for Normal, Heavyweight, and Mass Concrete (Reapproved 2009).” Accessed: Aug. 26, 2023. [Online]. Available: https://www.concrete.org/store/productdetail.aspx?ItemID=211191&Format=DOWNLOAD&Language=English&Units=US_Units
[94] CSA group, “CSA A23.1:19/CSA A23.2:19,” CSA Group. Accessed: Jul. 08, 2024. [Online]. Available: https://www.csagroup.org/store/product/CSA%20A23.1%3A19-CSA%20A23.2%3A19/?gad_source=1&gclid=CjwKCAjwnK60BhA9EiwAmpHZwxVgF3gkX8YO2YtZ5dMJ4asyyE1TY9JfR89GshdOmKBM0vZJjHI09RoCy88QAvD_BwE
[95] ASTM International, “ASTM C192/C192M-14 Standard Practice for Making and Curing Concrete Test Specimens in the Laboratory.” Accessed: Aug. 26, 2023. [Online]. Available: https://www.astm.org/c0192_c0192m-14.html

[96] “e-4574-carbon-dioxide-safety-data-sheet-sds.pdf.” Accessed: Aug. 30, 2024. [Online]. Available: https://www.lindecanada.ca/-/media/corporate/praxair-canada/documents-en/safety-data-sheet-linde-canada/e-4574-carbon-dioxide-safety-data-sheet-sds.pdf?la=en-ca
[97] “Empirical Math Model: Ideal Gas Law,” Energy.gov. Accessed: Jul. 14, 2024. [Online]. Available: https://www.energy.gov/ne/articles/empirical-math-model-ideal-gas-law
[98] “Mole to volume and weight conversions for common compounds.” Accessed: Sep. 05, 2024. [Online]. Available: https://www.aqua-calc.com/calculate/mole-to-volume-and-weight
[99] “ASTM C143/C143M-12 Standard Test Method for Slump of Hydraulic-Cement Concrete.” Accessed: Jul. 08, 2024. [Online]. Available: https://www.astm.org/c0143_c0143m-12.html
[100] “ASTM C231-09a Standard Test Method for Air Content of Freshly Mixed Concrete by the Pressure Method.” Accessed: Jul. 08, 2024. [Online]. Available: https://www.astm.org/c0231-09a.html
[101] “ASTM C39/C39M-21-Standard Test Method for Compressive Strength of Cylindrical Concrete Specimens.” Accessed: Apr. 05, 2024. [Online]. Available: https://www.astm.org/c0039_c0039m-21.html
[102] “ASTM C496-96-Standard Test Method for Splitting Tensile Strength of Cylindrical Concrete Specimens.” Accessed: Jul. 08, 2024. [Online]. Available: https://www.astm.org/c0496-96.html
[103] “ASTM C78-09 Standard Test Method for Flexural Strength of Concrete (Using Simple Beam with Third-Point Loading).” Accessed: Jul. 08, 2024. [Online]. Available: https://www.astm.org/c0078-09.html
[104] J. Dweck, P. M. Buchler, A. C. V. Coelho, and F. K. Cartledge, “Hydration of a Portland cement blended with calcium carbonate,” *Thermochimica Acta*, vol. 346, no. 1, pp. 105–113, Mar. 2000, doi: 10.1016/S0040-6031(99)00369-X.
[105] “ACI CODE-318-19(22): Building Code Requirements for Structural Concrete and Commentary (Reapproved 2022).” Accessed: Jul. 12, 2024. [Online]. Available: https://www.concrete.org/store/productdetail.aspx?ItemID=318U19&Language=English&Units=US_Units
[106] N. K. Lee and H. K. Lee, “Setting and mechanical properties of alkali-activated fly ash/slag concrete manufactured at room temperature,” *Construction and Building Materials*, vol. 47, pp. 1201–1209, Oct. 2013, doi: 10.1016/j.conbuildmat.2013.05.107.
[107] S. Mindess, J. F. Young, and D. Darwin, *Concrete*. in Prentice-Hall civil engineering and engineering mechanics series. Prentice Hall, 2003. [Online]. Available: https://books.google.ca/books?id=euMXnwEACAAJ
[108] P. Schober, C. Boer, and L. A. Schwarte, “Correlation Coefficients: Appropriate Use and Interpretation,” *Anesthesia & Analgesia*, vol. 126, no. 5, p. 1763, May 2018, doi: 10.1213/ANE.0000000000002864.
[109] “CarbonCure’s Impact on Concrete Mixture Type GU Cement – Mix Optimization - CarbonCure,” CarbonCure Technologies Inc. Accessed: Nov. 18, 2024. [Online]. Available: https://www.carboncure.com/resources/carboncures-impact-on-concrete-mixture-type-gu-cement-mix-optimization/
[110] S. Monkman, “Utilization of CO2 in Ready Mixed Concrete Production: A Project Case Study”.
[111] S. Rashid and M. Singh, “An Investigation on Carbon Dioxide Incorporated Sustainable Ready-Mix Concrete Using OPC and PPC,” *Arab J Sci Eng*, vol. 48, no. 10, pp. 14213–14236, Oct. 2023, doi: 10.1007/s13369-023-08106-y.
[112] D. Suescum-Morales, J. M. Fernández-Rodríguez, and J. R. Jiménez, “Use of carbonated water to improve the mechanical properties and reduce the carbon footprint of cement-

based materials with recycled aggregates," *Journal of CO2 Utilization*, vol. 57, p. 101886, Mar. 2022, doi: 10.1016/j.jcou.2022.101886.
[113] Y.-C. Wang, M.-G. Lee, W.-C. Wang, Y.-C. Kan, S.-H. Kao, and H.-W. Chang, "CO2 Curing on the Mechanical Properties of Portland Cement Concrete," *Buildings*, vol. 12, no. 6, Art. no. 6, Jun. 2022, doi: 10.3390/buildings12060817.
[114] B. Dziejarski, R. Krzyżyńska, and K. Andersson, "Current status of carbon capture, utilization, and storage technologies in the global economy: A survey of technical assessment," *Fuel*, vol. 342, p. 127776, Jun. 2023, doi: 10.1016/j.fuel.2023.127776.
[115] A. F. A. Fuhaid and A. Niaz, "Carbonation and Corrosion Problems in Reinforced Concrete Structures," *Buildings*, vol. 12, no. 5, Art. no. 5, May 2022, doi: 10.3390/buildings12050586.
[116] A. Leemann and F. Moro, "Carbonation of concrete: the role of CO2 concentration, relative humidity and CO2 buffer capacity," *Materials and Structures/Materiaux et Constructions*, vol. 50, no. 1, 2017, doi: 10.1617/s11527-016-0917-2.
[117] R. A. Robayo-Salazar, A. M. Aguirre-Guerrero, and R. Mejía de Gutiérrez, "Carbonation-induced corrosion of alkali-activated binary concrete based on natural volcanic pozzolan," *Construction and Building Materials*, vol. 232, p. 117189, Jan. 2020, doi: 10.1016/j.conbuildmat.2019.117189.
[118] A. Marani, T. Oyinkanola, and D. K. Panesar, "Probabilistic deep learning prediction of natural carbonation of low-carbon concrete incorporating SCMs," *Cement and Concrete Composites*, vol. 152, p. 105635, Sep. 2024, doi: 10.1016/j.cemconcomp.2024.105635.
[119] J. Broomfield, *Corrosion of Steel in Concrete: Understanding, Investigation and Repair*. 2022. doi: 10.1201/9781003223016.
[120] P. Claisse, *Transport Properties of Concrete: Measurements and Applications*. 2014.
[121] Y. Li, Z. Liu, and J. Jiang, "Microstructure and macroscopic properties of low-carbon concrete subjected to elevated temperature: State-of-the-Art Review," *Journal of Building Engineering*, vol. 86, p. 108731, Jun. 2024, doi: 10.1016/j.jobe.2024.108731.
[122] P. Azarsa and R. Gupta, "Electrical Resistivity of Concrete for Durability Evaluation: A Review," *Advances in Materials Science and Engineering*, vol. 2017, no. 1, p. 8453095, 2017, doi: 10.1155/2017/8453095.
[123] X. Li, Q. Xu, and S. Chen, "An experimental and numerical study on water permeability of concrete," *Construction and Building Materials*, vol. 105, pp. 503–510, Feb. 2016, doi: 10.1016/j.conbuildmat.2015.12.184.
[124] E. J. Garboczi, "Permeability, diffusivity, and microstructural parameters: A critical review," *Cement and Concrete Research*, vol. 20, no. 4, pp. 591–601, Jul. 1990, doi: 10.1016/0008-8846(90)90101-3.
[125] K. Li, F. Zhao, Y. Zhang, and 胡振中, "Influence of carbonation on the chloride ingress into concrete: Theoretical analysis and application to durability design," *Cement and Concrete Research*, vol. 123, Jun. 2019, doi: 10.1016/j.cemconres.2019.105788.
[126] G. A. Julio-Betancourt and R. D. Hooton, "Study of the Joule effect on rapid chloride permeability values and evaluation of related electrical properties of concretes," *Cement and Concrete Research*, vol. 34, no. 6, pp. 1007–1015, Jun. 2004, doi: 10.1016/j.cemconres.2003.11.012.
[127] R. Feldman, L. R. Prudencio, and G. Chan, "Rapid chloride permeability test on blended cement and other concretes: correlations between charge, initial current and conductivity," *Construction and Building Materials*, vol. 13, no. 3, pp. 149–154, Apr. 1999, doi: 10.1016/S0950-0618(98)00033-6.
[128] R. Spragg *et al.*, "Leaching of conductive species: Implications to measurements of electrical resistivity," *Cement and Concrete Composites*, vol. 79, pp. 94–105, May 2017, doi: 10.1016/j.cemconcomp.2017.02.003.

[129] A. A. Ramezanianpour, A. Pilvar, M. Mahdikhani, and F. Moodi, “Practical evaluation of relationship between concrete resistivity, water penetration, rapid chloride penetration and compressive strength,” *Construction and Building Materials*, vol. 25, no. 5, pp. 2472–2479, May 2011, doi: 10.1016/j.conbuildmat.2010.11.069.
[130] S. Gupta, “Carbon sequestration in cementitious matrix containing pyrogenic carbon from waste biomass: A comparison of external and internal carbonation approach,” *Journal of Building Engineering*, vol. 43, p. 102910, Nov. 2021, doi: 10.1016/j.jobe.2021.102910.
[131] N. Kamal, Z. Itam, Y. Sivaganese, and S. Beddu, “Carbon dioxide sequestration in concrete and its effects on concrete compressive strength,” *Materials Today: Proceedings*, vol. 31, Dec. 2020, doi: 10.1016/j.matpr.2020.11.185.
[132] I. Elkhaldi, E. Rozière, G. Villain, and A. Loukili, “Effect of accelerated carbonation on electrical resistivity and microstructure of clinker-slag-limestone cement based concretes,” *Materials and Structures*, vol. 57, Jan. 2024, doi: 10.1617/s11527-023-02290-x.
[133] D. Singh Gill and S. Mariam Abraham, “Feasibility of CO2 sequestration in concrete containing recycled aggregates,” *Materials Today: Proceedings*, Mar. 2023, doi: 10.1016/j.matpr.2023.03.186.
[134] Y. Zhao, S. Lian, J. Bi, C. Wang, and kun Zheng, “Study on Freezing-Thawing damage mechanism and evolution model of concrete,” *Theoretical and Applied Fracture Mechanics*, vol. 121, p. 103439, Oct. 2022, doi: 10.1016/j.tafmec.2022.103439.
[135] H. Cai and X. Liu, “Freeze-thaw durability of concrete: ice formation process in pores,” *Cement and Concrete Research*, vol. 28, no. 9, pp. 1281–1287, Sep. 1998, doi: 10.1016/S0008-8846(98)00103-3.
[136] “ACI 201.2R-16 Guide to Durable Concrete.” Accessed: Jul. 25, 2024. [Online]. Available: https://www.concrete.org/publications/internationalconcreteabstractsportal/m/details/id/51689514
[137] S. Fajardo, D. M. Bastidas, M. P. Ryan, M. Criado, D. S. McPhail, and J. M. Bastidas, “Low-nickel stainless steel passive film in simulated concrete pore solution: A SIMS study,” *Applied Surface Science*, vol. 256, no. 21, pp. 6139–6143, Aug. 2010, doi: 10.1016/j.apsusc.2010.03.140.
[138] F. Shaheen and B. Pradhan, “Influence of sulfate ion and associated cation type on steel reinforcement corrosion in concrete powder aqueous solution in the presence of chloride ions,” *Cement and Concrete Research*, vol. 91, pp. 73–86, Jan. 2017, doi: 10.1016/j.cemconres.2016.10.008.
[139] N. Silva, “Chloride Induced Corrosion of Reinforcement Steel in Concrete - Threshold Values and Ion Distributions at the Concrete-Steel Interface,” 2013. Accessed: Aug. 25, 2024. [Online]. Available: https://www.semanticscholar.org/paper/Chloride-Induced-Corrosion-of-Reinforcement-Steel-Silva/42906505c6370ea601f0e2946e17545fec08fb36
[140] B. Guo, G. Chu, R. Yu, Y. Wang, Q. Yu, and D. Niu, “Effects of sufficient carbonation on the strength and microstructure of CO2-cured concrete,” *Journal of Building Engineering*, vol. 76, p. 107311, Oct. 2023, doi: 10.1016/j.jobe.2023.107311.
[141] A. Steffens, D. Dinkler, and H. Ahrens, “Modeling carbonation for corrosion risk prediction of concrete structures,” *Cement and Concrete Research*, vol. 32, no. 6, pp. 935–941, Jun. 2002, doi: 10.1016/S0008-8846(02)00728-7.
[142] J. M. Chi, R. Huang, and C. C. Yang, “Effects of carbonation on mechanical properties and durability of concrete using accelerated testing method,” *Journal of Marine Science and Technology*, vol. 10, no. 1, pp. 14–20, 2002.
[143] S. Talukdar and N. Banthia, “Carbonation in concrete infrastructure in the context of global climate change: Development of a service lifespan model,” *Construction and Building Materials*, vol. 40, pp. 775–782, Mar. 2013, doi: 10.1016/j.conbuildmat.2012.11.026.

[144] X. Shen *et al.*, “Combine ingress of chloride and carbonation in marine-exposed concrete under unsaturated environment: A numerical study,” *Ocean Engineering*, vol. 189, p. 106350, Oct. 2019, doi: 10.1016/j.oceaneng.2019.106350.
[145] “CAN/CSA-A3000-03. Cementitious Materials Compendium (Consists of A3001, A3002, A3003, A3004 and A3005),” CSA Group. Accessed: Aug. 25, 2024. [Online]. Available: https://www.csagroup.org/store/product/2416710/
[146] ASTM International, “ASTM C595-08a Standard Specification for Blended Hydraulic Cements.” Accessed: Aug. 26, 2023. [Online]. Available: https://www.astm.org/c0595-08a.html
[147] ASTM International, “C494/C494M-17 Standard Specification for Chemical Admixtures for Concrete.” Accessed: Aug. 26, 2023. [Online]. Available: https://www.astm.org/c0494_c0494m-17.html
[148] “CSA A23.1:24/CSA A23.2:24,” CSA Group. Accessed: Feb. 13, 2025. [Online]. Available: https://www.csagroup.org/store/product/2701210/
[149] “AASHTO T 358-19: Method of Test for Surface Resistivity Indication of Concrete’s Ability to Resist Chloride Ion Penetration.” Accessed: Aug. 25, 2024. [Online]. Available: https://civilnode.com/download-standard/10672560484310/AASHTO-T-358-19-Method-of-Test-for-Surface-Resistivity-Indication-of-Concrete-s-Ability-to-Resist-Chloride-Ion-Penetration
[150] “Surf™ | Concrete Surface Resistivity,” Giatec Scientific Inc. Accessed: Feb. 13, 2025. [Online]. Available: https://www.giatecscientific.com/products/concrete-ndt-devices/surf-surface-resistivity-meter-giatec/
[151] “Giatec-SURF-UserManual-2023-07.pdf.” Accessed: Sep. 15, 2024. [Online]. Available: https://www.giatecscientific.com/documents/Shared%20Documents/1.0%20External%20Resources/1.11%20Surf/Technical%20support%20resources/User%20Manual/Giatec-SURF-UserManual-2023-07.pdf
[152] “ASTM C1202-22 Standard Test Method for Electrical Indication of Concrete’s Ability to Resist Chloride Ion Penetration.” Accessed: Aug. 25, 2024. [Online]. Available: https://www.astm.org/c1202-22.html
[153] “AASHTO T 277 - Standard Method of Test for Electrical Indication of Concrete’s Ability to Resist Chloride Ion Penetration | GlobalSpec.” Accessed: Feb. 13, 2025. [Online]. Available: https://standards.globalspec.com/std/13344840/aashto-t-277
[154] “Perma™ | Rapid Chloride Permeability,” Giatec Scientific Inc. Accessed: Feb. 13, 2025. [Online]. Available: https://www.giatecscientific.com/products/concrete-ndt-devices/perma-rapid-chloride-permeability/
[155] “Perma2-Manual-Final.pdf.” Accessed: Sep. 15, 2024. [Online]. Available: https://www.giatecscientific.com/wp-content/uploads/2013/06/Perma2-Manual-Final.pdf
[156] E. Standards, “BS EN 12390-8:2019 Testing hardened concrete Depth of penetration of water under pressure,” https://www.en-standard.eu. Accessed: Aug. 25, 2024. [Online]. Available: https://www.en-standard.eu/bs-en-12390-8-2019-testing-hardened-concrete-depth-of-penetration-of-water-under-pressure/
[157] P. Monteiro and P. Mehta, *Concrete: Microstructure, Properties and Materials*. 2006.
[158] M. Ibrahim and M. Issa, “Evaluation of chloride and water penetration in concrete with cement containing limestone and IPA,” *Construction and Building Materials*, vol. 129, pp. 278–288, Dec. 2016, doi: 10.1016/j.conbuildmat.2016.10.085.
[159] “ASTM C666-Standard Test Method for Resistance of Concrete to Rapid Freezing and Thawing.” Accessed: Sep. 15, 2024. [Online]. Available: https://www.astm.org/c0666-97.html
[160] “Elite Series Freeze Thaw Cabinet.” Accessed: Feb. 13, 2025. [Online]. Available: https://www.humboldtmfg.com/elite-series-freeze-thaw-cabinet.html

[161] “ASTM C215-19-Standard Test Method for Fundamental Transverse, Longitudinal, and Torsional Resonant Frequencies of Concrete Specimens.” Accessed: Sep. 15, 2024. [Online]. Available: https://www.astm.org/c0215-19.html
[162] “ASTM C597-22 Standard Test Method for Ultrasonic Pulse Velocity Through Concrete.” Accessed: Sep. 15, 2024. [Online]. Available: https://www.astm.org/c0597-22.html
[163] M. Mohana, “Assessment of concrete compressive strength by ultrasonic pulse velocity test,” *Iraqi Journal of Civil Engineering*, Accessed: Aug. 26, 2024. [Online]. Available: https://www.academia.edu/107709346/Assessment_of_concrete_compressive_strength_by_ultrasonic_pulse_velocity_test
[164] I. A. E. Agency, “Guidebook on Non-destructive Testing of Concrete Structures,” International Atomic Energy Agency, Text, 2002. Accessed: Feb. 13, 2025. [Online]. Available: https://www.iaea.org/publications/6347/guidebook-on-non-destructive-testing-of-concrete-structures
[165] R. Narayan Swamy, “Dynamic Poisson’s ratio of portland cement paste, mortar and concrete,” *Cement and Concrete Research*, vol. 1, no. 5, pp. 559–583, Sep. 1971, doi: 10.1016/0008-8846(71)90060-3.
[166] K. Tuutti, “Corrosion of steel in concrete,” Doctoral Thesis (monograph), Swedish Cement and Concrete Research Institute, Stockholm, 1982.
[167] “A proposed laboratory method to evaluate the durability of concrete pavement joints against freezing in the presence of deicer salts,” *Canadian Journal of Civil Engineering*, vol. 49, no. 8, pp. 1351–1365, Apr. 2022, doi: 10.1139/cjce-2021-0140.
[168] C. S. Rangel, M. Amario, M. Pepe, E. Martinelli, and R. D. Toledo Filho, “Influence of Wetting and Drying Cycles on Physical and Mechanical Behavior of Recycled Aggregate Concrete,” *Materials (Basel)*, vol. 13, no. 24, p. 5675, Dec. 2020, doi: 10.3390/ma13245675.
[169] “iCOR® Archives,” Giatec Scientific Inc. Accessed: Aug. 26, 2024. [Online]. Available: https://www.giatecscientific.com/category/giatec-icor/
[170] “Giatec-iCOR-User-Manual-V-2.0.pdf.” Accessed: Sep. 16, 2024. [Online]. Available: https://www.giatecscientific.com/wp-content/uploads/2013/06/Giatec-iCOR-User-Manual-V-2.0.pdf
[171] “ASTM C876-15-Standard Test Method for Corrosion Potentials of Uncoated Reinforcing Steel in Concrete.” Accessed: Sep. 16, 2024. [Online]. Available: https://www.astm.org/c0876-15.html
[172] P. Schober, C. Boer, and L. A. Schwarte, “Correlation Coefficients: Appropriate Use and Interpretation,” *Anesth Analg*, vol. 126, no. 5, pp. 1763–1768, May 2018, doi: 10.1213/ANE.0000000000002864.
[173] C. Andrade, “The P Value and Statistical Significance: Misunderstandings, Explanations, Challenges, and Alternatives,” *Indian J Psychol Med*, vol. 41, no. 3, pp. 210–215, 2019, doi: 10.4103/IJPSYM.IJPSYM_193_19.
[174] M. Ali *et al.*, “A review on chloride induced corrosion in reinforced concrete structures: lab and in situ investigation,” *RSC Advances*, vol. 14, no. 50, pp. 37252–37271, 2024, doi: 10.1039/D4RA05506C.
[175] H. Justnes, M. O. Kim, S. Ng, and X. Qian, “Methodology of calculating required chloride diffusion coefficient for intended service life as function of concrete cover in reinforced marine structures,” *Cement and Concrete Composites*, vol. 73, pp. 316–323, Oct. 2016, doi: 10.1016/j.cemconcomp.2016.08.006.
[176] D. V. Dinh, “Initiation time of corrosion in reinforced concrete structures exposed to chloride in marine environment,” *IJCIET*, vol. 8, no. 9, Art. no. 9, Sep. 2017.
[177] “ACI 365.1R-00: Service-Life Prediction.” Accessed: Sep. 29, 2024. [Online]. Available: https://www.concrete.org/store/productdetail.aspx?ItemID=365100&Format=DOWNLOAD&Language=English&Units=US_AND_METRIC

[178] P. Konečný, P. Lehner, T. Ponikiewski, and P. Miera, “Comparison of Chloride Diffusion Coefficient Evaluation Based on Electrochemical Methods,” *Procedia Engineering*, vol. 190, pp. 193–198, Jan. 2017, doi: 10.1016/j.proeng.2017.05.326.
[179] T. Kuhlman and J. Farrington, “What is Sustainability?,” *Sustainability*, vol. 2, no. 11, Art. no. 11, Nov. 2010, doi: 10.3390/su2113436.
[180] J. Li, F. Xiao, L. Zhang, and S. Amirkhanian, “Life cycle assessment and life cycle cost analysis of recycled solid waste materials in highway pavement: A review,” *Journal of Cleaner Production*, vol. 233, pp. 1182–1206, Oct. 2019, doi: 10.1016/j.jclepro.2019.06.061.
[181] “ISO 14040:2006,” ISO. Accessed: Oct. 05, 2024. [Online]. Available: https://www.iso.org/standard/37456.html
[182] E. and C. C. Canada, “Global warming potentials.” Accessed: Feb. 05, 2025. [Online]. Available: https://www.canada.ca/en/environment-climate-change/services/climate-change/greenhouse-gas-emissions/quantification-guidance/global-warming-potentials.html
[183] A. Atmaca, “Understanding carbon footprint: impact, assessment, and greenhouse gas emissions,” in *Advances and Technology Development in Greenhouse Gases: Emission, Capture and Conversion*, M. R. Rahimpour, M. A. Makarem, and M. Meshksar, Eds., Elsevier, 2024, pp. 497–516. doi: 10.1016/B978-0-443-19231-9.00015-6.
[184] K. Vázquez-Calle, V. Guillén-Mena, and F. Quesada-Molina, “Analysis of the Embodied Energy and CO2 Emissions of Ready-Mixed Concrete: A Case Study in Cuenca, Ecuador,” *Materials (Basel)*, vol. 15, no. 14, p. 4896, Jul. 2022, doi: 10.3390/ma15144896.
[185] R. Kahlon, “Ministerial Order No. BA 2023 10”.
[186] “LCI Databases | Athena Sustainable Materials Institute.” Accessed: Oct. 10, 2024. [Online]. Available: https://www.athenasmi.org/our-software-data/lca-databases/
[187] “EPD-DeltaNRMCAEPD20034.pdf.” Accessed: Oct. 09, 2024. [Online]. Available: https://www.nrmca.org/wp-content/uploads/2020/05/EPD-DeltaNRMCAEPD20034.pdf
[188] “appendix 7.pdf.” Accessed: Oct. 10, 2024. [Online]. Available: https://legacy.winnipeg.ca/finance/findata/matmgt/documents/2012/682-2012/682-2012_appendix_h-wstp_south_end_plant_process_selection_report/appendix%207.pdf
[189] “EPD for Polaris Materials Concrete Aggregates - ASTM International,” m.moam.info. Accessed: Feb. 06, 2025. [Online]. Available: https://m.moam.info/epd-for-polaris-materials-concrete-aggregates-astm-international_6479d1a8097c476d028bb86f.html
[190] “Sika Canada_EPD_5_Concrete Admixtures_Additives_2021-06-09.pdf.” Accessed: Oct. 09, 2024. [Online]. Available: https://can.sika.com/dam/dms/ca01/f/Sika%20Canada_EPD_5_Concrete%20Admixtures_Additives_2021-06-09.pdf
[191] “ISO 14044:2006/Amd 2:2020,” ISO. Accessed: Feb. 06, 2025. [Online]. Available: https://www.iso.org/standard/76122.html
[192] “Industrial carbon pricing explained,” Canadian Climate Institute. Accessed: Oct. 11, 2024. [Online]. Available: https://climateinstitute.ca/large-emitter-trading-systems-explained/

Appendix A

(a) (b) (c)

Figure A.1(a) Workability of the concrete mix before CO_2 addition, (b) Workability after 1% CO_2 addition and (c) Air content testing

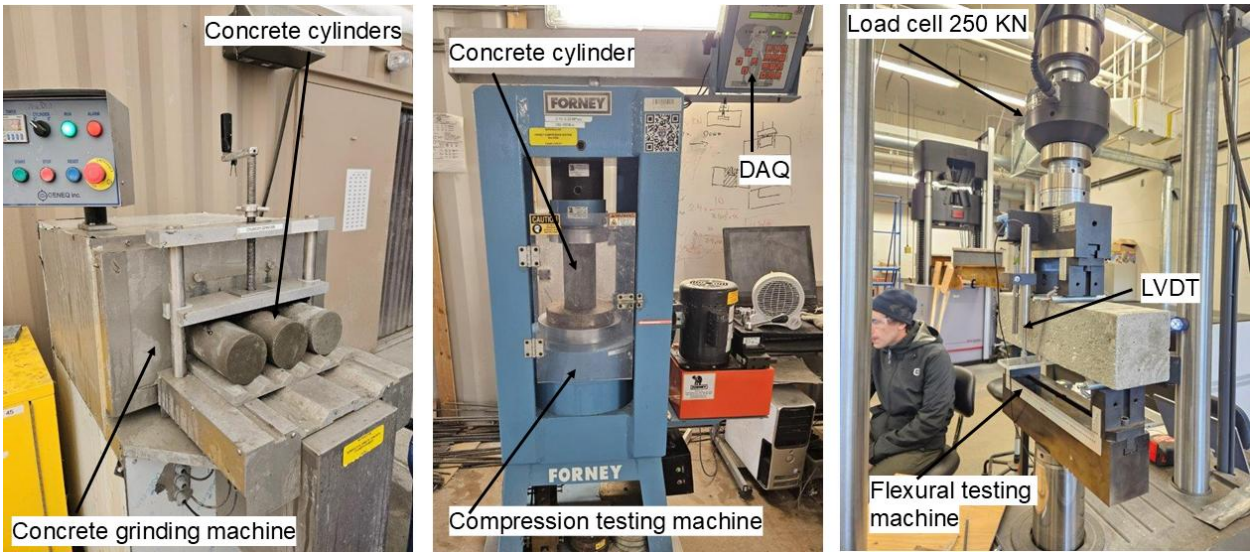

(a) (b) (c)

Figure A.2 (a) Concrete surface grinding machine, (b) Compression testing machine and (c) Flexural testing under third point loading

(a) (b) (c)

Figure A.3 Thermal Pyrolysis test (a) Marshall compactor, (b) Muffle furnace and (c) Digital weighing balance

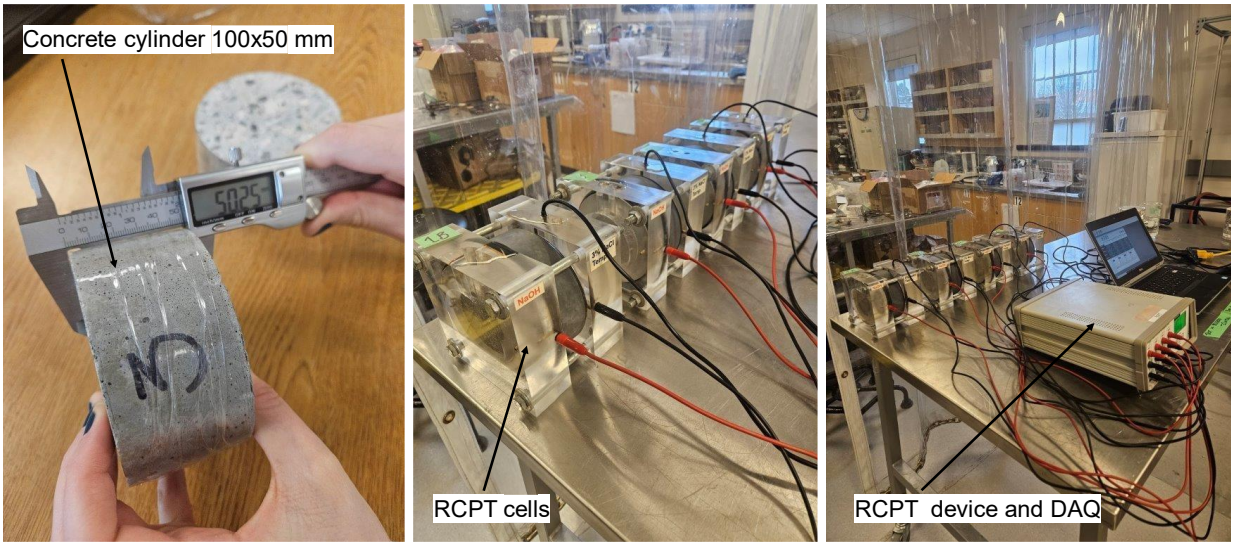

(a) (b) (c)

Figure A.4 (a) 50 mm thick concrete specimen covered with a waterproof tape, (b) RCPT cells with NaOH and NaCl reservoirs and (c) RCPT test setup

(a) (b) (c)

Figure A.5 (a) Water permeability testing setup, (b) Concrete cube splitting jig and (c) Water penetration depth measurement

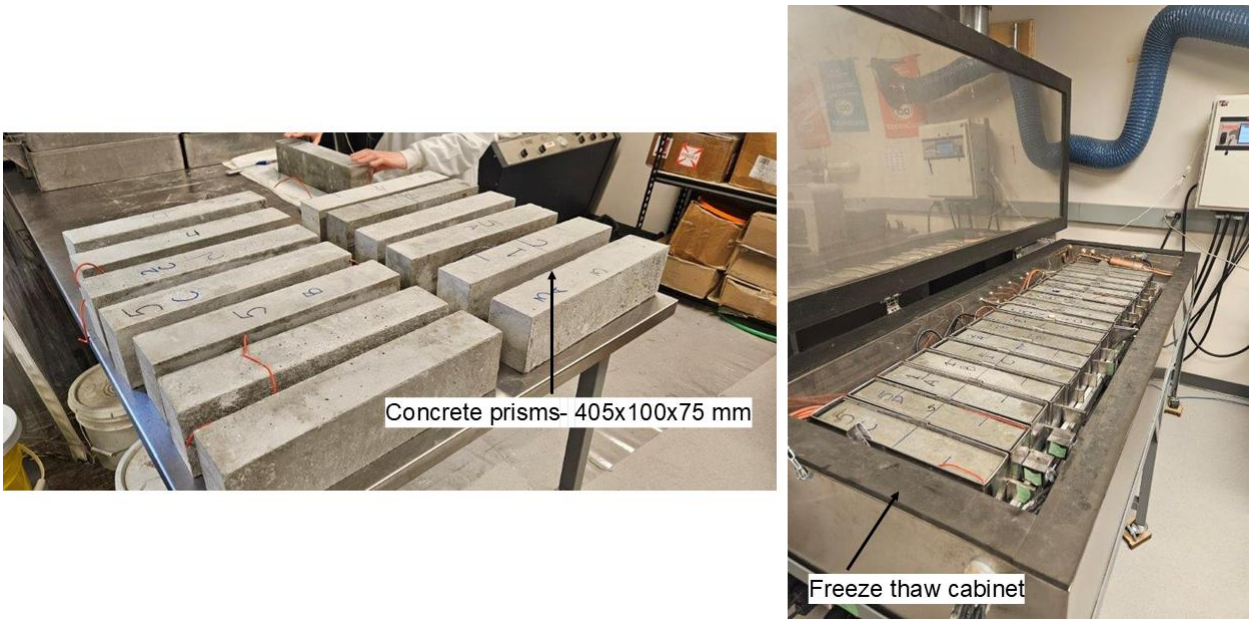

Figure A.6 (a) Concrete prisms for freeze-thaw testing and (b) Freeze-thaw testing cabinet

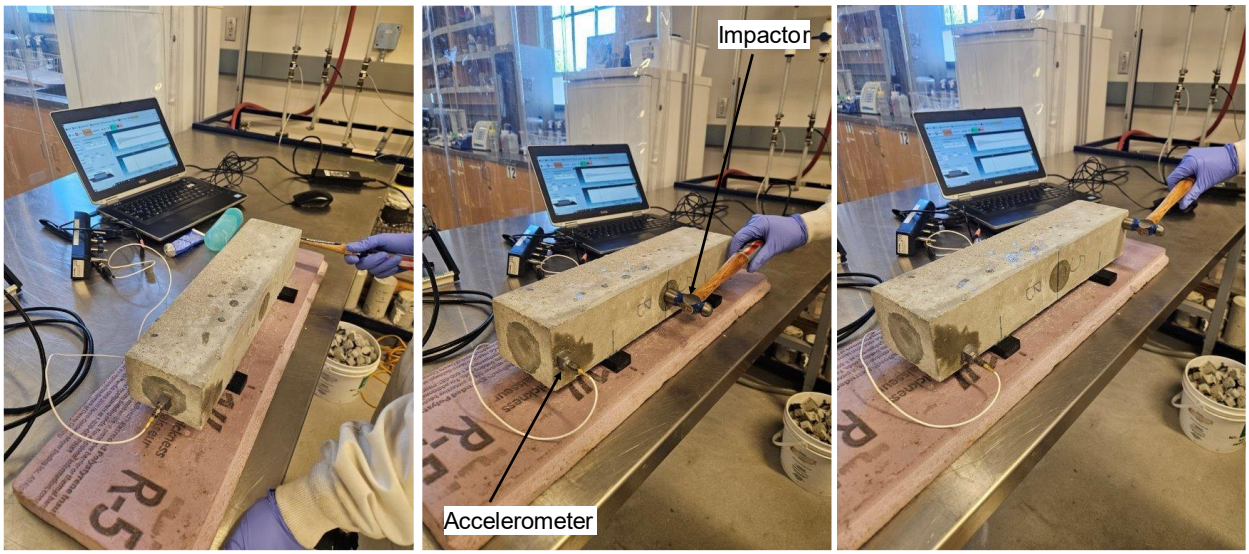

(a) (b) (c)

Figure A.7 Resonant frequency test (a) Longitudinal fundamental frequency, (b) Transverse fundamental frequency and (c) Torsional fundamental frequency of vibration test

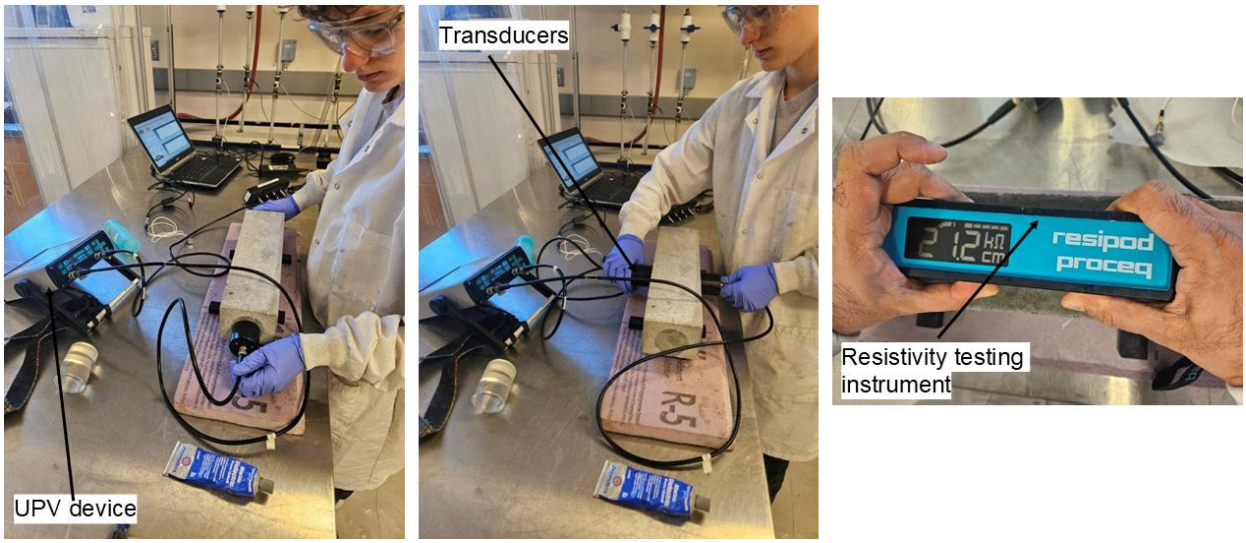

(a) (b) (c)

Figure A.8 Testing of concrete prisms subjected to freeze thaw cycles (a) UPV across longitudinal direction, (b) UPV across transverse direction, and (c) Concrete resistivity testing

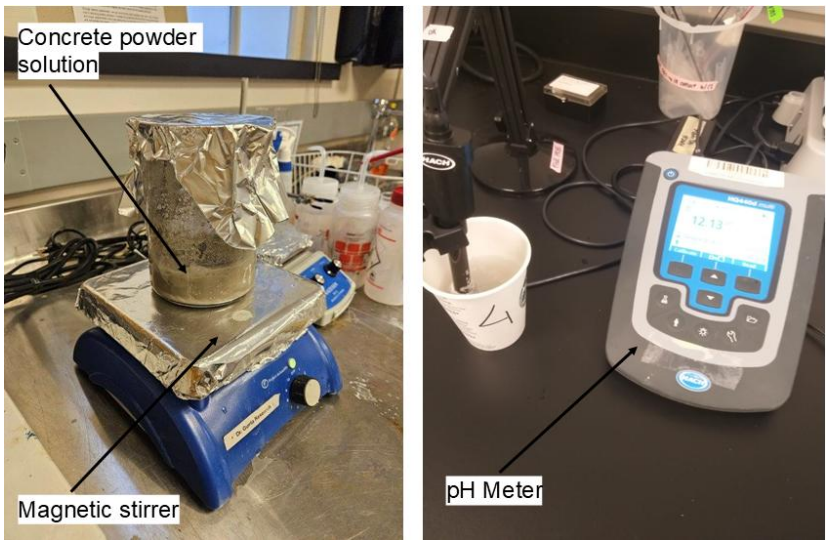

(a) (b)

Figure A.9 pH testing of concrete (a) Preparation of concrete powder solution using a magnetic stirrer and (b) pH testing using a digital pH meter

(a) (b)

Figure A.10 Alternative wetting and drying cycles test setup (a) Wetting cycle and (b) Drying cycle